The Energetics of Defects and Impurities in Metals and Ionic Materials from First Principles.

Alessandro De Vita
Dottore in Fisica.

Submitted in partial fulfilment of the requirements of the degree of
Doctor of Philosophy

Department of Physics, University of Keele.

September 1992

Abstract

The study of defects in metals and ionic solids has been the subject of great theoretical and experimental interest, in basic as well as applied research areas. The present work collects two series of calculations on the energetics of a variety of defective systems, in a metal host matrix (Al), and in two ionic oxides (MgO and Li_2O) . The energetics and the electronic ground state of the vacancy, of the self-interstitial, and of the hydrogen impurity systems in Al were investigated. The formation and migration energies of Schottky defects in MgO and Frenkel Defects in Li_2O were also studied. All results are in close agreement with experiment, while the work gives new insight into the localisation of defects, the role played by lattice relaxation effects, and the defect-induced redistribution of valence electrons. The calculations are based on density functional and pseudopotential theory, make use the supercell approach, and employ in different implementations the conjugate gradients technique to minimise the total energy functional. For the calculations on oxides, we made use of a newly developed parallel computing methodology.

to my parents Anna and Vincenzo

Contents

List of Figures

List of Tables

Introduction.

The study of defects in metals and ionic solids has been the subject of great theoretical and experimental interest, in basic as well as applied research areas. The availability of a coherent description of the properties of isolated defects in these materials is a mandatory condition for almost any kind of theoretical investigation on more complex defective structures, or for any advanced technological application involving non-pure samples or temperature regimes in which the presence of intrinsic defects is statistically relevant.

In the present work we report on two series of calculations which we have performed on a variety of defective systems, in a metal host matrix (Al), and in two ionic oxides (MgO and Li_2O). In the first series of calculations we investigated the simple vacancy, the self-interstitial, the hydrogen impurity and the hydrogen-vacancy systems in aluminium. In the second one, we studied the intrinsic Schottky defect pair system in MgO and Frenkel defect pair system in Li_2O.

Metal defects and impurity systems investigated.

The intrinsic isolated vacancy defect in aluminium is a typical example of simple defect in a technologically important material on which theoretical calculations and experiments have for long been in serious disagreement. Al is an high density "simple" (*sp*-bonded) metal, with a free-electron-like band structure. A simple model of the isolated vacancy in Al which has been extensively studied in the past consists of a Wigner sphere "hole" in the positive background of an otherwise uniform electron gas having the same average density of the metal. After solving self-consistently the electronic wave equation for this model system, most early theoretical models included the interaction of the vacancy with the metal ions lattice by means of perturbation expansions in the strength of the weak ionic core potential.

In more recent times, one first-principles supercell calculation of the formation energy of the aluminium vacancy was attempted, at first using a model Al potential, and subsequently an ab initio norm-conserving pseudopotential. The disagreement of the results with experiment suggested the conclusion that the supercell method was not suited for the physical system investigated.

The physics of hydrogen impurities in metals is also of great scientific interest. Hydrogen atoms occupy interstitial sites in metals lattices, and diffuse much faster than any other atoms in solids. The technological relevance of metal systems with hydrogen in solid solution is due to phenomena like metal embrittlement and fatigue in the presence of impurities, and is connected with the development of solid state energy storage systems. Again, a detailed description of the isolated defect is necessary to provide quantitative estimates of technologically relevant quantities like the hydrogen heat of solution. Moreover, information on the lattice distortion field associated with the defect self-trapped states are necessary to model the various mechanisms of hydrogen diffusion (*e.g.* by coherent or thermally activated tunneling, or by classical over-barrier jumps).

For the system constituted of an isolated hydrogen atom in aluminium host, no clear experimental picture is available on a number of issues like (i) the exact location of the stablest interstitial site and the the role played by lattice relaxation in the different interstitial geometries, (ii) the role of vacancy defects as trapping sites for hydrogen impurities, and (iii) the size of the energy barriers for hydrogen diffusion.

The existing theoretical results for this system have been obtained by models based on the embedding of hydrogen in pure jellium. The interaction of the defect with the ionic lattice is again included via perturbation theory, as in the early calculations on the isolated vacancy, or making a spherical approximation for the potential due to the ions. In no case has the explicit interaction of the hydrogen atom with the metal ions been treated self-consistently; most of the earlier work ignores lattice relaxation effects, on the belief that its effects on the energetics are negligible.

The goal of the first part of the present work was to re-examine the problem of calculating point-defect energies in aluminium, avoiding as far as possible the approximations made in earlier studies. Our aim was to investigate on how much the recent advances in total energy techniques could help us to provide supporting insight to the experimental activity concerning these systems.

Defects investigated in ionic solids.

The study of point defects in ionic materials is a well-assessed aspect of solid state theory. Ceramic oxides are materials of large (and ever increasing) technological importance, as refractory materials, insulators, and catalysts, in a wide range of applications from metallurgy to solid state batteries and fusion reactors. MgO and Li_2O are two representative examples of ceramic oxides whose physical properties (electrical conductivity, response to stress, high temperature behaviour) are determined by the energetics of intrinsic defects. The leading intrinsic defects in the two materials are the Schottky and Frenkel isolated pairs, respectively.

The first requirement in calculating defect parameters is to have a model of the crystal forces. In the past, the treatment of the energetics of defective ionic materials has relied on empirical interaction models, like the "shell model", or on the ab initio cluster techniques of various kind based on the Hartree-Fock method. The empirical models suffer to some extent from the intrinsic limitations of the chosen analytic pair interaction forms, and of the fitting procedure of the potentials parameters from experimental data. The Hartree-Fock based models can be limited by the small cluster size which can be handled, and by difficulties in achieving the convergence of the energies with respect to the size of the localised basis sets, while the evaluation of the forces exerted on the ions is made difficult by the occurrence of Pulay effects. In spite of the mentioned difficulties, these approaches have been successful in many cases.

In the second part of the present work we report on some of the first fully ab initio calculations on point defect energetics in ceramic oxides performed using the supercell method in the framework of the Pseudopotential Density Functional Plane Waves formalism. One of the aims of these calculations was to investigate the adequacy of this technical framework to a class of physical systems in which the ground state electronic density is strongly inhomogeneous and is expected to largely redistribute in the ionic solid from the isolated neutral atoms case. Moreover, the defects we investigated in MgO and Li_2O carry net charges, and therefore have an associated long-ranged polarisation field. The assumption of the Local Density Approximation for the electronic exchange and correlation energy, the use of norm-conserving pseudopotentials to represent the core ions, and the use of the repeated cell geometry for the defective systems, all involve systematic errors which need investigation, testing, and, if needed, the application of suitable corrections.

The treatment of supercells of oxide materials within the plane wave formalism requires large amounts of computer resources, in terms of processing time and memory allocations. An important feature of our calculations on oxides is that they have been performed on a parallel supercomputer (a 64-node Meiko Computing Surface), using a total energy minimisation code specifically designed for this kind of machine. High performance parallel computers able to compete (and surpass) the more conventional (CRAY-like) serial machines have become available only in recent times, and are expected to play an increasingly important role in all kind of large-scale scientific computational applications. The use of a machine of this kind in an ab initio total energy calculation introduces novel technical problems. In the practice of the calculations, the attention is continually driven to the structural aspects of the usual algorithms which dictate the parallelisation strategy and dominate the expense of computing resources at large system sizes. One of the aims of our calculations on MgO and Li_2O was to demonstrate in a practical application the effectiveness of total energy computations in this new parallel implementation.

Plan of the work.

In Chapter 1 we briefly summarise the standard theoretical background of the present work. The main results and approximations of Density Functional Theory are described, and a brief introduction to the features of pseudopotentials in solid state applications is given.

In Chapter 2 an outline of the computational techniques utilised in the work is provided. Two different procedures based on the conjugate gradients technique for accomplishing the total energy minimisation are presented and discussed. The adopted pseudopotential representation and optimisation in the plane waves formalism, and the non-linear core correction of the exchange and correlation potential, are introduced. The problems connected with the Brillouin Zone integration in metals are summarised. A novel analysis of the various Fermi energy smearing techniques is provided, and a general expression for a correction term to improve the accuracy of ground state energy values is presented.

In Chapter 3, after a brief historical sketch of the existing theoretical results, we report on our calculations on the energetics of the stable and migrating vacancy, the self-interstitial, the interstitial and migrating hydrogen impurity, and the hydrogen-vacancy system in aluminium host. The problem of correctly defining the defect formation energies and the associated volume relaxation using periodic boundary conditions is discussed. When possible, the results are compared with other recent first-principles theoretical predictions obtained making use of different techniques.

In Chapter 4 we briefly introduce the problem of performing total energy calculations on parallel computing machines, and report an analysis of some possible parallelisation strategies, leading to the one which was used for the calculations on oxide materials.

In Chapter 5 we report on our calculations on defect energetics in MgO and Li_2O. Some of the existing empirical models and Hartree Fock based techniques are briefly described, as alternative, or complementary, to our approach. The problem of studying the energetics of charged defects with the supercell method is addressed, and we provide the results of some empirical model calculations which we performed to study the convergence of results with respect to the size of the systems investigated. We then present results for the energetics and the ground state charge densities of Schottky defects in MgO, Frenkel defects in Li_2O, and of all the associated migrating-defect systems.

After some brief concluding notes, we report in Appendix A the results of some further calculations on some perfect lattice properties of Al, which we performed to demonstrate the validity of the Fermi energy smearing scheme presented at the end of Chapter 2 .

1 Density Functional Theory and Pseudopotentials.

1.1 Introduction.

In this chapter a brief summary of the standard theoretical background of the present work is given. The problem of solving the many-body Schrödinger equation for the electrons in a solid is stated in the framework of Density Functional Theory. The assumptions of the theory and the approximations involved in using it for real calculations are briefly discussed. The problems connected with the representation of the atoms as core ions, emitting a potential field in which only the valence electrons need to be treated in the calculations, is also discussed.

1.2 Density Functional Theory.

The general problem of finding the ground state many-body wavefunction for a system of N electrons in a given external potential is reduced within the Density Functional Theory (DFT)[1][2] to the problem of finding a scalar field $\rho(\boldsymbol{r})$ representing the ground state density of electrons. For any give external potential $V(\boldsymbol{r})$ such density can be determined from the exact solution of the associated Schrödinger equation. The main result of DFT is that also the opposite is true: for any given ground state density $\rho(\boldsymbol{r})$ for which there exist a potential $V(\boldsymbol{r})$ such that $\rho(\boldsymbol{r})$ is the ground state of the associated wave equation, it is possible to show that such potential is *unique*. Given the ground state density, the hamiltonian operator of the system is therefore completely determined, and so is its ground state expectation value $E[\rho]$, expressed as a functional of ρ (Hohenberg and Kohn theorem, 1964[1]):

$$E[\rho] = < \Psi | \ \hat{T} + \hat{V} + \hat{U} \ | \Psi > \tag{1.1}$$

where $\hat{T}$ and $\hat{U}$ are the kinetic energy and electron-electron interaction operators, and Ψ is the ground state many-body wavefunction.
It is important to notice that the functional $E[\rho]$ is defined only on the domain of real functions $\rho(\boldsymbol{r})$ which are ground state densities for some potential (v - representability).[1]

The functional in equation (1.1) can be regrouped as:

$$E[\rho] = G[\rho] + \int V(\boldsymbol{r})\rho(\boldsymbol{r})d\boldsymbol{r}; \qquad G[\rho] = < \Psi|\, T + U \,|\Psi > \tag{1.2}$$

to isolate the kinetic and interaction contributions. For a given external potential V_0 (in general not the one corresponding uniquely to ρ according to the HK theorem), it is also possible to show that the functional

$$E_{V_0}[\rho] = G[\rho] + \int V_0(\boldsymbol{r})\rho(\boldsymbol{r})d\boldsymbol{r} \ , \tag{1.3}$$

defined on the same domain as $E[\rho]$ in eqn. (1.1), has an absolute minimum on the ground state density ρ_0 corresponding to V_0, so that

$$E_{V_0}[\rho_0] = E[\rho_0] \ . \tag{1.4}$$

The problem of minimising the expectation value in eqn. (1.1) according to the Variational Principle on Ψ is therefore formally reduced to the much simpler problem of minimising the functional (1.3) with respect to ρ, for the given external potential V_0. Unfortunately the exact form of the functional $E[\rho]$ (or, equivalently, of the functional $G[\rho]$ in eqn. (1.3)) is not known, so that some approximation is required to represent the kinetic and exchange-correlation contributions. However, the theory provides a way to deal with the kinetic contribution by reformulating the minimization problem into that of solving a set of self-consistent single-particle equations.[2] For any density ρ the HK theorem identifies a unique potential whose corresponding non-interacting

---

[1] However, this does not seem to have posed serious limitations in the practice of calculations based on DFT.

[2] An accurate enough approximated expression for $G[\rho]$ to avoid such complication and solve the Thomas-Fermi problem directly has also not been yet found.

electron problem ($\hat{U} = 0$) has ρ as a ground state density. The minimum property of the therefore uniquely defined energy functional

$$\overline{E}_V[\rho] = \overline{T}[\rho] + \int V(\boldsymbol{r})\rho(\boldsymbol{r})d\boldsymbol{r} \tag{1.5}$$

for any given V, states that the functional reaches its absolute minimum on the ground state density of the non-interacting electron system with potential V.
It is convenient to rewrite the functional in eqn. (1.3) making use of the non-interacting kinetic energy functional $\overline{T}[\rho]$ and of the classic electrostatic energy term:

$$E_{V_0}[\rho] = \overline{T}[\rho] \ + \frac{e^2}{2}\int \frac{\rho(\boldsymbol{r})\rho(\boldsymbol{r}')}{|\boldsymbol{r} - \boldsymbol{r}'|}d\boldsymbol{r}\,d\boldsymbol{r}' \ + \int V_0(\boldsymbol{r})\rho(\boldsymbol{r})d\boldsymbol{r} \ + E_{xc}[\rho]\ . \tag{1.6}$$

This equation defines the exchange and correlation potential $E_{xc}[\rho]$. Imposing on the energy functionals in eqns. (1.5) and (1.6) that they both be minimized by the same electron density we get

$$V(\boldsymbol{r}) = V_0(\boldsymbol{r}) \ + \int \frac{\rho(\boldsymbol{r}')}{|\boldsymbol{r} - \boldsymbol{r}'|}d\boldsymbol{r}' \ + V_{xc}(\boldsymbol{r}) \ ; \ V_{xc}(\boldsymbol{r}) = \frac{\delta E_{xc}[\rho]}{\delta\rho(\boldsymbol{r})}\ , \tag{1.7}$$

where the exchange-correlation potential $V_{xc}(\boldsymbol{r})$ is in general non-local. Equation (1.7) shows how to construct a self-consistent potential for a non-interacting electrons system having the same ground state density of the original interacting system. For a non-interacting electron problem the ground-state solution has the form of a single Slater determinant of rank N:

$$\Psi = A[\phi_1(\boldsymbol{r}_1), .., \phi_N(\boldsymbol{r}_N)] \tag{1.8}$$

where the single-particle orbitals $\phi_i(\boldsymbol{r})$ satisfy the equations (Kohn and Sham, 1965[2]):

$$(-\frac{\hbar^2}{2m}\nabla^2 + V(\boldsymbol{r}))\phi_i(\boldsymbol{r}) = \epsilon_i\phi_i(\boldsymbol{r})\ , \tag{1.9}$$

and the particle density can be calculated as

$$\rho(\boldsymbol{r}) = \sum_{i=1}^{N} |\phi_i(\boldsymbol{r})|^2 \tag{1.10}$$

where the index i spans the set of N eigenstates with lowest eigenvalues ϵ_i. The ground state density ρ_0 is therefore given as in (1.10) by the the solution of equations (1.9), with the self-consistent potential given by (1.7). The ground state total energy of the interacting electrons system can then be evaluated as in (1.6), where by definition

$$\overline{T}[\rho_0] \;=\; \sum_{i=1}^{N} < \phi_i| - \frac{\hbar^2}{2m}\nabla^2|\phi_i > . \tag{1.11}$$

The original problem of solving the wave-equation for the electron system is therefore reduced to the solution of a self-consistent set of single-particle equations where the *only* error introduced is due to the approximated form adopted for the exchange and correlation energy functional $E_{xc}[\rho]$. Assuming $E_{xc}[\rho] = 0$, the problem reduces to a set of Hartree equations, while it is easily seen that substituting $E_{xc}[\rho]$ in the equations with the exchange term

$$-\sum_{i,j} \frac{e^2}{2} \int \frac{\phi_i^\dagger(\boldsymbol{r})\phi_j^\dagger(\boldsymbol{r}')\phi_i(\boldsymbol{r}')\phi_j(\boldsymbol{r})}{|\boldsymbol{r} - \boldsymbol{r}'|} d\boldsymbol{r}\, d\boldsymbol{r}' \tag{1.12}$$

the equations obtained form an Hartree-Fock set and their solution corresponds to the exact minimum of the energy expectation value of the many-body hamiltonian operator within the variational class (1.8).

1.3 The extension to finite temperatures.

An important extension to the ground state theory results is the generalisation of the Hohenberg-Kohn theorem to finite temperatures (Mermin, 1965 [33]). The essential result is that the grand potential of a system with a given finite temperature is a functional of the density at that temperature. The system is treated in the standard grand-canonical formalism with a given chemical potential μ and temperature $\tau = 1/\beta$. The proof is based on the fact that the grand potential

$$\Omega[\hat{\rho}] = tr[\hat{\rho}(\hat{H} - \mu\hat{N} + 1/\beta \log \hat{\rho})] \tag{1.13}$$

expressed as a function of a variable density matrix $\hat{\rho}$ subject to the constraint

$$tr[\hat{\rho}] = 1 \tag{1.14}$$

assumes its absolute minimum on the true grand canonical density matrix

$$\hat{\rho} = \frac{e^{-\beta(\hat{H}-\mu\hat{N})}}{tr[e^{-\beta(\hat{H}-\mu\hat{N})}]} \, . \tag{1.15}$$

Following essentially the same procedure of HK, Mermin shows that that the density $\rho(\boldsymbol{r})$ corresponding to minimum of the grand potential (1.13), in which some $v(\boldsymbol{r})$ is the external potential in the hamiltonian $\hat{H}$ acting on every single particle, also identifies uniquely the difference $v(\boldsymbol{r})-\mu$. This determines uniquely the operator $\hat{H}-\mu\hat{N}$ and so the grand potential itself and the true density matrix $\hat{\rho}$. Therefore the grand potential and in general all thermodynamic averages on the grand canonical ensemble for the given system can be written as functionals of the density of particles $\rho(\boldsymbol{r})$ for the given temperature. Moreover, it can be proved that the functional

$$\omega_v[\rho'] = \int (v(\boldsymbol{r}) - \mu)\rho'(\boldsymbol{r})d\boldsymbol{r} + F[\rho'] \tag{1.16}$$

for a *given* external potential $v(\boldsymbol{r})$, with

$$F[\rho] = tr\{\hat{\rho}(\hat{T} + \hat{U} + 1/\beta \log \hat{\rho})\} = T[\rho] + U[\rho] - \tau S[\rho] \tag{1.17}$$

reaches its absolute minimum on its domain of definition when $\rho'(\boldsymbol{r}) = \rho(\boldsymbol{r})$, *i.e.* on the ground state particle density corresponding to $v(\boldsymbol{r}) - \mu$.

Again it is possible to deal with the (unknown) kinetic and entropy functionals approximating them with their correct expression for a system of non-interacting fermions:

$$\omega_v[\rho] = \int (v(\boldsymbol{r}) - \mu)\rho'(\boldsymbol{r})d\boldsymbol{r} + \overline{T}[\rho] - \tau\overline{S}[\rho] + E_{xc}[\rho] + \frac{e^2}{2}\int \frac{\rho(\boldsymbol{r})\rho(\boldsymbol{r}')}{|\boldsymbol{r}-\boldsymbol{r}'|}d\boldsymbol{r}\,d\boldsymbol{r}' \tag{1.18}$$

and formally including the remainder in the definition of the exchange and correlation functional $E_{xc}[\rho]$. Varying eqn. (1.18) one obtains:

$$\frac{\delta(\overline{T}[\rho] - \tau\overline{S}[\rho])}{\delta\rho(\boldsymbol{r})} + (V(\boldsymbol{r}) - \mu) = 0 \tag{1.19}$$

which is equivalent to the minimum problem for a system of non-interacting electrons in the external potential

$$V_{eff}(\boldsymbol{r}) = v(\boldsymbol{r}) + \int \frac{\rho(\boldsymbol{r}')}{|\boldsymbol{r}-\boldsymbol{r}'|}d\boldsymbol{r}' + V_{xc}(\boldsymbol{r}) \, ; \qquad V_{xc}(\boldsymbol{r}) = \frac{\delta E_{xc}[\rho]}{\delta\rho(\boldsymbol{r})} \, . \tag{1.20}$$

For such system the spectrum of energy states $\{\epsilon_i\}$ determines the occupation probability f_i of each state via the Fermi-Dirac expression

$$f_i = \frac{1}{e^{\beta(\epsilon_i - \mu)} + 1} , \tag{1.21}$$

and the total number of particles is given by

$$N = \sum_i^{\infty} f_i . \tag{1.22}$$

The expression for the charge density is

$$\rho(\boldsymbol{r}) = \sum_{i=1}^{\infty} f_i |\phi_i(\boldsymbol{r})|^2 , \tag{1.23}$$

in which the single-particle states $\phi_i(\boldsymbol{r})$ can be calculated as the self-consistent solution of the equations

$$(-\frac{\hbar^2}{2m}\nabla^2 + V_{eff}(\boldsymbol{r}))\phi_i(\boldsymbol{r}) = \epsilon_i \phi_i(\boldsymbol{r}) , \tag{1.24}$$

which also determine the eigenvalues ϵ_i. The charge density obtained from (1.23) may be then substituted in eqn. (1.18), where the thermally averaged kinetic term is evaluated as

$$\overline{T}[\rho_0] = \sum_{i=1}^{\infty} f_i < \phi_i | -\frac{\hbar^2}{2m}\nabla^2 | \phi_i > , \tag{1.25}$$

and the entropy term S is a function of the occupations:

$$S = -\sum_i [f_i \log(f_i) + (1 - f_i) \log(1 - f_i)] . \tag{1.26}$$

It is important to notice that the expression for the exchange and correlation potential defined by eqn. (1.18) for a system of interacting fermions must contain some kinetic and entropic contributions, and in general depends on the temperature τ, though it must converge to the usual HK definition (eqn. (1.6)) in the limit $\tau \rightarrow 0$. In the cases in which the system has a fixed number N of particles the chemical potential μ can be adjusted as a free parameter in eqn. (1.21) to satisfy at self-consistency eqn. (1.22), now taken as a constraint on the occupations f_i. The Helmholtz free energy of the system of N fermions can be calculated from the self-consistent value of μ from equation (1.18) and from the definition

$$F[\rho] = \omega[\rho] + \mu N[\rho]. \tag{1.27}$$

It is, finally, worth mentioning a further generalisation of the uniqueness theorems and related self-consistent calculation procedures which have been described so far, which include spin into the general formalism. In such generalisation[106], the main results leading to a minimum principle on $E[\rho]$ or $\Omega[\rho]$ for paramagnetic systems are formally extended to the spin-dependent case, the main change introduced being that the KS single-particle equations (1.9) have to be re-expressed and solved self-consistently in the appropriate (2x2) matrix form. The subject will not be discussed here in more details because it is of no relevance in the present work.

1.4 The Local Density Approximation.

To perform calculations based on DFT, an appropriate expression for the functional $E_{xc}[\rho]$ has to be determined. For simplicity we discuss here the case of a paramagnetic system at zero temperature. It has first of all to be noted that from the definition given in eqn. (1.6), the functional $E_{xc}[\rho]$ must include a contribution coming from the true interacting kinetic energy functional $T[\rho]$, which is not reproduced by the non-interacting term $T_S[\rho]$ in the same equation. Moreover, the definition is given in terms of functionals which are only known to be unique, if they exist, via the HK theorem. The theorem itself is demonstrated through a *reductio ad absurdum* of the non-uniqueness hypothesis, and gives no insight into the structure of the functionals. The exact form of $E_{xc}[\rho]$ is up to date unknown, and is probably very complicated, while a large production of computational work based on DFT has been performed using approximated expressions to evaluate the functional.

The approximation which has so far been most widely used with (often surprisingly) good results, is the Local Density Approximation (LDA). Within LDA, it is assumed that the exchange and correlation energy is a function of position which depends only on the value of the particle density in that position, and is therefore a local property. The exchange and correlation functional is then evaluated as

$$E_{xc}[\rho] = \int d\boldsymbol{r}\, \epsilon_{xc}(\rho(\boldsymbol{r}))\rho(\boldsymbol{r}) \ , \tag{1.28}$$

where the function $\epsilon_{xc}(\rho)$ employed is the exchange and correlation energy for the uniform electron gas of density ρ. Given this expression, the exchange and correlation potential $V_{xc}(\boldsymbol{r})$ defined in eqn. (1.7) is also local, and corresponds to

$$V_{xc}(\boldsymbol{r}) = \mu(\rho(\boldsymbol{r})) \ ; \qquad \mu = \epsilon' \rho + \epsilon \ . \tag{1.29}$$

The analytic behaviour of $\epsilon(\rho)$ has been long ago determined in the limits of very high and very low densities. More recently its values for several densities in the intermediate region have also been determined by accurate Diffusion Monte Carlo simulations[3], so that a number of interpolation formulas are available to be used in the calculations[146]. The LDA approximation is by definition exact in the limit of very slowly varying charge density, and should in principle give reliable results *only* for such systems as nearly free-electron-gas metals. However, LDA is known to produce rather accurate results for systems where the ground state electronic density is far from being uniform, like atoms, molecules, semiconductor and ionic solids. A partial account of this success can be probably given by the fact that the LDA exchange and correlation function reproduces some exact features of the exact functional. For example it is possible to show[5] that the exact functional can be rigorously written as

$$E_{xc}[\rho] = \frac{e^2}{2} \int d\boldsymbol{r}\, d\boldsymbol{r}' \frac{\rho(\boldsymbol{r})\rho^h(\boldsymbol{r},\boldsymbol{r}')}{|\boldsymbol{r} - \boldsymbol{r}'|} \ , \tag{1.30}$$

where the function $\rho^h(\boldsymbol{r},\boldsymbol{r}')$ has to fulfill the screening sum rule

$$\int d\boldsymbol{r}' \rho^h(\boldsymbol{r},\boldsymbol{r}') = -1 \tag{1.31}$$

and can be pictorially thought to describe the exchange and correlation “hole”, or depletion, in the density expectation value in $\boldsymbol{r}'$ originating from the presence of an

electron in $\boldsymbol{r}$. The interaction between such a hole and the charge density of the system gives the total exchange and correlation energy value in eqn. (1.30). It is straightforward to expand the hole function in spherical harmonics and show that such value depends only on the zero (spherical) component $\rho_0^h(|\boldsymbol{r}-\boldsymbol{r}'|,\boldsymbol{r})$ of the expansion, all the contributions from the non spherical terms averaging to zero in the integral. So, in spite of the fact that the true exchange and correlation hole may be strongly asymmetric in most systems, it is only its spherical component that contributes to the total energy value.
The local density approximated hole function, which depends only on the density value in $\boldsymbol{r}$ and is spherical by symmetry:

$$\rho_{LDA}^h(|\boldsymbol{r}-\boldsymbol{r}'|,\boldsymbol{r}) = h_{LDA}(|\boldsymbol{r}-\boldsymbol{r}'|,\rho(\boldsymbol{r})) \tag{1.32}$$

has therefore the relevant structure for calculating the energy, while by comparison with an uniform electron gas of density $\rho(\boldsymbol{r})$ it still satisfies the constraint (1.31). The exchange and correlation energy is, in other words, calculated within the LDA in a way which is formally equivalent to summing the electrostatic Coulomb interaction between the self-consistent charge in each point and the correct amount of hole charge around it, although the hole charge radial distribution is an approximation of the unknown exact one.

1.5 The pseudopotential approximation.

The apparatus of Density Functional Theory provides in principle a way to deal computationally with any finite system of interacting fermions in a completely arbitrary local external potential, the only approximation involved being the recipe used to evaluate the exchange and correlation energy, as discussed in the former section. A natural kind of system for the computational applications is represented by atoms and molecules. The solution of a set of atomic KS equations is by far the simplest application, thanks to the enormous computational simplifications originating from the spherical symmetry of the self-consistent potential. The resulting atomic single-particle states, conveniently organised in shells and multiplets structure according to their energies and angular symmetries (in total similarity with the classic Hartree-Fock treatment), are the starting point for any further application connected with the study of polyatomic systems. The fast spatial oscillations of the inner states, obviously connected with their associated high kinetic energy, usually requires a representation based on some logarithmic (or equivalent) real-space mesh for solving the radial differential equations. Such representation is also required in the treatment of the higher states, due to their complicated core nodal structure imposed by the orthogonality to the low-lying states. Although no direct physical meaning can be attributed to these single-particle states within DFT, the only true physical quantity being the density calculated from them, most of the computational burden involved in their determination has to do with their detailed structure, in itself uninteresting, in the inner (core) real-space region closely surrounding the nucleus.

The passage from the atom to the simplest diatomic or polyatomic molecules brings in the computational problem of basis set representation, which becomes increasingly serious with the progressive loss of symmetry. At the same time, it becomes evident that only the outer electronic charge density of atoms actually participates in the formation of chemical bonds, while the core charge surrounding the nuclei maintains more or less exactly its size and shape while passing from the atomic to the molecular arrangement. From the point of view of a single-particle description, this is equivalent to the fact that the strongly localised core orbitals are rather insensitive to the external chemical environment, so that only the less bound and more extended *valence* orbitals are sensibly modified by the presence of neighbouring atoms. There are then strong computational and physical reasons to develop a procedure to exclude the core electrons from the calculations, since they are difficult to represent numerically and since they play a negligible part in the chemical behaviour of atoms. This clearly has to be achieved without losing a correct representation of the valence charge density chemical behaviour.

Ideally, a substitutive atomic "pseudo" potential, to be used in the calculations instead of the Coulomb potential, and whose full spectrum of states $\{\psi_i\}$ were perfectly coincident with the spectrum of the original atom starting from the first valence state, would be the solution to the technical problems connected with the core electrons, provided also that such an operator could display good "transferability" properties when performing calculations on the valence electrons in molecules or solids.

1.5.1 Pseudopotentials.

Various classes of pseudopotentials have been so far utilised in the practice of calculations, which can generally be regrouped in the two categories of (1) empirical pseudopotentials fitted to experimental data, and (2) "ab initio" pseudopotentials, whose construction is based on some exact theoretical justification, without referring to observed properties.

1.5.1.1 Empirical pseudopotentials.

In the construction of empirical pseudopotentials, observed data (usually, the atomic energy levels) are used to fit some simple analytic form for the pseudopotential[6]. The simplest models consist of a Coulomb potential for distances beyond a fixed "core" radius r_c:

$$V(r) = \begin{cases} -\frac{Ze}{r} & r > r_c \\ A & r \leq r_c\,. \end{cases} \tag{1.33}$$

Inside such radius the potential function is set to a constant A which does not necessarily match the potential at r_c to guarantee continuity (so that the second derivatives of the solutions are in general discontinuous). A possible choice for A is simply to set it equal to zero ("empty core potential"[7]), or to adjust it to a different value A_l for each angular momentum eigenvalue. An effectively non-local (angular momentum dependent) potential is in this last case introduced in the calculation, the term "non-local" (in a single-particle picture) meaning simply that the potential acting on the particle at the position $\boldsymbol{r}$ is not a function of the particle position only, but in general depends on other (and therefore "non-local") properties of the particle, such as its angular momentum.

Another approach is based on the direct fit of the atomic potential operator in the wave-number representation $V_a(\boldsymbol{G})$ to the experimental band structure. It is assumed that the crystal potential is a linear superposition of atomic potentials:

$$V(\boldsymbol{r}) = \sum_{\boldsymbol{G}} V_a(\boldsymbol{G}) S(\boldsymbol{G}) e^{i\boldsymbol{G} \cdot \boldsymbol{r}} \ . \tag{1.34}$$

This expression, in which the atomic positions enter through the structure factor $S(\boldsymbol{G})$, can be usefully implemented to solve the secular equation associated with the single-particle problem in a periodic crystal:

$$\left[-\frac{\hbar^2}{2m}\nabla^2 + V(\boldsymbol{r})\right] \phi_{n,\boldsymbol{k}}(\boldsymbol{r}) = \epsilon_n(\boldsymbol{k})\phi_{n,\boldsymbol{k}}(\boldsymbol{r}) \ , \tag{1.35}$$

to give as output the energy band structure $\epsilon_n(\boldsymbol{k})$ and the eigenfunctions $\phi_{n,\boldsymbol{k}}(\boldsymbol{r})$ in the Bloch form. If the function $V_a(\boldsymbol{G})$ is fast-decaying (*i.e.* if its real-space Fourier Transform is relatively smooth), very few coefficients on the reciprocal lattice expansion will be significantly different from zero. Such coefficients can easily be optimised through a self-consistent procedure in which their values are updated up to the best fit between the output band structure and the experimental data.

This approach, known as "Empirical Pseudopotential Method", provides surprisingly good results in describing the band structure of semiconductors and simple metals. Moreover, the idea of constructing a smooth model potential can be combined with the analytic requirement of the correct Coulomb tail, typical of forms such as (1.33), to provide parametrised potentials to be fitted again to experimental data by a self-consistent procedure. Using the electronic charge distribution obtained from the pseudo-wavefunctions, it is possible to unscreen such potentials from the Hartree and exchange-correlation contributions, to get atomic pseudopotentials which can assumed to be transferable. Such potentials can then be used in the calculations for atomic geometries such as surfaces, where the Fourier expansion coefficients of the full potential are known *not* to be negligible after the first few G-vectors, and where therefore the screening potential has to be calculated with some self-consistent procedure such as the one described in Section 1.2.

1.5.1.2 First-principles pseudopotentials.

A brief discussion about the properties and the construction of "ab initio" pseudopotentials can usefully start from some considerations originally developed within the framework of the Orthogonalised-Plane-Wave (OPW) method for band structures[8]. One of the essential properties of a true valence wavefunction ψ is its orthogonality to the underlying core states ϕ_c. An OPW wavefunction is expressed as the sum of a smooth wavefunction ϕ and a sum over the occupied core states ϕ_c. From the orthogonality condition one gets:

$$\psi = \phi - \sum_c < \phi_c | \phi > \phi_c \tag{1.36}$$

Substituting this expression into the Schrödinger equation $H\psi = E\psi$ it is easy to show that also is

$$[H + V_{PS}]\phi = E\phi \tag{1.37}$$

with the "orthogonality" potential V_{PS} defined as

$$V_{PS}\phi = \sum_c (E - \epsilon_c) < \phi_c | \phi > \phi_c \; . \tag{1.38}$$

This potential added to the true crystal potential in the hamiltonian $\hat{H}$ of eqn. (1.37) forms an "exact" pseudopotential[9], which reproduces the correct valence eigenvalue E. Any solution ϕ is a smooth function which may be represented by a fast-converging expansion of plane waves. It should be noted that given the angular symmetry of the core states, the non-local potential can be naturally decomposed into a sum of projections over all the angular momentum components present in the core:

$$V_{PS} = V_s\hat{P}_s + V_p\hat{P}_p + V_d\hat{P}_d + ... \tag{1.39}$$

Each projection V_l includes the repulsive effect originating from the constraint of orthogonality to the core states of symmetry l. The degree of localisation of the pseudowavefunctions is therefore much sensitive to the presence or not in the core of lower-lying electrons of the same angular symmetry (so that for example p pseudo-orbitals in second row elements like carbon or oxygen are expected to be much more contracted on the atomic nucleus than the third row correspondent elements silicon and sulphur). The potential (1.38) is short-ranged, being by definition zero in the region outside the atomic core. In such domain clearly ϕ and ψ are solutions of the same differential equation, so that the "pseudofunction" ϕ may be said to well represent the true solution ψ in the valence region. It shold be pointed out that there is a difference in the normalisation of the two functions: if $<\psi|\psi>= 1$ then must be $<\phi|\phi>= 1+\sum_c |<\phi_c|\phi>|^2$, *i.e.* the smooth solution ϕ is not normalised, or alternatively if normalised puts too much charge in the core region and too little in the valence region. In self-consistent calculations this charge shift can in principle be corrected before calculating the charge distribution, through direct orthogonalisation of ϕ to the core states, although this would be much time consuming in the calculations, so that the advantages of using a pseudopotential would be partially lost. Pseudopotential operators leading to pseudowavefunctions with a built-in norm conservation (that is to say leading to single-particle eigenstates which when normalised distribute correctly the charge between core and valence regions, therefore coinciding exactly with the all-electron eigenfunctions outside a chosen core radius) are therefore much more convenient to use.

1.5.2 Norm-conserving pseudopotentials.

For any solution regular at the origin (not necessarily an eigenstate) of the radial atomic Schrödinger equation, the following identity holds (atomic units):

$$-\left[r^2\phi^2\frac{d}{d\epsilon}\frac{d}{dr}\log\phi\right]_R = 2\int_0^R r^2\phi^2 dr \ , \qquad (1.40)$$

for any fixed radius R. It is also possible to relate the radial logarithmic derivative in the left term of this equation to the phase shifts which describe the potential scattering properties, so that for two different potentials leading to solutions which coincide for $r \geq R$ at some given energies, the scattering properties at close energy values will vary in the same way to leading order. A norm-conserving pseudopotential is by construction reproducing the all-electron eigenvalues, and the corresponding eigenstates beyond a chosen core radius. From what said, it must therefore share with the all-electron potential also the scattering properties within first order in the valence eigenvalues shifts when the potential is transferred to chemical environments other than the isolated atom. Although this does not imply any *exact* transferability property, the errors from the pseudopotential approximation involved here are very often negligible when compared with errors originating from other sources, such as the approximations adopted in the underlying single-particle theory (*e.g.* the LDA in DFT, or the neglect of correlation in pure Hartree-Fock).

A detailed account on the possible construction techniques to generate effective norm-conserving pseudopotentials is beyond our scope here, while more will be said in a forthcoming chapter about some recent techniques to optimise other pseudopotential characteristics than the norm-conservation property. We will therefore only sketch a standard construction procedure (the one originally followed by Bachelet *et al.*[11] after the introduction of the norm-conservation scheme by Hamann *et al.*[10]), suitable for DFT-LDA-based total energy calculations in solid state, of the kind performed in the present work.

A non-local "pseudo" potential is needed for reproducing a certain valence electrons configuration, not necessarily the ground state. An all-electron self-consistent calculation is firstly performed to generate a KS potential in this chosen configuration. The potential is then matched to a parametrised smooth function within a certain "core" radius r_c, and the parameters (if more than one) are adjusted to reproduce the correct eigenvalue for its first eigenstate of the chosen angular symmetry. Such eigenstate is coincident with the correspondent all-electron state outside r_c, and can be modified inside the core radius to get a smooth (nodeless) normalised state. Direct inversion of the Schrödinger equation provides then the necessary (small) correction to modify the pseudopotential accordingly. Finally, the potential is unscreened from the Hartree and exchange-correlation contributions arising from the pseudo-valence charge, which leaves it in its final form.

The solution of the all-electron problems for heavy atoms normally requires a relativistic treatment, *i.e.* the description of the deep core multiplets within the Dirac's formalism, implicitly including the spin-orbit interaction. Weighted averages of the self-consistent potentials obtained for $l = 1, 2, 3$ at various values j of the total angular momentum have therefore to be taken for producing a pseudopotential which can be consistently implemented in a non-relativistic calculation.

Norm-conserving pseudopotentials constructed in this way perform typically very well in DFT-LDA total energy calculations, leading to predicted values for lattice constants, bulk moduli and elastic constants, cohesive energies, and phonon frequencies which are in agreement within a few percent with experiment. The pseudopotential single-particle band energies are typically in agreement with the all-electron values within few hundredths of an eV.

2 Computational techniques.

2.1 Introduction.

In this chapter an outline of the computational techniques utilised in the present work is given. The solution approach to the Kohn-Sham problem through the conjugate gradients global minimisation of the total energy functional is presented and discussed. Two different procedures for accomplishing the minimisation are described. The pseudopotential representation in the plane-waves formalism is discussed, together with the problem of obtaining a transferable pseudopotential well optimised for convergence with respect to energy cutoff. The non-linear core correction to the exchange and correlation potential is discussed. The problems related to the treatment of metals in total energy calculations are discussed and the subspace rotation and smearing techniques utilised in the calculations for improving the efficiency of the Brillouin Zone (BZ) sampling are presented.

2.2 Conjugate gradients minimisation of the energy functional.

In this section we discuss the problem of performing a direct minimisation of the DFT energy functional, some reasons to adopt minimisation techniques based on the evaluation of energy "gradients" with respect to the electronic expansion coefficients on the plane-waves (PW) basis set, and the conjugate gradients technique for performing non-linear minimisations.

2.2.1 Direct functional minimisation in the PW representation.

We have shown in the former chapter how the problem of finding the true minimum of the DFT energy functional (1.6), corresponding to a system of interacting electrons, can be reduced to the problem of determining the self-consistent solution of a set of single-particle equations (1.9) for a non-interacting electron gas immersed in an effective potential. The self-consistent electron density extracted from such procedure is by construction a minimum (or at least a point of null first order variation) of the interacting electrons problem. We want now to illustrate how a direct global minimisation of the energy functional can be performed without explicitly solving a KS set of equations (*i.e.* the correspondent secular problem).

The electron density can be here expressed again, as in eqn.(1.10), as the sum of squared moduli of normalised single particle functions

$$\rho(\boldsymbol{r}) = \sum_{i=1}^{N} |\phi_i(\boldsymbol{r})|^2 \, . \tag{2.1}$$

By *imposing* mutual orthogonality between different orbitals ($< \phi_i|\phi_j >= \delta_{ij}$) and then varying the orbitals under such constraint to minimise the total energy functional (written as in eqn. (1.6), with the kinetic contribution defined as in (1.11)), it is easily shown that the charge density obtained at the minimum coincides with the one obtained from the solution of the KS equations in the self-consistent screening potential. Therefore from Section (1.2) we can conclude that such minimum procedure also leads to the true minimum of the energy functional, independently from the representation of the density as a sum of orbitals implied by eqn. (2.1), while the total energy at the minimum can still be calculated in the normal way through the orbitals matrix elements.

The traditional self-consistent eigenvalue problem of inverting the hamiltonian matrix to solve the KS equations is therefore perfectly equivalent to the problem of performing a constrained search of the global minimum in the domain of the expansion coefficients representing the single particle orbitals on the chosen basis set. The basis set most largely utilised for total energy calculations in solid state, including all the calculations presented in the present work, is the plane waves one. Since the calculations are performed using periodic boundary conditions, the single-particle orbitals representing the electron states can be written as Bloch expansions on the reciprocal space G-vector basis set

$$\psi_{\boldsymbol{k}}(\boldsymbol{r}) = e^{i\boldsymbol{k}\cdot\boldsymbol{r}} \sum_{\boldsymbol{G}} a_{\boldsymbol{k},\,\boldsymbol{G}}\, e^{i\boldsymbol{G}\cdot\boldsymbol{r}} \tag{2.2}$$

for any given BZ vector $\boldsymbol{k}$. The dimension of the basis set depends on the size of the system, and on the energy cutoff assumed for the PW kinetic energy. In any case, the truncation of the PW basis set will lead to an error in the value of the computed total energy. It is, however, possible to monitor and reduce such error by progressively increasing (not always necessarily up to full convergence) the value of the cutoff utilised. Provided that this cutoff issue is under control, the PW basis set representation has the advantage of being unbiased, since it is not necessary to modify and tune it for the particular system under examination, as it is instead customary when employing localised basis sets. Moreover, the expression for the total electronic kinetic energy in the PW representation assumes the very simple diagonal form (atomic units)

$$E_K = \sum_{\boldsymbol{k},G,i} \omega_{\boldsymbol{k}} \left|a_{\boldsymbol{k},i,\boldsymbol{G}}\right|^2 \frac{G^2}{2} \tag{2.3}$$

for the given set of BZ sampling points and weights $\{\boldsymbol{k}, \omega_{\boldsymbol{k}}\}$ utilised (the subscript i is the band index for each k-point), and in such form can be economically and straightforwardly calculated.

Systems having low translational symmetry and requiring an high cutoff treatment are the hardest to deal with computationally, since large amounts of processing time and computer memory are necessary to operate with all the electronic orbitals present in the calculation, while the algorithm employed must be well balanced to deal efficiently with the minimisation problem when the basis set spans a very large energy interval. In the present work various systems of isolated defects have been studied, still adopting the periodic boundary conditions approach, with increasingly large repeating "supercells" surrounding the defects, and either with the need of a large number of orbitals to deal with the problem of BZ sampling in metals, or with the need of an explicit high cutoff treatment to deal with ceramic materials containing oxygen.

The typical basis sets utilised can count up to 20,000 plane waves, with a number of electrons in the system of the order of one hundred. For these large basis dimensions, evaluating and storing a full Kohn-Sham hamiltonian matrix would be highly inefficient (if not impossible) because of the prohibitive memory requirements, so that some alternative and less memory-intensive technique has to be used. While some techniques for efficient iterative matrix inversion have been available for some time[18], it is only recently that the direct density functional minimisation approach adopted in this work has been proposed [16][17],[19] and has entered in the practice of ab initio calculations.

2.2.2 Energy minimisation techniques for total energy calculations.

The problem of minimising a non-linear function within a parameter domain of large dimensionality is a traditionally difficult one[12]. Some stochastic procedures like the simulated annealing search are available, which are almost guaranteed to provide the absolute minimum of the function considered without the risk of the algorithm getting stuck in a local minimum. Moreover, they only require a sampling of the function considered, and being based on a random-walk search in the given parametric domain, the computer time required is formally independent from the dimensionality of the search domain itself. These methods, however, are more convenient than less robust ones only when the function considered is known to display several concurrent minima, the lowest of which has to be identified, and when the parameters in question are highly correlated and have a dishomogeneous "meaning" as variables of the function to be minimised.

The DFT energy functional as a function of the coefficients $a_{\mathbf{k},i,\mathbf{G}}$ displays normally a unique and well identified minimum, while the values of the parameters at the minimum, being the Fourier coefficients of the ground state KS orbitals, display a "smooth" behaviour with varying G, so that the functional variation when varying the coefficients of G-vectors close to each other (for example: in the high cutoff region, dominated by the kinetic contribution) is expected to be homogeneous. Because of these characteristics, a minimum search technique which relies on analytic information such as the functional derivatives with respect to the coefficients, and which is known to fast-converge in the quadratic region surrounding the minimum in the coefficients space, is expected to be the best suited for the problem under consideration.

Writing the functional for the electronic problem in the ionic field V_0 (in atomic units, dropping here, for simplicity, the k-point index) as

$$E_{V_0}[\{\psi_i\}] = \sum_i < \psi_i | -\frac{1}{2}\nabla^2 | \psi_i > \; + E_{xc}[\rho] \; + \frac{1}{2}\int \frac{\rho(\boldsymbol{r})\rho(\boldsymbol{r}')}{|\boldsymbol{r} - \boldsymbol{r}'|} d\boldsymbol{r}\, d\boldsymbol{r}' \; + \int V_0(\boldsymbol{r})\rho(\boldsymbol{r}) d\boldsymbol{r} \;, \tag{2.4}$$

and formally taking the partial derivatives with respect to the complex conjugate coefficients $a^{\dagger}_{i,G}$ (or equivalently, with respect to the bra orbital $< \psi_i|$), one gets the expression for the energy derivative ("force" on the orbital i):

$$F_i = -[\hat{T} + \hat{V}]\ |\psi_i >= \begin{pmatrix} -\frac{\partial E}{\partial a^{\dagger}_{i,G_1}} \\ \vdots \\ -\frac{\partial E}{\partial a^{\dagger}_{i,G_{N_{plw}}}} \end{pmatrix} \tag{2.5}$$

as an array with the same dimension N_{plw} of the PW basis set, defining the direction of maximum energy decrease in the subset of the i-th orbital plane waves coefficients. The direction is simply obtained applying the self-consistent hamiltonian $\hat{H}$ ($\hat{V}$ is the same as in eqn. (1.7)) to the orbital considered.

The gradient defined by eqn. (2.5) can be used to construct a direct minimisation algorithm for the total energy functional, simply performing a line search along its direction for each orbital. Provided that all the orbitals are updated in some order, and that the orthogonality constraint between orbitals is maintained, it does not matter in line of principle which exact sequence of band gradient evaluations, line minimisations, and orthonormalisations is adopted. An immediate possible strategy is to evaluate the gradients F_i for all the orbitals, therefore constructing a global gradient

$$\mathcal{F} = \begin{pmatrix} F_1 \\ \vdots \\ F_{N_{orb}} \end{pmatrix} \tag{2.6}$$

and minimising the functional along the line which such vector defines in the $N_{plw}N_{orb}$-dimensional space of the wavefunctions coefficients. It should be noted that outside convergence the single particle orbitals to be updated are *not* yet eigenstates of the self-consistent hamiltonian operator (the one calculated with the charge density obtained from those orbitals). More precisely, they cannot be transformed into eigenstates through a unitary transformation within the Hilbert space which they define[1]. The normalised updated orbitals

$$\psi_i' = \frac{1}{\sqrt{1+\alpha^2}} \left(\psi_i + \alpha \frac{F_i}{|F_i|}\right) \tag{2.7}$$

are therefore not orthogonal to each other, and some orthogonalisation strategy must be applied. (On the other hand when the convergence is nearly reached the orbitals approximate increasingly better, still within a unitary transformation, the lowest set of eigenstates of the self-consistent hamiltonian.)

In any case a line search direction defined by gradients should span an ensemble of *orthonormal* sets $\{\psi_{i,\alpha}'\}$ varying the line coordinate α, and to achieve this orthogonality constraints have to be applied to the gradient expressions (2.5).

If all the bands are updated simultaneously as in (2.7), by imposing to the gradient F_i the condition

$$< F_i|\psi_j >= 0 \; ; \; j = 1, N_{orb} \tag{2.8}$$

we obtain a set of trial states $\{\psi_{i,\alpha}'\}$ which are mutually orthogonal only within first order in α, so that an exact orthogonalisation has to be performed before evaluating (self-consistently) the energy functional on each point along the line.

If the bands are instead updated one by one, the condition (2.8) on the direction of search F_i ensures *exact* orthogonality. There are both memory and computer-time

---

[1] Such transformation would not, of course, change the value of the functional (2.4).

reasons for which the second strategy (*i.e.* updating the bands one by one) is more efficient for the study of systems of large size. For relatively small sizes (some tens of atoms) the calculations are less dominated by the orthogonalisation procedure, and other considerations influence the choice of the optimal algorithm. In the present work both strategies have been applied, and the relative procedures will be both described and discussed in Section 2.3.

Before any further analysis of the global structure of the constrained total energy minimisation, it should be noted that the search directions along which the orbitals are updated do not have to coincide with the energy gradient of eqn. (2.5) as done in equation (2.7). The search directions actually used in all the calculations of the present work were constructed with the "conjugate gradients" technique, described in the next section.

2.2.3 Conjugate gradients techniques.

We discuss here briefly the conjugate gradients (CG) minimisation algorithm[13][14]. For simplicity, we do not include considerations regarding the orthonormality of electron states, or the self-consistent nature of the functional which has to be minimised. All the considerations in this section can be thought as referring to the total energy minimisation for a single particle in a fixed external potential, or equally well to a general multi-dimensional minimum search problem.

Given a function $E[\{a_G\}]$ whose value is determined by a N-dimensional set of parameters $\{a_G\}$ $G = 1, 2, .., N$, and provided that for a given set of parameters the values of the function and of its gradient vector $F = -\partial E / \partial a_G$ are both known, the simplest minimisation technique implies a search along the gradient direction to identify the relative line minimum. Once this is achieved, the new gradient is evaluated at the minimum point, and another line search is started. This procedure is known as "steepest descent" algorithm[12][15], and the value of E is guaranteed to decrease at each minimisation. Note that any gradient is bound to be orthogonal to the preceding one, since it must have null projection on the direction of the old line search on whose minimum it has been evaluated. Also note that this orthogonality relation is satisfied for successive gradients *only*, and that no memory of the minimisation directions before the last one is in fact included at each iterative step in the current search direction. It is easy to construct examples of functions E for which this "short memory" problem of the steepest descent algorithm is responsible for an highly inefficient minimisation path. Consider the example in two dimensions of a long narrow valley with steep walls in one direction, and a much more shallow minimum in the orthogonal direction. A steepest descent path will include many steps along gradients whose components along the steepest direction have alternate sign. Even a simple quadratic form like $E = \alpha a_1^2 + \beta a_2^2$, $\alpha, \beta > 0$ will take several iterations for the minimum to be reached if $\alpha << \beta$, successive gradients having alternate sign on the direction of the minimisation variable a_2. Clearly a more effective strategy for determining the search direction should inhibit such oscillatory behaviour, for example by *summing* at each step to the current gradient a small contribution of the last (and orthogonal) search direction:

$$S_n = F_n + \alpha_n S_{n-1} \ . \tag{2.9}$$

Here S_n is the search direction at iteration n, and F_n is the relative gradient. A minimisation strategy of this kind, when completed by the definitions:

$$S_1 = F_1 \ , \qquad \alpha = \frac{|F_n|^2}{|F_{n-1}|^2} \ , \tag{2.10}$$

is called "conjugate gradients"[13] technique, and leads to a far more efficient minimisation path. It can be proven that for a N-dimensional quadratic form the method reaches the absolute minimum after N conjugate gradients steps only, the N associated gradient directions being all mutually orthogonal[2]. Therefore near an isolated minimum of a non-pathological function, where the second order expansion terms give the leading contributions to the function's value, the conjugate gradients technique is guaranteed to reach the minimum in a reasonably controlled number of steps using the

---

[2] The recipe for α in order for the algorithm to have this property is not unique: see for example reference [12].

function's gradients only, and no more than two of them at the same time. This clearly eliminates the necessity of ever storing an amount of information corresponding to the full Hessian matrix of second partial derivatives of the function at the minimum.

In the domain regions far away from the minimum, the function to be minimised is not in general approximately quadratic, so that the argument above concerning the *maximum* amount of gradient steps to reach the minimum does not hold if the minimisation procedures begins from an arbitrary starting point, for example chosen at random. Moreover, when the number of parameters is very large, such property is of no help, the algorithm being expected anyway to determine the function's minimum in much less than N steps.

Finally, it should be noted that so far we have discussed the efficiency of a technique for choosing search directions in a parameter space, while the overall efficiency of the algorithm has to be discussed in terms of the global computing resources for reaching the function's minimum. The cost of a multi-dimensional minimisation depends on how many times the function to be minimised and its gradient have to be evaluated. Performing the minimisation along the direction determined by eqn. (2.9) implies some function evaluations, and is in itself time consuming. Different strategies for performing the line minimisation have been adopted in this work, and will be discussed in the next section.

We only mention here that when using a search direction technique like the conjugate gradients one, based at each iteration on the local properties of the function, it is always possible to restart the algorithm at some intermediate point from a steepest descent step. This in turn permits to tune the computational effort spent in line minimisations: such effort can be lowered and the minimisation made much faster allowing for some error in the detection of the minimum. The building up of these errors would eventually lead the CG algorithm to select less and less efficient search directions. Restarting the algorithm from time to time forbids any propagation of errors to the whole descent path, the overall procedure resulting fast and robust without loosing its essential simplicity.

2.3 Total energy minimisation schemes.

In the present section we describe in more detail some features of the two minimisation schemes utilised throughout the present work, corresponding to two separate computer codes of independent origin and different structure, which have been used to perform the calculations described in the next chapters.

The first has been explicitly designed (Gillan, 1989 [17]) for studying the energetics of medium sized metal systems, and performs the task of minimising a total free energy functional of the kind discussed in Section 1.3 . Its main features are connected with the finite temperature formalism which it uses. This formalism requires to deal efficiently with fractionally occupied orbitals, while permitting us to keep under technical control the problems arising from the metal discontinuities at the Fermi level. The scheme has been used in the present work to perform calculations on the energetics of defects and impurity systems in aluminium host.

The second scheme (Teter *et al.*, 1989 [19]) has been developed for large scale calculations on semiconducting and insulating materials, and performs the minimisation of the DFT energy functional using a band-by-band technique which reduces to the minimum the amount of memory storage required.

While the target physical systems and the general architecture of the first scheme make it suitable for a vectorial (Cray-like) supercomputer, the features of the second scheme make possible its implementation on a parallel computer, provided that a parallelisation strategy is designed in the most compatible way with the program tasks and purposes. The calculations on ceramic insulators described in the present work have all been performed on a parallel supercomputing device (a 64-nodes Meiko Computing Surface, in Edinburgh University). A description of some relevant technical features of the two calculation strategies is given hereafter.

2.3.1 Calculation features, first strategy.

The starting point of a self-consistent energy minimisation run consists of a full initial set of electronic orbitals $\{\phi_i^0\}$. In this scheme such set is generated by solving the KS eigenvalues problem in the fixed screening potential derived by the superposition of atomic densities, considering only the plane wave components up to some small cutoff (two or three Ry). Along the minimisation, the conjugate gradients (initially: steepest descent) directions are recursively used to lower the total free energy updating each time the "current" set of orbitals $\{\phi_i^n\}$.

At each step the "force" gradient on the electronic degrees of freedom is evaluated as in eqn. (2.6) from the self-consistent hamiltonian generated with such orbitals. For each BZ vector $\boldsymbol{k}$ each gradient F_i has components both in the "parallel" Hilbert space spanned by the $\{\phi^n_{\boldsymbol{k},i}\}$ and in the "orthogonal" space of wavefunctions which are not linear combinations of them.

2.3.1.1 Minimisation within the parallel subspace.

For total energy calculations on semiconducting and insulating materials, in which no fractional band occupation is needed, we could just ignore any band updating within the parallel subspace, which would correspond to a unitary rotation leaving the ground state density (and therefore the energy functional) unchanged.

Introducing the fractional occupation of orbitals we also introduce the possibility of changing the charge density when rotating the orbitals and re-computing their occupation numbers accordingly to their new energy expectation values. This can obviously lower the value of the total energy. At each iteration n, the relevant object taking part in this procedure is the Hamiltonian matrix

$$h_{\boldsymbol{k},i,j} = < \psi^n_{\boldsymbol{k},i} | \hat{H} | \psi^n_{\boldsymbol{k},j} > \qquad\qquad i,j = 1,..,N_{orb} \,, \qquad (2.11)$$

the elements of which are easily calculated as a subproduct of the gradient evaluation (2.5). Such matrix is *not* diagonal out of convergence, and being of a comparatively small size it could for example be directly diagonalised. However, this would *not* give any evident advantage towards the final goal of reaching the global eigenfunctions set, since the diagonalisation (i) would take place within a Hilbert subspace being still not the ground state one, and (ii) would not be done self-consistently[3], and therefore it could lead to an *increase* of the total energy when the energy is calculated self-consistently after the subspace rotation.

The procedure which we have applied to update the wavefunctions within the parallel subspace is designed[17] to guarantee that the total energy decreases, as an alternative way to the conjugate gradients technique to define the search direction. If the parallel displacement of the wavevectors is written as

$$\delta_{\|}\psi_{\boldsymbol{k},i}(\boldsymbol{r}) \; = \; \alpha \sum_{i} W_{\boldsymbol{k},i,j} \psi_{\boldsymbol{k},j}(\boldsymbol{r}) \; , \tag{2.12}$$

and imposing to the matrix W to be anti-Hermitian in order to preserve the orthonormality of orbitals within first order in α, a condition to ensure the energy decrease for small positive values of α writes

$$\sum_{i,j} h_{\boldsymbol{k},i,j} W_{\boldsymbol{k},i,j} (f_{\boldsymbol{k},i} - f_{\boldsymbol{k},j}) \; < \; 0 \; , \tag{2.13}$$

where the $f_{\boldsymbol{k},i}$ are as usual the orbital occupation numbers. We write the coefficients $W_{\boldsymbol{k},i,j}$ at each sampling point $\boldsymbol{k}$, as[4]:

$$W_{\boldsymbol{k},i,j} = \frac{\xi_{i,j} h_{\boldsymbol{k},j,i}}{(h_{\boldsymbol{k},i,i} - h_{\boldsymbol{k},j,j})} \qquad i \neq j \tag{2.14}$$

and then define a symmetric matrix $\xi_{i,j}$ which set to be the unit matrix would make the (2.14) correspond to the first order perturbation matrix for obtaining the eigenstates of $h_{\boldsymbol{k},i,j}$. In some cases during the run a "wrong" ordering of occupancies given the calculated expectation values can occur, *i.e.* when the inequalities $f_i < f_j$ and $h_{i,i} < h_{j,j}$

---

[3] Sometimes a "charge slosh" behaviour is observed when diagonalising this matrix, when high-lying eigenstates which are equivalent by symmetry have different eigenvalues due to lack of self-consistency, so that their occupation numbers oscillate.

[4] Note that the diagonal matrix elements must be zero and do not need to be defined.

hold simultaneously for some couple of indexes i, j.[5] By imposing $\xi_{i,j} = 0$ in all these cases the condition 2.13 is always satisfied. Moreover, when necessary we lower the value of $\xi_{i,j}$ to satisfy for each matrix element the inequality

$$|W_{\boldsymbol{k},i,j}| < \epsilon \tag{2.15}$$

where the maximum value ϵ (normally put equal to 0.2) has the scope to keep the matrix elements within the limits where perturbation theory is valid. The value of $\xi_{i,j}$ is otherwise always set equal to one.

2.3.1.2 Minimisation within the orthogonal subspace.

The orthogonal subspace is the Hilbert space of the states generated by the PW basis set which are orthogonal to the current set of wavefunctions $\{\psi^n_{\boldsymbol{k},i}\}$. The search direction to minimise the energy functional in this space is determined with the conjugate gradients technique. The orthogonality constraint is then applied on the search direction. Starting from the expression for $S^n_{\boldsymbol{k},i,\boldsymbol{G}}$ obtained from eqn. (2.9) for the i-th orbital at the sampling point $\boldsymbol{k}$, we project the search direction onto the orthogonal (or "tangent" to the constraint) manifold, rewriting it as:

$$\overline{S^n}_{\boldsymbol{k},i} = S^n_{\boldsymbol{k},i,\boldsymbol{G}} - \frac{1}{2} \sum_{j,\boldsymbol{G}'} \{S^n_{\boldsymbol{k},i,\boldsymbol{G}'} a^{n\dagger}_{\boldsymbol{k},j,\boldsymbol{G}'} + a^n_{\boldsymbol{k},i,\boldsymbol{G}'} S^{n\dagger}_{\boldsymbol{k},j,\boldsymbol{G}'}\} a^n_{\boldsymbol{k},j,\boldsymbol{G}} , \tag{2.16}$$

where like in eqn. (2.2) the $a^n_{\boldsymbol{k},i,\boldsymbol{G}}$ are the orbital expansion coefficients at the minimisation step n. Formula (2.16) provides a search direction S^n along which the updated wavefunctions given by

$$a^{n+1}_{\boldsymbol{k},i,\boldsymbol{G}'} = a^n_{\boldsymbol{k},i,\boldsymbol{G}'} + \beta^n \overline{S^n}_{\boldsymbol{k},i,\boldsymbol{G}} \tag{2.17}$$

are still mutually orthonormal within first order in β^n.

---

[5] The reason is that the occupation numbers themselves are treated as minimisation variables, and are recursively updated before reaching the Fermi-Dirac distribution at self-consistency. If we *imposed* the Fermi-Dirac distribution, the "right" ordering would be obviously automatically satisfied.

2.3.1.3 Minimisation with respect to the occupation numbers.

Once the search directions in both the parallel and the orthogonal subspaces have been determined, all is needed to define completely a global minimisation direction is a strategy for varying the occupation numbers $f^n_{\boldsymbol{k},i}$. It should be noted that during the run the wavefunctions are expected converge to the correct KS eigenstates because of the successive "first order" rotations in the parallel subspace (as it can be easily verified checking the size of the off-diagonal matrix elements (2.11)). The final statistical distribution of the occupation numbers is known to be Fermi-Dirac-like at the minimum of the free energy functional (1.27).

A very simple strategy has been applied for the updating of the $f^n_{\boldsymbol{k},i}$: at each iteration n, using the energy expectation values $h_{\boldsymbol{k},i,i}$ and the Fermi-Dirac expression (1.21) we calculate new values for the orbital occupations which can be written as $f^{n+1}_{\boldsymbol{k},i} = f^n_{\boldsymbol{k},i} + \Delta f^n_{\boldsymbol{k},i}$. Again this establishes a search direction $\Delta f^n_{\boldsymbol{k},i}$ in the space of the occupation degrees of freedom, along which a minimisation search can be performed calculating the occupations as

$$f^{n+1}_{\boldsymbol{k},i} = f^n_{\boldsymbol{k},i} + \gamma^n \Delta f^n_{\boldsymbol{k},i} \, . \tag{2.18}$$

at positive values of the line variable γ^n. It can be shown that the free energy is guaranteed to be reduced for some positive value of γ^n.

It will be shown in Section (2.5) that the the zero-temperature ground state energy of the electronic system can be calculated from the minimum value of the free energy functional independently of the details of the distribution of the coefficients $\{f_{\boldsymbol{k},i}\}$ at the minimum, so that the smearing of the Fermi Surface can in practice be performed using other occupation functions than the Fermi-Dirac distribution.

2.3.1.4 Line minimisation.

Once the global search direction has been completely specified with respect to the orbital occupation variables and the plane wave coefficients both in the parallel and in the orthogonal subspaces, the following step consists in the minimisation along the line spanned by the three associated line variables $\{\alpha^n, \beta^n, \gamma^n\}$.

The asymptotic value for the parameter γ in eqn. (2.18) can be assumed to be equal to one, provided that the unnormalised vector $\Delta f^n_{\boldsymbol{k},i}$ is used as search direction. Analogously, the asymptotic value of the parameter α in eqn. (2.14) using as a search direction the unnormalised vector $\sum_i W_{\boldsymbol{k},i,j} \psi_{\boldsymbol{k},j}(\boldsymbol{r})$ corresponds to unity, while the actual displacement connected with the subspace rotation becomes infinitesimal as the orbitals approach the self-consistent KS set. The values for parameters α and γ at the beginning of a new minimisation step are therefore both set to one. Experience shows that the search in the orthogonal subspace is the slowest (and most system-sensitive) component of the whole minimisation process to reach convergence, and is also the one to be accounted for almost all the energy lowering obtained in a minimisation step. To provide a trial value for the displacement parameter β (eqn.(2.17)) on the *normalised* search direction $S_{\boldsymbol{k},i,G}$ it is therefore sufficient to estimate the amount of energy decrease expected from the whole present minimisation step.

A reasonable way to do this is to assume some simple golden-ratio rule for the expected energy lowering, based on the experience on the convergence properties of the algorithm on the class of systems investigated. Given that at the current point in the minimisation path both the total free energy and its gradient are known, an expected energy gain provides the third numerical value for a simple parabolic fit which is used to extrapolate the position of the minimum along the search line, so to fix the value of the parameter β. At this point a trial displacement is defined, and a check on the orthogonality of the updated states is performed to confirm that the displaced orbitals are orthogonal within first order, as they should by construction from what said so far. If the trial states are *not* orthogonal within first order (*i.e.* within 10-20%) the extrapolation is reduced halving the values of the line variables $\{\alpha^n, \beta^n, \gamma^n\}$, and the test is repeated *before* any time-consuming energy evaluation is performed. When the condition is satisfied the states are eventually orthonormalised *exactly* through a Gram-Schmidt procedure, to obtain the trial set of states for the new energy evaluation.

Once the new total free energy has been calculated, its value is used to check on the efficiency of the extrapolation. The free energy decrease obtained from the calculation is compared with its extrapolated linear decrease ΔF_{lin}, calculated as the product of the gradients and the displacements for all the minimisation variables. If the calculated energy decrease is too small (less than 10% of ΔF_{lin}, in cases of overestimation of the minimum position) or too large (more than 90% of ΔF_{lin}, when the minimum position is underestimated and the decrease is almost linear) the displacement is rejected. The rejected value is however used for a new parabolic fit (this time not biased by a guess on the expected energy lowering) and a new minimum position is estimated.

This calculation procedure produces typically a 50% of rejections: fifteen total energy evaluations are in other words usually needed for every ten accepted conjugate gradients step, the first-guess minimum point usually being good enough half of the times. This good acceptance rate is a consequence of the quadratic shape of the free energy functional close to its absolute minimum, where most of the time is spent in the calculations. Such shape is what we assume when adopting the parabolic extrapolation.

It should be noted that the procedure described (i) allows to save computer time with respect to other line search algorithms which evaluate systematically at least one extra point besides the starting one before fitting the minimum position, and (ii) is always guaranteed to decrease the total energy, which is always evaluated self-consistently[6].

Its most obvious drawbacks are its loss of efficiency far away from the minimum (for example if we wanted to start the calculations from *random* wavefunctions) and its large use of orthogonalisations between orbitals when tuning up the displacement. For extremely large physical systems, in spite of the Gram-Schmidt procedure being highly vectorisable on most computers, the orthogonalisation of orbitals would became by far the most cpu-intensive operation, and the procedure described would eventually have to be abandoned. This is *not* the case for the physical systems on which this procedure was used in the present work, which go up to a maximum of 7000 plane waves per orbital in the biggest supercell (41 orbitals) studied, and for which the Fourier trans-

---

[6] For the description of a conjugate gradients scheme which is *not* evaluating the energy self-consistently while performing the line search, see [18].

formations between direct and reciprocal spaces are the leading operation in terms of computer time cost.

2.3.1.5 Relaxation of ionic position.

The relaxation of the ionic position within the fixed constraint of the supercell geometry represents the last (and somewhat independent) operation to be performed during the calculation when the goal is to determine the ground state energy of a relaxed atomic structure. Following the original ideal of Car and Parrinello[16], the total energy is minimised in the present technique with respect to *all* the variables (electronic and ionic in our case) at the same time, although the technique does not make use of annealed dynamics to reach the global minimum values for such variables. As in the case of the electronic orbitals, a single well defined minimum is expected, the systems investigated having in all cases a high degree of symmetry. Moreover, since we look for the global minimum of the free energy, and since we are *not* modelling any physical ionic dynamics, the gradient directions which come into play for the ionic relaxation procedure do not need to be the Hellmann-Feynman forces[20] for the given ionic position at the associated electronic ground state. Instead, at each electronic iteration the ions are relaxed to their "zero-force" positions given by the expression

$$\frac{\partial E}{\partial \boldsymbol{R}_i} = 0 \qquad i = 1, N_{ions} \ , \tag{2.19}$$

while the (unconverged) electronic charge density is kept fixed. Only the Madelung energy and the electrons-ions interaction contribute to the gradient in eqn. (2.19). The procedure proves to work well in all the situations in which the relaxation effects expected are not extremely large (in which case forcing the ionic positions slightly beyond the minimum along the search direction is known to speed up the overall minimisation procedure), and is almost negligible in terms of computer time in comparison to the orbital relaxation. Some more about *constrained* atomic relaxation when applied to defective systems will be said in the following chapter.

2.3.2 Calculation features, second strategy.

In this section we provide a description of the total energy minimisation technique used in the present work for the study of defect energetics in ceramic insulators. Due to the much less efficient electronic screening of the defects taking place in insulators, and to the necessity of high cutoff treatment of the oxygen atoms, the calculations on these compounds are extremely demanding in terms of system sizes (number of orbitals) and dimension of the PW basis sets.

Although given the increasing power of modern computers the speed at which calculations can be performed is constantly improving, and the amount of memory which can be asked for in a single calculation is rapidly growing, a fast and moderately memory intensive algorithm is indispensable for approaching very large calculations.

At the present time a highly desirable feature of any calculation procedure is the possibility of implementing it efficiently onto a distributed-memory parallel machine, since beyond a certain system size the dynamic memory and the speed obtainable with vectorial machines are no more sufficient.

2.3.2.1 The band-by-band updating.

In a pseudopotential total energy calculation using a PW basis set the memory requirements are dominated by the necessity of storing the wavefunctions arrays[7]. A way to retain all the advantages of the conjugate gradients procedure without increasing the memory requirements to more than a *single* storage of the full set of orbital coefficients is to update by conjugate gradients one single band at time[19].

An order must be chosen for the band updating. For insulators and semiconductors the final set of states will eventually correspond only within a unitary transformation to the self-consistent KS set of states, while for metals the KS states will have to be

---

[7] Note that the necessity of treating a full set of orbitals in a *direct* minimisation of the energy functional is due to the fact that a better representation of the kinetic energy functional $T_s[\rho]$ is not available: it is not in itself a feature of DFT.

reproduced *exactly*. In the following we will assume that subspace rotation is always applied (which does not represent a large additional computational load), and that the sequence of orbital updating follows in ascending order the spectrum of the orbital energy expectation values $\{\eta_i\}$, $i = 1, N_{orb}$. The steepest descent gradient for a given band ψ_i is given by

$$F_i = -(H - \eta_i)\psi_i \; ; \qquad \eta_i = < \psi_i|\hat{H}|\psi_i > , \tag{2.20}$$

where only the orthogonality of the gradient to the state itself has been added to the previous definition (2.5). Note that this gradient vanishes when the state ψ_i approaches an eigenstate of the self-consistent hamiltonian H.

Before any band updating can start, the direction F_i needs to be orthogonalised to the other wavefunctions, which are kept fixed during the process:

$$F_i' = F_i - \sum_{j \neq i} < \psi_j|F_i > \psi_j \; . \tag{2.21}$$

It should be noted that any displacement $\delta\psi_i$ along the direction F_i' will now keep the state orthogonal to *all* the other states, and not, for example, to only the lower-lying states which have already been updated during the present global CG iteration.

One reason for this comes from the way in which the present scheme deals with the self-consistent nature of the minimisation problem: ensuring the complete orthogonality as in eqn. (2.21), only the change in the charge density from the single band needs to be computed to evaluate the total charge density while the band is updated by the CG procedure. Since the updating of the self-consistent screening potential is also a straightforward operation, the CG optimisation of the single wavefunction to minimise the total energy can be done always calculating the energy in a fully self-consistent way.[8]

---

[8] Even in a non self-consistent calculation in which the hamiltonian is kept fixed while all the bands are updated one by one, there are reasons to impose full orthogonality, for example to avoid large gradient vectors parallel to quasi-degenerate upper-lying bands, which would introduce instabilities in the calculations.

In systems with large number of states, and in particular in the initial part of the minimisation, when the changes in the screening potential due to the orbital optimisation are expected to be large, it is essential to update the effective hamiltonian while the bands are optimised to lower the total energy. Proceeding in such way, it is ensured (i) that the conjugate search directions along which the optimisation takes place are the most effective ones available at each stage of the calculation (since they are evaluated as in (2.20) from the self-consistent hamiltonian), and (ii) that the total energy will be decreased after all the band minimisations have been performed, since the energy does not have to be evaluated only at that point, for the first time, in the correct variational way (2.4). In other words, the whole procedure allows to the hamiltonian operator to converge smoothly to its self-consistent value, while the total energy after a global CG step is assured to be effectively lowered even in the case of large density rearrangements.

2.3.2.2 Preconditioning of the steepest descent vector.

The total energy calculations on oxide materials, which will be described in chapter 5 of this work, were all initialised assigning pseudo-random values to the expansion coefficients $a_{\mathbf{k},i,\mathbf{G}}$ which represent the orbitals. The advantage of this is that no predetermined knowledge on the electronic ground state (such as the symmetry, or in general the shape of the charge distribution) is incorporated in the initial conditions, and therefore somewhat propagated to the complete minimisation procedure[9].

A drawback of this is that the large kinetic energy of the initial orbitals is by far the dominant term in the total energy during the first iterations of each run, and therefore has to be efficiently removed to reach the ground state in a reasonable time. The analysis of the problem suggests a technique, called "preconditioning" of the steepest descent direction, which helps in doing so[21].

---

[9] The numerical noise in the calculations would *never* be big enough for the CG procedure to break an imposed symmetry and find a lower less symmetric ground state, even if the charge density were not kept symmetric along the run by explicit symmetrisation.

The high-energy excited eigenstates of the KS hamiltonian conduction bands can be thought as free quasi-particle unoccupied states, whose energy is essentially kinetic. With starting condition like the ones described above, there are in the initial orbitals large contributions from these high states, especially if the PW energy cutoff is itself large. The highest plane wave vectors randomly occupied carry the largest amount of kinetic energy, and are very little scattered into each other by the potential operator. The problem of annealing a set of electronic orbitals from random initial conditions will therefore look very much like the problem of minimising with conjugate gradients a system of noninteracting electrons, as long as the kinetic energy in the system is high (hundreds of eV per band), and if we focus on the high kinetic energy components in the orbitals (*i.e.* the PW coefficients $a_{\mathbf{k},i,\mathbf{G}}$ with large $|\mathbf{G}|$).

For a single-electron hamiltonian consisting of the kinetic operator $\hat{T}$ only, the steepest descent direction

$$F_i \; = \; -(\hat{T} - \eta_i)|\psi_i> \; = \; -\sum_{\mathbf{G}}(\frac{G^2}{2} - \eta_i)a_{i,\mathbf{G}}|\mathbf{G}> \; ; \qquad \eta_i \; = \; \sum_{\mathbf{G}} \frac{G^2}{2}|a_{i,\mathbf{G}}|^2 \; , \quad (2.22)$$

is obviously not parallel to the error vector, which in this case is the function $|\psi_i>$ itself. The search direction is not proportional to the state because of the coefficients $\frac{G^2}{2}$ in the prefactors, which project the search direction more than necessary onto the high G-space wave-vector components.

A way of suppressing this effect is to operate on the gradient (2.22) with a diagonal matrix $K_{\mathbf{G},\mathbf{G}'}$ effectively correcting the gradient at kinetic energies beyond the average orbital's one. A possible choice, used in this work, is

$$K_{\mathbf{G},\mathbf{G}'} \; = \; \delta_{\mathbf{G},\mathbf{G}'} \frac{27 + 18x + 12x^2 + 8x^3}{27 + 18x + 12x^2 + 8x^3 + 16x^4} \qquad x = \frac{G^2}{2\eta_i} \; , \qquad (2.23)$$

which has the advantage of approaching the $G = 0$ limit with the first three derivatives equal to zero (*i.e.* no corrections is applied in the low kinetic energy regime). At high kinetic energies, well beyond $x = 1$, the preconditioned search direction

$$F_i^{prec} \; = \; K \; F_i \qquad (2.24)$$

causes all the large wave-vector components to converge at the same rate. Since the preconditioning procedure has to be followed by a further orthogonalisation of the gradient to all the existing bands, and therefore involves some non-negligible additional computer work, it is preferable to use it only when large components from the high-lying KS eigenstates are expected to be still present in the wavefunctions being updated[10], *i.e.* in the initial part of the calculation.

2.3.2.3 Line minimisation.

Once the CG procedure has been applied to the preconditioned steepest descent vector to obtain for the current band a normalised search direction S_i which is orthogonal to all the other bands, the following linear combination:

$$\psi_i \cos(\theta) + S_i \sin(\theta) \qquad \theta \in [0, 2\pi] \tag{2.25}$$

is also normalised and orthogonal to all the other bands $\{\psi_j;\ i \neq j\ \}$ for any real value of the angle θ which here represents the line displacement coordinate. The minimisation is again based on some assumption on the Energy analytic behaviour. The charge density is a periodic function of θ with period π, and the Kohn-Sham energy can be rewritten as the Fourier expansion

$$E(\theta) = E_{avg} + \sum_{n=1,\infty} A_n \cos(2n\theta) + B_n \sin(2n\theta)\ . \tag{2.26}$$

Assuming from experience on simple systems[21] that the first Fourier component is the leading term in the expansion, and rewriting the energy as

$$E(\theta) = E_{avg} + A_1 \cos(2\theta) + B_1 \sin(2\theta)\ , \tag{2.27}$$

the minimum can be located from this expression provided that three independent values of the function or of its derivatives are available for a fit of the three parameters

---

[10] The simple form of preconditioning we use is based on the assumption that we can approximate the orbitals components on the high-lying KS states with the coefficients $a_{i,\mathbf{G}}$ of their PW expansion: this approximation does not hold near convergence, where the mentioned components tend to zero.

E_{avg}, A_1, B_1 . Since the value of the function and its derivative at $\theta = 0$ are already known from the CG procedure, one more energy evaluation at some $\theta' \neq 0$ is sufficient for extrapolating a good value for the minimum. A typical value $\theta' = \pi/300$ has been utilised in all the calculations, and found large enough to avoid rounding errors when subtracting the values at $\theta = 0$ and small enough to guarantee good values for the fitted minimum near self-consistency in the runs, when the minima are expected to occur at very small values of θ.

2.3.2.4 Computational procedure.

For a minimisation run to be completed, the CG procedure updating all the orbitals one by one as described so far, has to be repeated for the number of times which is necessary to reach the total energy convergence. The number N of CG steps performed at each iteration on each band should not be very high, not to waste computer effort in optimising the bands while the screening potential has not yet reached self-consistency (see also the final considerations of Section (2.2.3), on page 31). Although for simplicity such number has been fixed to a value of three or four for all orbitals in the energy minimisations, it is clear that for calculations involving subspace rotations, where the character of the bands and the associated convergence properties are expected to vary along the spectrum, a more sophisticated algorithm can be applied to maximise the convergence speed, tuning an individual value for N for each band([22]).

2.4 The pseudopotential representation in the PW formalism.

We discuss hereafter the way in which the interaction between ionic cores and valence electrons is treated in the calculations. In the present work norm-conserving ab initio pseudopotentials of the kind proposed by Hamann, Schlüter and Chiang (HSC) [10] have been used for all the constituent atoms, with the only exception of hydrogen, for

which we used the bare Coulomb energy potential $-e^2/r$.
The total potential for the interaction is simply the sum over ionic position of the atomic pseudopotentials:

$$V = \sum_I v_{ps}(|\mathbf{r} - \mathbf{R_I}|) \ . \tag{2.28}$$

As discussed in Section (1.5.1), a natural form for the atomic pseudopotential is given by

$$v_{ps} = \sum_{l=0}^{\infty} v_l \hat{P}_l \ , \tag{2.29}$$

where the expansion is usually arrested at the highest angular component in the atomic valence shell, and the potential is rewritten as the sum of a local and a non-local parts

$$v_{ps} = v_{loc}(r) + v^{sl} \ ; \qquad v^{sl} = \sum_{l=0}^{l_{max}} (v_l(r) - v_{loc}(r))\hat{P}_l \ , \tag{2.30}$$

where now the angular components higher than l_{max} of the pseudopotential have been approximated with the local part v_{loc}. In the HSC formulation v_{loc} is shown to carry all the long-range interactions between the valence electrons and the pseudoion, while the angular waves $v_l^{sl} = v_l - v_{loc}$ of the non-local part v^{sl} [11] are short-ranged functions of the distance from the nucleus, which vanish outside the core radius r_c. It is customary in the calculations to set $v_{loc}(r) = v_{l_0}(r)$ for some chosen angular momentum l_0: the pseudopotential is then normally said to be l_0-local (renaming l_0 with s, p, d, f in practical use).
In the CG procedure the steepest descent vector we need (for the i$-th$ band) has G-space coefficients:

$$\begin{aligned} F_{i,\mathbf{G}} = - < \mathbf{G}|\hat{H}|\psi_i > = \\ -\sum_{\mathbf{G}'} a_{i,\mathbf{G}'} \Big\{ < \mathbf{G}|\hat{T}|\mathbf{G}' > + < \mathbf{G}|\hat{V}_{loc} + \hat{V}_{screen}|\mathbf{G}' > \\ + < \mathbf{G}|\hat{V}_{nonloc}|\mathbf{G}' > \Big\} \ , \end{aligned} \tag{2.31}$$

---

[11] Being a multiplicative operator on the radial part, but treating differently the different angular components of the orbitals, this potential v^{sl} is sometimes called "semilocal".

(capital V meaning a sum on the ionic positions as in (2.28)), where $\hat{V}_{nonloc}$ is obtained summing the potential v^{sl} of expression (2.30) on the ionic positions. Since the kinetic operator $\hat{T}$ is diagonal in G-space, and since each integral $< \mathbf{G}|\hat{V}_{loc} + \hat{V}_{screen}|\mathbf{G}' >$ in expression (2.31) is a Fourier coefficient (of the reciprocal space vector $|\mathbf{G} - \mathbf{G}' >$) of the local part of the KS potential, no operation scaling like N^2_{plw} is involved in these first two terms. The third integral

$$< \mathbf{G}|\hat{V}_{nonloc}|\mathbf{G}' > \tag{2.32}$$

involves matrix elements between plane waves of radial functions and angular projectors, and should in principle be calculated separately for each couple of G-vectors $(\mathbf{G}, \mathbf{G}')$, therefore introducing a N^2_{plw}-scaling operation in the calculations.

This problem can be overcome by rewriting the pseudopotential v_{ps} in the Kleinman-Bylander (KB) representation[23], given by

$$v_{ps}^{KB} = v_{loc}(r) + \sum_{lm} \frac{|v_l^{sl}(r)\chi_l(r)Y_{lm} >< Y_{lm}\chi_l(r)v_l^{sl}(r)|}{< \chi_l(r)Y_{lm}|v_l^{sl}(r)|\chi_l(r)Y_{lm} >} , \tag{2.33}$$

where $\chi_l(r)Y_{lm}$ is an eigenfunction of the atomic pseudo-hamiltonian. Note that the operator so obtained is *not* exactly equal to v_{ps} in equation (2.29), although it acts in the same way on the reference atomic pseudostates, and is therefore expected to be norm-conserving and transferable like v_{ps}[12].

The immediate effect in the calculation of the KB representation is that the matrix elements of the non-local pseudopotential on the PW basis set can be expressed in the separate form:

$$< \mathbf{G}|\hat{v}^{sl}|\mathbf{G}' >= \sum_l f_l(G) f_l(G') , \tag{2.34}$$

so that the integral (2.32) does never imply double sums on the PW basis set.

---

[12] It may happen that some spurious deep bound states are introduced by the KB representation, when the local part v_{loc} is badly chosen. A discussion on the occurrence of these rare "ghost" states can be found in reference [24].

2.4.1 Pseudopotential optimisation and non-linear core correction.

The number of PW which has to be included in a total energy calculation depends both on the volume of the supercell used and on the energy cutoff necessary for the PW basis set to reproduce correctly the valence electron orbitals. For first row elements and transition metals a very large number of PW is normally needed to reproduce the sharply peaked valence states which arise respectively from the strongly attractive *p* and *d* pseudopotential components.

It should be noted that if the quantities of interest are energy differences between different atomic arrangements, it is sufficient to use an energy cutoff large enough to obtain a converged charge density distribution in the bond region, since the errors arising from the incomplete convergence of the kinetic energy contributions from the peaked core regions of the pseudo-orbitals are structure-factor independent, and therefore largely cancel in the results. However, it is still highly desirable not to operate too much below the cutoff at which the energy can be considered fully converged, since the residual errors after the cancellation are difficult to predict and time-expensive to monitor directly for every result.

In the calculations presented in this work, which do not involve transition metals, the only "hard" element in need of a large cutoff treatment is oxygen, for which a pseudopotential explicitly optimised for fast PW convergence has been used. The general scheme of the optimisation procedure used in this case was recently proposed by Rappe, Rabe, Kaxiras and Joannopoulos (RRKJ)[25], and is summarised in the next section. For simple metals like Al, Mg, and Li, the pseudopotentials are weak, the convergency properties of the pseudopotentials do not represent a problem (and in fact improve passing from the atom to the metal solids, where the valence electrons are nearly uniformly distributed), and no optimisation was needed.

2.4.1.1 RRKJ optimisation.

The only degree of freedom left in the pseudopotential formulation after the requirement of norm conservation and exact reproduction of the all-electron wave functions beyond the chosen core radius r_c (cf. Section (1.5.2)) is the shape of the pseudopotential within such radius. It follows immediately that a small core radius, leading to a very accurate reproduction of all-electron atomic results, will leave very little variational freedom for the optimisation procedure, so that a compromise has to be reached between cutoff energy convergence and transferability properties.

Once r_c has been set, RRKJ point out that the total energy convergence in the high cutoff region resembles closely the cutoff convergence of the isolated pseudoatoms used in the calculation, and that the leading part of the residual error while approaching convergence derives from the kinetic energy of the orbitals. RRJK therefore parametrise directly the pseudo-wavefunctions $\psi_l(r)$ inside r_c, and adjust the parameters to minimise for each l the expression

$$\Delta E_{kin} = \int_{|\mathbf{G}|>q_c} d\mathbf{G}\, \frac{|\mathbf{G}|^2}{2}\, |\psi_l(\mathbf{G})|^2 \tag{2.35}$$

which represents the residual kinetic energy beyond a cutoff q_c. In this scheme the value of q_c is not fixed, but results from the calculations as the minimum possible cutoff which gives after the minimisation procedure a residual energy ΔE_{kin} lower than a fixed tolerance value (of the order of 1 mRy).

With some minor adjustments from the original scheme in the choice of the parametrisation of the pseudo-wavefunctions[13] and in the determination of q_c, this procedure has been applied[26] to generate the oxygen pseudopotential used in the calculations. More about the testing of the performance of this pseudopotential, and about how such performance compares with the available literature results for other oxygen pseudopotentials, will be said in Chapter 5.

---

[13] The parameters are adjusted so that $\psi_l(r)$ matches up to the second derivative the all-electron solution at r_c, and is normalised correctly, so that anyway more than *four* free parameters are needed to fulfill all the constraints.

2.4.2 The non-linear core correction.

One last technical issue is described here, which arises from an approximation inherent to the way pseudopotentials are constructed. The approximation in question consists of a forced linearisation of the exchange-correlation potential which is implicit in the construction of the norm-conserving pseudopotentials in all the cases in which the core and valence electron densities overlap significantly in the all-electron atomic calculations. When generating the pseudopotentials from such calculations, the total effective KS potential has to be "unscreened"[11] at some stage to subtract from it the Hartree and exchange-correlation potentials arising from the valence charge distribution (the Hartree and the exchange-correlation potentials due to the core charge can be considered included as a frozen contribution into the final pseudopotential):

$$v_l(r) = v_l^{scr}(r) \; - \; \int d\mathbf{r}' \frac{\rho_{val}(\mathbf{r}')}{|\mathbf{r}' - \mathbf{r}|} \; - \; v_{xc}^{val}(r) \; , \tag{2.36}$$

where the exchange-correlation potential arising from the atomic valence charge $\rho_{val}(r)$ is defined as in (1.29) by the equation

$$v_{xc}^{val}(r) \; = \; \mu_{xc}(\rho_{val}(r)) \; . \tag{2.37}$$

The unscreened pseudopotential v_l obtained with the (2.36) implicitly contains a term

$$v_l^{xc} = \mu_{xc}(\rho_{core}(r) + \rho_{val}(r)) - \mu_{xc}(\rho_{val}(r)) \tag{2.38}$$

representing the contribution to the the KS potential of the self-consistent calculation on the pseudoatom which added to the explicit exchange-correlation potential (2.37) of such calculation would give back the original exchange-correlation potential of the all-electron calculation[14]. Since the exchange-correlation potential is *not* linear in the charge (unlike the Hartree potential), we cannot in general assume also

$$v_l^{xc} = \mu_{xc}(\rho_{core}(r)) \qquad \forall\, r \; , \tag{2.39}$$

---

[14] Note that the pseudo-valence charge differs from the valence charge of the all-electron calculation within the core radius, since, for example, the pseudo-wavefunctions are nodeless unlike the all-electrons valence states. Because of the norm conservation, the distinction can be dropped here introducing only a small error[27].

unless the core orbitals for the atom in question are so contracted that the overlap region between core and valence charge is negligible, or unless we think to perform the calculation in exactly the reference atomic configuration, in which case the errors committed assuming the equivalence of (2.39) and (2.38) would cancel exactly.

Suppose now that calculations have to be performed in a solid where the self-consistent pseudo-valence distribution $\rho_{sc}(r)$ differs from the atomic one. A way to include exchange and correlation effects correctly consists of modifying the exchange-correlation potential

$$\mu_{xc}(\rho_{sc}(r)) \tag{2.40}$$

normally used in the calculations into the corrected form introduced by Louie, Froyen and Cohen[27]:

$$\mu_{xc}(\rho_{val}(r)) - \mu_{xc}(\rho_{core}(r) + \rho_{val}(r)) + \mu_{xc}(\rho_{core}(r) + \rho_{sc}(r)) \ . \tag{2.41}$$

The three terms in expression (2.41) correspond respectively to (i) re-screening the pseudopotential with the atomic pseudo-valence charge density (ii) unscreening it of the exchange-correlation potential of the full charge in the atom and (iii) finally adding the correct exchange-correlation potential (in the frozen core approximation) for the self-consistent calculation in the solid.

Two more source of approximation have to be added to the correction as described so far: (1) the strongly peaked frozen core charge $\rho_{core}(r)$ that has to be used throughout the calculations is typically *not* representable on the PW basis set, due to insufficient energy cutoff and (2) the pseudopotentials components $v_l(r)$ are usually evaluated for each angular momentum l in a different atomic reference configuration, so that in principle different core charge density should be used somehow in performing the correction.

Being clear from expression (2.41) that the correction only exists in the overlap region which is usually well outside the main core charge peak, it has become common practice to replace the full atomic core charge with a much smoother "effective core" distribution which is equal to the core charge density in (at least most of) the overlap region. This solves the problem (1), although some testing is needed to monitor the error introduced with the smoothing procedure. The second approximation consists of neglecting the core relaxations between two different reference configurations. Even if such relaxation is expected to be too small to affect the results, this has in practice to be checked comparing the corrected results obtained with the different reference core charge distributions.

Although in most cases the use of (2.41) instead of (2.40) leads to negligible changes in the results (the two expressions being equivalent in the limit of no valence-core overlap), for some other cases the correction is relevant, especially when relatively extended orbitals have to be put in the core[28], and in general when the valence distribution in the solid is much different than in the isolated atom[29]. In this latter case the non-linear core correction in expression (2.41) is expected to improve the transferability of the pseudopotential, making it fearly independent from the reference configuration which was used to generate it.

In the present work, calculations have been performed on ceramics like MgO, where the cation Mg, which in the neutral atomic ground state is known to have a significant core-valence overlap, undergoes ionisation from the neighbouring O atoms, the valence charge distribution in the solid being therefore radically different from the atomic case. Some results on the effects of the non-linear core correction implemented to treat this specific case will be reported in Chapter 5.

2.5 Metal smearing techniques for BZ integration.

As a final topic in the present chapter about computational techniques, we address the problems connected with the necessity of performing Brillouin Zone integrals in a total energy calculation using periodic boundary conditions and the DFT-KS scheme (or any other single-particle formulation). Such problem is serious in supercell calculations if the material investigated is a metal. In the present work the smearing technique introduced by Gillan[17], based on the finite temperature formalism[33][39] discussed in Section (1.3), has been used for the calculations on defect energetics in aluminium.

During the course of the work the relations between that proposed method and other methods existing in literature has been studied. The results of such investigation led to a general formulation[34] for the smearing technique which is independent of the smearing function used, and includes as sub-cases the most relevant smearing schemes available in the past [35][36][17][38], improving some of them [35][36] by the introduction of an appropriate smearing-dependent correction to the calculated ground state energy. The improvements on former results are particularly encouraging when the correction scheme is applied to the much used "gaussian smearing technique" introduced by Fu and Ho[35], and later discussed and modified by Needs[36].
What follows hereafter is a brief analysis of the metal BZ integration problem, and a description of the method used to deal with it in the present work on Al. Some more results on Al obtained with the corrected gaussian smearing technique are reported in Appendix A.

2.5.1 BZ sampling and smearing schemes.

To take into account the contribution to the self-consistent potential of *all* the electronic states in the periodic solid, and since the eigenstates of the KS hamiltonian are Bloch functions

$$\psi_{\boldsymbol{k}}(\boldsymbol{r}) = e^{i\boldsymbol{k}\cdot\boldsymbol{r}} \sum_{\boldsymbol{G}} a_{\boldsymbol{k},\,\boldsymbol{G}}\, e^{i\boldsymbol{G}\cdot\boldsymbol{r}} \tag{2.42}$$

due to the translational symmetry of the KS potential, the total energy of a unit cell of the infinite solid

$$E[\rho] = \frac{1}{\Omega_{BZ}} \int_{BZ} d\mathbf{k} \sum_i \epsilon_i(\mathbf{k}) f_\mu(\epsilon_i(\mathbf{k})) \; + \; \int_{cell} d\mathbf{r}(\; \epsilon_{xc}(\mathbf{r}) - v_{xc}(\mathbf{r}) - \frac{1}{2} v_H(\mathbf{r}) \;)\rho(\mathbf{r}) \tag{2.43}$$

includes the contribution of each **k** in the Brillouin Zone through a "band energy" term (first integral on the right term in (2.43)) and through the screening terms constructed from the self-consistent charge density (second integral). The charge density is given by

$$\rho(\mathbf{r}) = \frac{1}{\Omega_{BZ}} \int_{BZ} d\mathbf{k} \sum_i f_\mu(\epsilon_i(\mathbf{k})) |\psi^i_{\mathbf{k}}(\mathbf{r})|^2 \, , \tag{2.44}$$

where the LDA occupation function $f_\mu(\epsilon)$ for a given chemical potential μ corresponds to the step function

$$f_\mu(\epsilon) = \begin{cases} 2 & \epsilon < \mu \\ 1 & \epsilon = \mu \\ 0 & \epsilon > \mu \,. \end{cases} \tag{2.45}$$

In a real calculation the BZ integrals (2.43), (2.44) have to be approximated by a discrete sum on weighted points. Given the translational symmetry, the eigenvalue and eigenstate integrands

$$\epsilon_i(\mathbf{k}) f_\mu(\epsilon_i(\mathbf{k})) \qquad\qquad f_\mu(\epsilon_i(\mathbf{k}))|\psi^i_{\mathbf{k}}(\mathbf{r})|^2 \tag{2.46}$$

from equations (2.43), (2.44) are periodic in reciprocal space. The discrete integration problem corresponds therefore to the problem of determining the average of a periodic function of a given translational symmetry over its domain. As recognised long ago (Baldereschi, 1973 [30]), the symmetry properties alone are already sufficient for determining a single "mean value" point in the BZ which constitutes a minimal and accurate sampling set for performing the integrals, provided that the integrands are sufficiently smooth in G-space, as is the case for most semiconductors and insulators. Various refinements have been proposed since then to provide recipes for enlarged symmetry-dependent BZ sampling sets of increasing size and accuracy[31][32].

In the case of metals the integrands deriving from partially occupied conduction bands are discontinuous in G-space, although still periodical, due to the cut in the occupation number when, moving along some **k** direction in the BZ, the eigenvalue $\epsilon_i(\mathbf{k})$ crosses the Fermi level μ. The performance of the "special" sampling sets is in these cases expected to be much poorer, since the fast-convergence hypothesis on the integrands when expanded on the appropriately symmetrised sets of plane waves[30] is no more valid. The alternatives to reach a given precision in the integration are traditionally (1) to increase the size of the k-points sampling sets, therefore increasing (at least linearly) the computational load[15], (2) to modify the integrands (and therefore the functional

---

[15] Dropping the idea of performing the calculation in a fully self-consistent way, or on the complete PW set instead than on some limited basis set constructed with few k-points, it is however often possible to effectively include many sampling points in the calculations without an enormous expense of cpu time[37].

evaluated) to somewhat smoother functions, easier to integrate in the BZ, which reduce to the original form in the zero limit of an appropriate "smearing" linewidth parameter σ.

The density of states from a calculation can be represented as a sum on delta functions on the self-consistent KS eigenvalues (we drop here for simplicity the weighted summation on k-points):

$$n(\epsilon) = \sum_i \delta(\epsilon - \epsilon_i) \ . \tag{2.47}$$

With "smearing" of the Fermi surface a procedure is usually meant with which a different (normalised) distribution function is substituted to the delta functions. This function g (for example, a gaussian[35]) tends to the delta function in the limit of zero linewidth:

$$\frac{1}{\sigma} g(\frac{\epsilon - \epsilon_i}{\sigma}) \sim \delta(\epsilon - \epsilon_i) \qquad\qquad \sigma \sim 0 \ . \tag{2.48}$$

At finite values of σ, the occupancy f_i of the $i-th$ orbital is evaluated as

$$f_i = f(x_i) = \int_{-\infty}^{x_i} g(t)dt \qquad\qquad x_i = \frac{(\mu - \epsilon_i)}{\sigma} \ , \tag{2.49}$$

after the chemical potential μ has been determined imposing the constraint of the conservation of the number of electrons:

$$\sum_i f_\mu(\epsilon_i) = N_{elect.} \ . \tag{2.50}$$

For a general choice of the smearing function $g(x)$ and for any fixed σ, a set of occupation numbers is therefore determined, which is then used to evaluate the charge density as

$$\rho(\mathbf{r}) = \sum_{i=1}^{\infty} f_i |\phi_i(\mathbf{r})|^2 \ . \tag{2.51}$$

The band-energy contribution to the total energy (2.43) is evaluated either as the energy integral

$$E_{band} = \int_{-\infty}^{\mu} d\epsilon \ \tilde{n}(\epsilon)\epsilon \ = \int_{-\infty}^{\mu} d\epsilon \sum_i \frac{1}{\sigma} g(\frac{\epsilon - \epsilon_i}{\sigma}) \ \epsilon \tag{2.52}$$

on the smeared density of states $\tilde{n}(\epsilon)$, or as a sum weighted by the occupancies of the self-consistent eigenvalues of the calculation:

$$E_{band} = \sum_i f_i \, \epsilon_i \; = \; \sum_i \epsilon_i \int_{-\infty}^{\mu} d\epsilon \, \frac{1}{\sigma} \, g(\frac{\epsilon - \epsilon_i}{\sigma}) \; . \tag{2.53}$$

These two expressions are not equivalent, although they converge to the same value when σ approaches zero.[16] The use of a density of states "smeared" around each calculated eigenvalue $\epsilon_i(\mathbf{k}_j)$ as in the first expression (2.52) has been proposed[35] to take into account the Bloch states at points $\mathbf{k}$ close to the sampling point $\mathbf{k}_j$. The smearing parameter σ is therefore chosen to resemble the average band dispersion between neighbouring sampling points, and is systematically reduced when the dimension of the sampling set increases. The second expression (2.53) has been proposed[36] as an alternative to the first one, which improves the stability of the calculations, since the total energy defined in (2.43) has to be a functional of the density (2.51) represented within the calculation, and consistently should *not* include terms originating from states which do not contribute to the density itself. This is clear when considering that taking the variation with respect to wavefunctions of the total energy calculated as in (2.52) does not result in the Schrödinger equation that is actually solved.

Note that within these schemes no systematic way to control or correct the "smearing error" introduced with a finite σ is provided, and small values of σ (of the order of 0.1 eV, or less) have to be used to keep such error small.

There is a strong resemblance between expressions (2.51), (2.49) and the (1.23), (1.21) discussed in Section (1.3) and related to the generalisation of DFT to finite temperatures, the linewidth σ playing here a role similar to the one played by the temperature in that formulation. This has suggested a novel way[34] to (i) correct for the smearing error, enabling the use of much bigger values of σ, and (ii) clarify the issue raised above of the variational nature of the energy expression minimised within the smearing scheme.

---

[16] It is easily seen that they differ for a leading quadratic term in σ if the function $g(x)$ is even.

2.5.2 Generalised free energy.

For any chosen σ we can write a "free energy" functional of the wavefunctions, occupancies, and smearing, as:

$$\begin{aligned} F[\ \{\psi_i\},\{f_i\},\sigma\ ] &= \\ &\sum_i f_i < \psi_i|\hat{H}|\psi_i > + \int_{cell} d\mathbf{r}(\ \epsilon_{xc}(\mathbf{r}) - v_{xc}(\mathbf{r}) - \frac{1}{2}v_H(\mathbf{r})\ )\rho(\mathbf{r}) \\ &-\sigma S(\{f_i\}) - \mu(\sum_i f_i - N_{el}) + \sum_i f_i\epsilon_i(1- < \psi_i|\psi_i >)\ , \end{aligned} \tag{2.54}$$

with the charge density $\rho(\mathbf{r})$ evaluated as in eqn. (2.51). Here μ and the ϵ_i are Lagrange multipliers ensuring the conservation of the number of electrons and the normalisation of the orbitals. The "entropic" term S has been added here as a function of the occupation numbers only.

As in the standard formulation one obtains at the minimum the KS set of equations for orthonormal states:

$$\frac{\delta F}{\delta\psi_i^\dagger} = 0 \ \rightarrow\ \hat{H}|\psi_i >= \epsilon_i|\psi_i > \tag{2.55}$$

$$\frac{\partial F}{\partial\epsilon_i} = 0 \ \rightarrow\ < \psi_i|\psi_j >= \delta_{i,j}\ , \tag{2.56}$$

and two more conditions are added imposing to F to be stationary with respect to the occupancies $\{f_i\}$, the sum of which is fixed:

$$\frac{\partial F}{\partial\mu} = 0 \ \rightarrow\ \sum_i f_i = N_{el} \tag{2.57}$$

$$\frac{\partial F}{\partial f_i} = 0 \ \rightarrow\ < \psi_i|\hat{H}|\psi_i > -\mu = \sigma\frac{\partial S}{\partial f_i} \qquad \forall i\ . \tag{2.58}$$

The system (2.59) provides the $N_{orb}+1$ equations necessary to determine the "chemical potential" μ and the occupancies $\{f_i\}$. Suppose now that a *given* smearing function $g(x)$ is used in the calculations, and that we want to *determine* the appropriate entropy term $S(\{f_i\})$ which is minimised by the occupation function $f(x)$ corresponding to $g(x)$ as in eqn. (2.48). A natural choice for the functional form of S is:

$$S(\{f_i\}) = \sum_i A(f_i) \ , \tag{2.59}$$

where $A(f)$ is an undetermined function, so that from the (2.58) at self-consistency we obtain:

$$\frac{\partial S}{\partial f_i} = \frac{\epsilon_i - \mu}{\sigma} \qquad \rightarrow \qquad \frac{dA}{df} = -x \ , \tag{2.60}$$

where $x = (\mu - \epsilon)/\sigma$ as in eqn. (2.49). With a straightforward change of variables in the differentiation we obtain

$$\frac{dA}{dx} = -x \, \frac{df}{dx} \ , \tag{2.61}$$

which[17] leads to the values of $A(f)$ in the implicit form $A(f(x))$ via direct integration

$$A = \int_{-\infty}^{x} -t \ g(t) \ dt \tag{2.62}$$

so that finally the value of S is given by

$$S = \sum_i A(f(x_i)) \qquad x_i = \frac{\mu - \epsilon_i}{\sigma} \ . \tag{2.63}$$

A completely analogous strategy consists in choosing a suitable form for the occupation function $f(x)$ instead of the smearing function, and repeating the procedure described above, after noticing that

$$g(x) = f'(x) \ . \tag{2.64}$$

For example the choice of the occupation function

$$f_i = \frac{2}{e^{(\epsilon_i - \mu)/\sigma} + 1} \tag{2.65}$$

leads to the expression for the S :

$$S = -2 \ \sum_i [y_i \log(y_i) + (1 - y_i) \log(1 - y_i)] \qquad y_i = f_i/2 \tag{2.66}$$

which is the known entropy form for the degenerate non interacting Fermi-Dirac gas provided that $\sigma = 1/\beta$.

---

[17] Note that we are assuming here that $f(x)$ is a monotonic function of x, as it is always the case if $g(x)$ is everywhere positive. With some precaution more general choices can be made for $g(x)$ [38], leading to values for the orbitals occupation f_i which can be bigger than two, or *negative*.

2.5.3 The entropy correction.

We have seen so far that the addition of an adequate "entropy" term S to the standard energy functional makes it possible to treat the system with fractional occupancies within a global minimisation procedure with respect of wavefunction coefficients *and* occupation numbers for any given fixed σ in the "free energy" functional $F = E - \sigma S$. The reason for doing this is that it is now possible to analyse the behaviour of the functions $F(\sigma)$ and $E(\sigma)$ defined by the minimum procedure in order to estimate the non-smeared ground state energy corresponding to their $\sigma = 0$ value

$$E_0 = E(0) = F(0) \tag{2.67}$$

in terms of the values of the same functions at finite values of σ, where they are much easier to evaluate by BZ integration. While there is no reason why the the values of function $F(\sigma)$ should converge faster than those of $E(\sigma)$ (calculated as in (2.43) with any of the literature recipes for the band energy like (2.52), (2.53)), it can be shown that the correction term needed to obtain E_0 can be expressed in terms of the difference of the two, *i.e.* of the entropy function S (which is the ultimate reason why such term has been introduced).

From the minimum condition and the definition of F one obtains the system

$$\frac{\partial F}{\partial \sigma} = \frac{dF}{d\sigma} \tag{2.68}$$

$$\frac{\partial F}{\partial \sigma} = -S(\sigma)\,. \tag{2.69}$$

It can also be shown[40] that for small values of σ the entropy function $S(\sigma)$ tends to zero at least linearly with σ, so that

$$S \approx c_2\, \sigma\, n(\mu) = \gamma\sigma \tag{2.70}$$

$$c_2 = \int_{-\infty}^{\infty} dt\; t^2\, g(t)\;, \tag{2.71}$$

where $n(\mu)$ is the non-smeared density of states (2.47) at the Fermi level μ from a calculation performed at the given small value of σ.

From the system (2.70) it follows immediately that for small values of σ

$$F(\sigma) = E_0 - \frac{1}{2}\gamma\sigma^2 + O(\sigma^3) \tag{2.72}$$

$$E(\sigma) = E_0 + \frac{1}{2}\gamma\sigma^2 + O(\sigma^3) \tag{2.73}$$

and therefore the zero-smearing energy E_0 is obtained as

$$E_0 = \frac{E(\sigma) + F(\sigma)}{2} + O(\sigma^3) = E(\sigma) - \frac{\sigma}{2}S(\sigma) + O(\sigma^3) \tag{2.74}$$

by simply adding to $E(\sigma)$ the correction term

$$\Delta E_{corr}(\sigma) = -\frac{\sigma}{2}S(\sigma) = -\frac{\sigma}{2}\sum_{\mathbf{k}_j,i} w_{\mathbf{k}_j} A(f(\frac{\mu - \epsilon_i(\mathbf{k}_j)}{\sigma})) \tag{2.75}$$

(the summation on the right being the correction as it reads in the general case of a BZ sampling points set $\{\mathbf{k}_j\}$ with associated weights $\{w_{\mathbf{k}_j}\}$).

Adding this correction[18] to the computed value of the total energy an accurate prediction of E_0 can be expected even if the calculations have been performed at large values of σ [19], of the order of some eV, *i.e.* in a regime of very fast convergence of the calculated results with respect to BZ sampling.

It should be noted that although expressions corresponding to E and F have previously been used as the energy functionals to be minimised in different gaussian smearing schemes[20], the correction derived above has never before been applied to improve such schemes. We report in Appendix A some results obtained from the gaussian smearing

---

[18] Note that for smearing schemes in which the integral c_2 of eqn. (2.71) is identically zero (due to an appropriate choice of the smearing function $g(x)$), the correction ΔE_{corr} is also null.

[19] There are some indications that the error committed in expression (2.75) might be of order $O(\sigma^4)$. The analysis on this point is still in progress.

[20] Using the band energies (2.52) and (2.53) in the total energy expression (2.43) leads to functionals identical to our F and E respectively, although we obtained them through a different procedure.

function and the associated entropy correction

$$g(x) = \frac{2}{\sigma\sqrt{\pi}} e^{-(\frac{\epsilon-\mu}{\sigma})^2} \qquad \Delta E_{corr}(\sigma) = -\frac{\sigma}{2\sqrt{\pi}} \sum_{\mathbf{k}_j,i} w_{\mathbf{k}_j} e^{-(\frac{\mu-\epsilon_i(\mathbf{k}_j)}{\sigma})^2} , \tag{2.76}$$

which were used to study the BZ sampling convergence of the total energy and the C_{44} elastic constant in Al. For all the calculations on defect energetics in Al host, presented in the following chapter, we have made use of the Fermi-Dirac smearing scheme defined by expressions (2.65), (2.66), and we have applied to the results the entropy correction (2.75), as was done in reference[17] .

3 The ab initio calculation of defect energetics in aluminium.

3.1 Introduction.

In this chapter the theoretical background and the computational techniques described in Chapter 1 and Chapter 2 are applied to the problem of determining reliable ab initio theoretical values for the energetics of the stable and migrating vacancy, the self-interstitial, and the interstitial and migrating hydrogen impurity in aluminium host. The results of this investigation on the Al vacancy and the H-Al systems have already appeared in published form (references [58] and [59], respectively).

This choice of investigated systems has various motivations. Al is a technologically important material, representative of the class of "simple" (*sp*-bonded) metals. The Al vacancy is the simplest and most common isolated defect in the material, and as such it has attracted much experimental work. The self-interstitial is the next most natural isolated defect in the pure material, and given the close-packed structure of the metal, issues like the shape and the relevance for the energetics of the ionic relaxation around the defect are raised.

The introduction of H as a small isolated impurity in the metal permits the investigation of the electronic screening properties in a situation in which the balance is uncertain between the physical picture of H immersed into an almost uniform electron gas only slightly modulated by the presence of Al ions, and the possibility of a pronounced interaction between the proton (with its surrounding electron cloud) and the ionic cores.

In the following we provide a brief historical sketch of the various theoretical approaches reported in literature to the mentioned problems. We then address the problem of correctly calculating the vacancy formation energy taking into account the volume relaxation effects in periodic boundary conditions, and define the quantities of interest for the defect energetics. We then provide results for the perfect Al crystal, the equi-

librium vacancy, the migrating vacancy , and the self interstitial. When it is possible the results are compared with recent theoretical predictions making use of different techniques.
The introduction of hydrogen in the metal host, represented as a bare Coulomb potential, leads to some further technical refinements needed to deal with the wavefunctions cusps and the related G-space convergence problem. The case of hydrogen embedded in jellium is investigated as the elective test-system for checking the adequacy of our techniques. Numerical results are then provided for the hydrogen heath of solution, for the relative stability of the lattice interstitial sites, for the hydrogen migration energy along a chosen crystal direction, and for the energetics and geometry of the hydrogen bound to a vacancy. The metal screening in the defective systems investigated is discussed in terms of the ground state density distributions obtained from the calculations.

3.2 Previous modelling of aluminium systems.

The nearly-free-electron band structure of aluminium has made of this system the object of a series of theoretical investigations since the early times of pseudopotential theory. The specific goal was that of deriving an accurate formulation for the structure dependence of the total energy in terms of pseudopotentials[41][42]. A way to do this was provided by second order perturbation theory in the strength of the valence electrons interaction with the ionic cores, under the assumption that the observed small deviations from the free-electron band structure implied that in these materials the weak electron scattering by the metallic ions could be modelled through a correspondently weak model pseudopotential. The analysis could then proceed in explaining some structural properties of the material in terms of the detailed interaction between the pseudopotential in the G-space representation and the geometry of the reciprocal space vectors associated with the metal lattice[43]. Although the perturbative approach was successful in some respect, it was later proven to give unreliable predictions if applied to defects like the isolated vacancy.

3.2.1 The Al vacancy system.

The starting point for investigating the vacancy system was the simple picture of a vacancy in pure jellium at the metal density, in which the vacancy is simulated by a spherical "hole" in the uniform positive background charge[44]. The self-consistent (DFT) solution of such system was then used within first order perturbation theory for studying the system in which the discrete lattice of pseudoions had been substituted to the jellium positive background, to calculate the value of the vacancy formation energy in the actual metal[45]. The additional perturbative contribution for a polyvalent metal like Al turns out to be large and positive[1]

Another approach[41] consisted in rewriting the total energy for the perfect crystal obtained within second order perturbation theory in terms of a sum of pair interatomic potentials (plus a structure-independent volume term), and simply calculate the vacancy formation energy by subtracting the energy of the perfect lattice from that of the defective system. In this scheme lattice relaxation could easily be included, and good agreement with experiment was found by various authors [47][48][165].

The two approaches described were eventually proved to be inadequate (and the mentioned agreement has therefore to be considered purely fortuituos) by Evans and Finnis[49], who investigated the convergence to next (second) order in the first approach and looked at the results obtained with the second approach adopting more realistic choices of the pseudopotential, finding for the vacancy formation energy in Al values which were *negative* or anyway in very poor agreement with the experimental well assessed value of 0.66 eV [50][51][52]. Some later accurate work on the linear-response value of the formation energy confirms such conclusion, giving a result close to zero[53], which does not clearly improve by going to higher order in the perturbation expansion[54], on the convergence properties of which conclusive results are still lacking.

---

[1] Note that at the jellium-vacancy model cannot possibly represent the vacancy system in the real metal, since the vacancy formation energy in jellium is ***negative*** at the Al density[44].

A fully ab initio calculation was therefore needed for the aluminium vacancy system. The first two attempts in this direction were made in the early eighties by Chakraborty *et al.*, who investigated the Al vacancy using the DFT-LDA-PW formalism, representing the metal ions at first with an empirical model pseudopotential fitted on the crystalline properties[55], and subsequently with an ab-initio norm-conserving pseudopotential[56]. These were probably the first two calculations of this kind on defect energies in a metal ever attempted, and although they gave a rather consistent picture of the efficient electronic screening effects, they led to largely overestimated values for the vacancy formation energy (1.9 eV [55], and 1.5 eV [56]), probably because of some technical issue not completely under control. The authors concluded that the whole supercell method was not suitable for accurate formation energy calculations within the computational limitations of that time.

The next attempt on the same problem has been made in more recent times by Gillan[17](1989), using the minimisation approach described in Section 2.3.1 and a local potential for Al, constructed to reproduce the equilibrium lattice parameter and known to give satisfactory results for the bulk modulus and phonon frequencies [57]. Apart from the errors inherent to LDA and pseudopotential approximation, the calculations were shown through comparison with third order perturbation theory to be fully converged with respect to BZ sampling, supercell size, and energy cutoff, and led to a predicted value of 0.54 eV for the vacancy formation energy.

The calculations reported later in the present chapter[58] extend those results investigating the relaxed vacancy and other defective systems with the use of a norm-conserving non-local pseudopotential[11] for modelling the Al host atoms.

Meanwhile, a number of new calculations on the Al vacancy have been performed, making use of different techniques, including the use of pseudopotentials with mixed basis sets (Jansen and Klein, 1989 [166]), and of the all-electron APW technique (Mehl and Klein, 1990 [61]; Soler, 1990 [62]). The results of this last generation of calculations are all in substantial agreement with the experiment, and will be compared with our results on this system in a following section.

3.2.2 The H-Al system.

The investigation on hydrogen atoms (and other light impurities) in metals has also been the object of a large number of theoretical works over many years[63][64][65][66] [67][68]. Apart from technological reasons connected with the alteration of mechanical properties of the metals due to presence of hydrogen impurities (embrittlement, fatigue) and with the possibility of using metal hydrides as energy storage systems, there are various theoretical reasons why these systems are interesting.

One reason is connected with the hypothesis that the light hydrogen atoms are in band states in which wave functions are extended over periodic arrays of interstitial sites. If this were true, only a fully quantum mechanical treatment of the proton in the calculations could provide an adequate description of the physics of the system, and techniques like the ones utilised in the present work, which treat quantum-mechanically the electrons *only* in the solid, would be ruled out. However, the experimental observations (using ion channelling[69], or inelastic neutron scattering[70]) indicate that even in bcc metals, where extended states are more likely to form than in fcc metals due to the smaller separation between interstitial sites, the H atoms are always localised in space, *i.e.* they self-trap at the lowest-energy interstitial site in the pure metal.

The solubility of H_2 molecule in simple metals is very low (contrarily to what happens in some transition metals like Pd and Ta), of the order of 1 ppm in Al[71]. The molecule is known to dissolve in the metal and, given the low concentration, the resulting picture is that of independent screened protons as isolated impurities with no complicated core-electron structure. We have in other words the simplest possible impurity system treatable studying the ground state electronic properties *only*, in a class of materials for which the (spherically symmetric) free-electron gas approximation constitutes a reasonable starting point for modelling the valence electrons. Note that now a much stronger (point-like) defect than a vacancy is introduced in the pure material, the screening of which can accordingly be expected to be much less dependent on the metal ions arrangement than in the vacancy case. It is therefore not surprising that much theoretical work has been devoted to this system, and that the first attempts to study its energetics were performed taking in account the ionic lattice by perturbation theory.

Following this line Popovic and Stott (1974) [72] found that the octahedral site in Al (rather than the tetrahedral site) was the most stable position for the interstitial hydrogen, while a much lower energy than in either cases was found for the substitutional hydrogen system. To give some idea of the reliability of this *first order* perturbation treatment of the metal ions (the non-linear screening having been treated self-consistently in the DFT scheme by the mentioned authors) we anticipate here that *none* of these conclusions is in agreement with the results of the fully self-consistent calculations of the present work[59]. The model was also predicting a value of 0.45 eV for the hydrogen heat of solution[73] (non-inclusive of ions relaxation[2]), in good agreement with the experimental results 0.66 eV[71], 0.83 eV[74]. However, a later systematic study of the energy profiles for light impurities in simple metals using a number of different pseudopotentials, proved that the question of the relative stability of the interstitial sites could not be answered within the model, since the results were too much pseudopotential-dependent[75].

A different approach was based on the idea of spherically averaging the pseudopotential effects around the high symmetry interstitial (or substitutional) sites, and then solving self-consistently the resulting symmetric problem[76]. Such approach was applied to the H-Al system by Manninen and Nieminen[77], who found the interstitial octahedral site to be the most stable one (in particular, *more* stable than the substitutional H arrangement). In spite of the rather crude spherical modelling of the interaction of the electrons with the ions (reducing to a spherical distribution the *four* or *six* Al atoms nearest neighbours to the defect) and in spite of the rather simple form of the pseudopotential itself (an empirical "empty core" potential[7], cf. eqn. (1.33)), the resulting heat of solution of 0.19 eV was in reasonable agreement with the experimental value. The addition of non-spherical corrections[78] and ionic relaxation[79] to the same

---

[2] The heat of solution is *positive*, *i.e.* hydrogen is not spontaneously absorbed by the metal. The value reported in ref.[73] would be *lowered* by the inclusion of relaxation effects.

model was later proven to introduce negligible corrections to the heat of solution[78], while the choice of a similar but smoother empirical potential (in a modified Heine-Abarenkov form[81]) led to the new result of 0.593 eV [80].

Channelling experiments by Bugeat *et al.* on H-Al samples prepared by ion implantation [69][82] had meanwhile brought some evidence that hydrogen at low temperature (35-300^oK) occupies the tetrahedral interstitial site, or more probably gets trapped close to a vacant site occupying a displaced position towards one of the eight tetrahedral sites which surround the vacancy in the fcc lattice. Similar conclusions were also reached from μSR experiments on pure Al[83] and Al alloyed with Mn[84], which showed that (i) vacancy defects have a determinant role in trapping muons and that (ii) tetrahedral coordination of the μ site is found down to below 20^oK, due to presence of defects. The conclusions at this stage, given the theoretical results available, were[69] that it was not possible to exclude (considering the difference of masses between H and μ) some interstitial trapping of H in Al, although the evidence was for vacancy-induced tetrahedral trapping, and that it was still possible that the most stable trapping site were the octahedral one at very low temperature ($\approx$ 5^oK), although all the experiments down to 20^oK had shown the tetrahedral site to be most stable one.

The first-order perturbation methods were at this point extended to the case of non-substitutional pairs of H atoms in a dumbbell arrangement at the vacancy site[85], and re-investigated with more precise density distributions for the screening charge in the jellium calculations[86]. It was found that the non-substitutional off-centre H at the vacancy was in fact the most stable configuration (with a trapping energy of 1 eV), while the tetrahedral site was now predicted to be the interstitial site associated with the lowest energy[87]. A new value of 1.3 eV for the H heat of solution in the perfect metal lattice was also calculated[87], using an Al pseudopotential substantially identical to the ones used previously in refs. [73] and [77].

The models described so far suffered at least from two major sources of errors. The first and most important was clearly the extreme sensitivity of the results to the model pseudopotential choice. The second was the assumption that the local environment in

the solid could be simulated for all the screening properties with an uniform background of valence charge at the average density of the metal. This second approximation was investigated in a series of works in which the energy of light neutral atomic impurities in a metallic host was assumed to be function of the value and of the local gradients of the host valence density at the interstitial site considered. The energy terms up to second order in the charge distortion from the jellium case were then included in the calculations through different formulations ("Effective Medium Theory", Nørskov, 1980 [88]; "Quasiatoms approach", Stott and Zaremba, 1980 [89]).
The ideas at the basis of these formulations were overall not dissimilar from those behind the local density approximation for electronic exchange and correlation (see Section 1.4). The main assumption was that the electronic structure and the total energy of the impurity atom depend primarily on the local environment, reflecting the balance between the tendency to charge neutrality (*i.e.* the screening) and the energy terms originating from orthonormality and exchange and correlation. The immersion energy of atoms in an electron gas as a function of density was therefore extensively studied, to provide a database for more sophisticate modelling, and to help in discuss issues such as the identity of the preferred impurity trapping-sites on the basis of the valence charge modulation in the pure solid host[88][89][90].

The calculations we report in the present work provide results which can be usefully discussed on the basis of the previous treatments of the H-Al system described above, but do not suffer from the most serious approximations made in those works. In all our calculations the ions were relaxed to their zero-force positions (the lattice relaxation has been mostly ignored as unimportant in precedent calculations, with very few exceptions[79][91]). The core-valence interaction for aluminium is represented by a fully ab-initio pseudopotential[11], and we adopt the local density approximation, these two being the only approximations in the calculations whose effects cannot be systematically monitored. The calculations concern isolated defects, but adopt periodic boundary conditions, and in principle this could introduce spurious effects of interactions between (screened) defects situated in neighbouring supercells. Moreover, a finite cutoff must be used to truncate the PW basis set. Evidence that both these issues are under adequate technical control will be provided with the results.

3.3 Definitions of defect energies.

From the point of view of the practical calculations involving the use of periodic boundary conditions, quantities like the energy of formation of an isolated defect need an operative definition taking into account the volume relaxation effects. The energy of formation E_f of the vacancy is the energy change when an atom is removed from the perfect bulk crystal and replaced on a new bulk site. Note that in any realistic sample of "perfect crystal" all the bulk sites would be by definition occupied, and the ion displaced to create the vacancy would have to be put on the surface. This can still be thought to induce one of the atoms previously on the surface to sink into the bulk crystal, so that the definition given above of vacancy formation energy makes sense in real experiments, in which the vacancy defects are activated and annealed by thermal treatment[52][92][93], the total number of metal atoms remaining constant.

A more detailed definition depends on the conditions under which the vacancy is formed. In the calculations there are three natural conditions, which correspond to the vacancy being formed at constant *volume*, at constant *pressure*, or at constant *lattice parameter*. We shall denote with $E(N, \nu_v; \Omega)$ the energy of a system of N atoms and ν_v vacancies atoms occupying $N + \nu_v$ regular lattice sites, in the total volume Ω. The formation energy at constant *volume* is is defined by

$$E_f^v = E(N, 1; \Omega) - E(N, 0; \Omega) . \tag{3.1}$$

In the limit of infinite system (N and Ω going to infinity with the ratio N/Ω kept fixed at the perfect lattice value) this definition gives the quantity of physical interest. The formation energies at constant pressure E_f^p or at constant lattice parameter E_f^a are defined in an analogous way, substituting the explicit dependence in the function E.

The meaning of E_f^a is easily seen writing it in terms of volume

$$E_f^a = E(N,1;\frac{N+1}{N}\Omega_a) - E(N,0;\Omega_a) , \tag{3.2}$$

as the energy of formation obtained when the vacancy is allowed to form with the addition of one atomic volume, Ω_a being the volume of N atoms in the perfect crystal of lattice constant a.

The relation between E_f^p and E_f^v involves the vacancy volume of formation Ω_f, which is defined as the volume change in the system considered when a vacancy is formed at constant pressure. If we denote with $\Omega(N,\nu_v;p)$ the equilibrium volume of the system of N atoms and ν_v vacancies at pressure p, we obtain:

$$\Omega_f = \Omega(N,1;p) - \Omega(N,0;p) . \tag{3.3}$$

The energy of formation at constant pressure can therefore be written as

$$E_f^p = E(N,1;\Omega_0 + \Omega_f) - E(N,0;\Omega_0) , \tag{3.4}$$

where $\Omega_0 = \Omega(N,0;p)$. We then expand the energy up to quadratic order in the small volume change Ω_f, and obtain:

$$E_f^p = E_f^v + \Omega_f \frac{\partial E}{\partial \Omega}(N,1;\Omega_0) + \frac{1}{2}\Omega_f^2 \frac{\partial^2 E}{\partial \Omega^2}(N,1;\Omega_0) , \tag{3.5}$$

which rewritten in terms of pressure p and bulk modulus B in the vacancy system gives

$$E_f^v = E_f^p + p\Omega_f + \frac{1}{2}\Omega_f^2 B/\Omega . \tag{3.6}$$

A similar relation is readily obtained for E_f^a

$$E_f^a = E_f^p + p(\Omega_c - \Omega_f) + \frac{1}{2}(\Omega_c - \Omega_f)^2 B/\Omega , \tag{3.7}$$

where now Ω_c is the equilibrium volume[3] for one atom in the perfect system at pressure p . Given the relations (3.6) and (3.7), each of the three defined formation energies

---

[3] It does not matter to which of the conditions examined the bulk modulus B refers to, since it appears in the second order term, and its own dependence on volume changes would introduce corrections of third order at most.

can be calculated with good accuracy from any of the other two, provided that some information is known about the volumic relaxation of the system when the vacancy is created.

Note that in the case $p = 0$, which is usually the one of interest in literature, all the definitions converge to the same value in the limit of infinite systems, so that the relations (3.6) and (3.7) provide in this case a simple check to investigate the convergence with respect to system size. Since the systems treatable in actual calculations are finite, the actual recipe for performing the calculations should be the one which exploits the fastest convergence with respect to system size. Since it has been shown in a precedent work[17] that fast convergence can be expected for the vacancy energy of formation calculated at constant volume (3.1), we have chosen to calculate E_f^v.

The periodic boundary conditions pose some restrictions on the geometry of the systems investigated. The calculations have to be performed with supercells of atoms, having the same number of regular lattice sites both in the perfect and in the defective system. The definition in (3.1) for E_f^v has to be adapted for practical use in the calculations, rewriting it into the form

$$E_f^v = E(N-1,1;(N-1)\Omega/N) - \frac{N-1}{N}E(N,0;\Omega) \ , \tag{3.8}$$

where now both the energy terms in the right term of the equations refer to the same number of lattice sites $N + \nu_v$.

The self-interstitial energy is defined as the energy difference between a system of N atoms sitting on $N-1$ regular lattice sites and one interstitial site, minus the energy of N atoms in the perfect crystal, and we calculate it as

$$E_f^{self} \ = \ E(N,\nu_{self}=1;\Omega) \ - \ \frac{N+1}{N}E(N,\nu_{self}=0;\Omega) \ , \tag{3.9}$$

where now ν_{self} is the number of self-interstitial atoms in the system, and Ω is the equilibrium volume of a perfect system of N atoms.

In an analogous way we define the embedding energy of H in Al as the change of energy when going from perfect bulk aluminium plus an isolated hydrogen atom to the metal system of same volume and same number of atoms plus an hydrogen atom sitting at an interstitial site. The heat of solution of H in Al is obtained in the analogous way starting from molecular (instead of atomic) hydrogen in the reference system.

Furthermore, we define the vacancy migration energy as the energy barrier which has to be surmounted by the vacancy when moving from one site to a neighbouring site previously occupied by an atom which moves during the process into the original vacant site. We assume that in the saddle-point configuration the migrating atom is midway between two nearest-neighbour lattice sites. The vacancy migration energy E_m^{vac} is then the energy difference between this fully relaxed saddle-point configuration and the fully relaxed system in which the vacancy is on a regular site.

Finally, we define the migration energy E_m^H for the diffusion of H in Al as the energy barrier which hydrogen has to surmount when diffusing between interstitial sites. Some further considerations on the geometry of the diffusion process are included in a later section.

3.4 Setting up of calculations and bulk results.

In this section some technical details of the calculations are provided. It is customary before proceeding with the larger defect calculations to test the techniques determining some properties of the perfect crystal, and some results are therefore included on the pure Al bulk. We will refer to Chapters 1 and 2 for the description of the energy minimisation procedure, and describe here only the actual calculation setting up.

The total free energy is minimised with the strategy described in Section 2.3.1. To evaluate the exchange and correlation contribution to the total energy within the local density approximation (see Section 1.4), we adopt the Perdew and Zunger parametrisation[146] of the results for the electron-gas correlation energy originally calculated by Ceperley and Alder[3]. For the Al pseudopotential we use a pseudopotential as constructed by Bachelet *et al.* [11] in the form discussed in Section 1.5.2, and we represent it in the fully non local form due to Kleinman and Bylander (cf. eqn. (2.33)). The $d-$wave v_2 is used as local part in the semilocal form (eqn. (2.30)), and all the terms with $l > 2$ are not included in the pseudopotential expansion. The possibility that "ghost states" might occur in the KB form we adopt for the pseudopotential has been investigated and ruled out by a recent systematic study[94]. The transferability properties of the pseudopotential can be expected to be good from the behaviour of the logarithmic derivatives of the pseudo-wavefunctions versus the all-electron wavefunctions, which for each angular symmetry match each other well within a window of about 1 Hartree around the atomic eigenvalues.

The calculations are performed on three supercells of 8 (fcc) , 16 (bcc), and 27 (fcc) regular lattice sites. The k-point sampling sets are Monkhorst-Pack special-point grids[32] of various sizes, reduced by symmetry to the minimal set of k-points inequivalent by point-group rotations. Symmetrisation is performed accordingly during the runs on the charge density and the non-local forces on the ions. The smearing of the Fermi energy surface is performed with fractional occupation of orbitals using the Fermi-Dirac occupation function[17] as discussed in Section 2.5, and the ground state energy E_0 of the system is estimated through the entropy correction defined by eqn. (2.75), as the average of F and E extracted from the calculations at finite smearing. The smearing linewidth kT (cf. eqn.(2.65)) has been set in all calculation to one tenth of the Fermi energy of jellium at the system's average electron density. Tests performed at different values of T indicate that the deviation of *total* energy from its value at $T = 0$ is less than a few hundredths of an eV per atom. Extensive tests on the convergence of the total corrected energy in Al with respect to smearing width and number of BZ sampling points are reported in Appendix A.

In all calculations involving defects the ions are relaxed to complete equilibrium with a steepest descent procedure while the electronic charge is kept fixed as described in Section 2.3.1.5 . The ionic displacements take place along the gradient directions (or "forces") of eqn. (2.19). As previously mentioned these directions are constrained not to break the initial symmetry of the system while the ions are displaced. In our calculations this means that all the cubic point group elements (space rotations centered on the defect site combined or not with inversion) which leave invariant the system at the beginning of each calculation are used along all the run for symmetrising the self-consistent charge density and the forces over the ions. This means that in cases in which the energy could be lowered by symmetry-breaking, the algorithm would *fail* to detect the true ground state. In the situations studied in the present work it is highly unlikely that symmetry-breaking mechanisms could lead to lower energies, so that all the symmetry constraints compatible with the initially unrelaxed defect geometry have been imposed in all cases to maximise the efficiency of the algorithm and the speed of calculations.

The calculations on the bulk crystal give results which confirm the adequacy of the techniques used. The parabolic fit of a series of five calculations made on the 16-atom system with two inequivalent k-points at uniformly spaced values of the lattice parameter a, gives the values $a_0 = 7.66$ *a.u.*, and $B = 0.722$ *Mbar* for the equilibrium lattice parameter and the bulk modulus, in good agreement with the experimental values $a_0 = 7.64$ *a.u.* and $B = 0.722$ *Mbar* (taken from ref. [56] and references therein). The calculations were made at constant number of plane waves, with an energy cutoff which at the experimental value of a_0 equals 13 Hartree. A close spacing of 0.025 *a.u.* was used between nearest values of the lattice parameter, and the residual variance of the calculated energies from the parabolic distribution resulted completely negligible.

3.5 The jellium correction and the equilibrium vacancy.

The energy cutoff of 13 Hartree has been used in the calculations on all defective systems. Given the fast G-space convergency properties which can be expected studying a supercell containing aluminium atoms only, this cutoff is probably more than enough for the calculations on the the vacancy system, in which the errors due to the incompleteness of the basis set should be negligible.

The ground state energy of the bulk, the unrelaxed vacancy and the relaxed vacancy have been calculated[4] for the 8-atoms, 16-atoms, and 27-atoms systems, holding fixed in all the bulk calculations the lattice parameter at the experimental value of 7.64 *a.u.*, and lowering it in the calculations involving vacancies to keep constant the number of atoms per unit volume (*i.e.* the average electron density).

The technical errors which can be expect to be left in the calculations are due to (i) interaction of defects between supercells (of direct chemical nature, or because of interference between periodic constraints and ionic relaxation), and (ii) imperfection of the BZ sampling, in spite of the smearing scheme utilised. The results for the vacancy formation energy are obtained as differences of large calculated energies for supercells of very dissimilar ionic arrangements, so that the BZ integration on a small fixed number of special points (*two* in the irreducible BZ wedge for the two bigger supercells) can introduce a sampling error which does not cancel away in the differences, although it is expected to decrease increasing the system size. A correction for this error can however be applied to the calculated results, based on the hypothesis that the sampling error we commit is similar to that which we would commit in calculations on pure jellium.

The calculated formation energy of equation (3.8) can be thought as the difference between the results of two BZ integrations referring to two metal systems of same average electron density. The leading error in the integrations is made in the band energy contribution, and is mostly connected with imperfect sampling of the electronic kinetic energy in the proximity of the Fermi level, as previously discussed. The band structure of the two systems at the Fermi level is also expected to be very similar, if we assume that the electrons close to the Fermi energy in a nearly free-electron-gas metal of given density do not strongly couple with the ionic positions.

In particular, if we "smear out" the (weak) atomic pseudopotentials to a positive uniform charge distribution we get the jellium model, with a band structure at the Fermi level still similar to those of our starting systems, but for which the vacancy formation energy represented by the difference (3.8) is *exactly* zero. However, the two total-energy calculations needed for the difference have to be made using a BZ sampling

---

[4] In the 8-atom supercell the ionic relaxation is forbidden by symmetry.

set of special points which is the same in the *relative* reciprocal space coordinate systems of the two calculations[32], while is not the same in *absolute* reciprocal space coordinates, since the two supercells of the calculations have different volumes.
The value ΔE_{jell} of the difference $E(N-1,1;(N-1)/N\ \Omega)\ -\ E(N,0;\Omega)(N-1)/N$ calculated for supercells of pure jellium is therefore a nonzero quantity, since it contains a sampling error. This error is hopefully almost identical to the one we commit in the pseudopotential calculation of E_f^v using the same supercells. A better value for the vacancy formation energy can therefore be readily obtained by subtracting from E_f^v the jellium correction ΔE_{jell} calculated for the same system geometry and BZ sampling.[5]
Since the defect screening in the metal is expected to be very efficient, the spurious interaction between defects due to periodicity is expected to quickly vanish with encreasing system size, the only error left for well separated defects and limited special points sets being the one committed on the BZ averages. If applying the described procedure to correct the BZ sampling error we obtain good convergence of the vacancy formation energy with respect to system size, it is reasonable to assume that both the sources of error have been removed within the convergence accuracy by the time we get to the biggest supercell.
The results we have obtained for the fully relaxed vacancy formation energy in Al are summarised in the table (3.1) on page 83, for the three supercell sizes. The results are reported both without (uncorrected) and with (corrected) the jellium correction. The values for the relaxation displacement of the vacancy neighbours are given in units of the nearest neighbour distance in the perfect fcc lattice (2.86 *a.u.*).

The convergence of corrected energies appears to be reached within 0.1 *eV* by the time we get to the value of 0.55 *eV*, which should be the most reliable result, to be compared with the experimental enthalpy of formation 0.66 *eV*. Values for the relaxation displacements of other ions than the nearest neighbours to the vacancy are

---

[5] Obviously the jellium correction is *not* calculated at the same energy cutoff used for the actual metal: because of the PW basis set used, the additional computer time for calculating the correction is insignificant.

not reported since such relaxation is found to be extremely small (less than 10^{-2} *a.u.*). An illustration of the valence charge density distribution around a relaxed vacancy is given in figures 3.1 and 3.2 on page 84, respectively for the two planes (100) and (110), corresponding to a face and to a diagonal section of the unit face-centered cube with origin in the vacant site. The units for the numbers on the contour levels are 10^{-2} *a.u.* ($a.u. = e/a_0^3$). The main feature of the pictures is the strong charge density deviation in the vacancy region from its values in the surrounding lattice, with a minimum value of 0.29 in the vacancy center, to be compared with the average electronic density value of 2.7 in the bulk metal.

A plot of the valence electron density from the vacancy center along the (100), (110), and (111) directions is reported in figure 3.3 on page 85. The full circles correspond to the calculated values from the original investigation of Chakraborty *et al.*[56], as reported in reference [95]. The charge distribution is essentially symmetric with a shallow minimum at the vacant site. The strong anisotropy from a spherical charge distribution arises with the build-up of valence charge when approaching the nearest neighbour atom in the centre of the face ((110) direction), the charge saddle point between the vacancy and the octahedral site ((111) direction) and the second nearest neighbour at the opposite vertex of the fcc cube when moving along the cube's edge direction (100). Such anisotropy is mostly due to the localisation of the neighbouring Al atoms (and *not* to the actual chemical interaction between the defect and the valence charge screening the core ions).[6]

This is evident in the plots of figures 3.4 and 3.5 (page 86), which have been obtained from unrelaxed vacancy calculations by subtracting the bulk valence density from the ground state distribution, both systems having the same lattice parameter. The plots refer again to the 27-atom system, length scales, units, and plane geometries being exactly the same as in figures 3.1 and 3.2 (page 86).

---

[6] For a collection of radial charge distributions obtained within spherical approximation in the jellium model ref. [49] should be consulted. The main disagreement between the predictions of the various approximated models seems to be for the value of the density charge in the center of the vacancy, while all the models seem to be equivalent in the outer vacancy region, where however the

The shape of the displaced charge is seen to be almost spherical although some features are left of the underlying subtracted lattice in correspondence with the neighbouring atoms positions. Such features appear to interfere with the Friedel oscillations visible in the outer screening regions, which are the only displaced charge structures left by the subtraction in the physical space between the periodically repeated vacancies. The entity of such oscillations is easily seen to be very small after the first three or four *a.u.* from the defect centre. This suggests that the electronic interaction between vacancies for this largest cell-size should be negligible.

We turn now to the analysis of the dependence of the calculated value of the vacancy formation energy from the particular definition adopted since to each different definition corresponds a slightly different recipe for the volume at which the calculation on the defective system has to be performed, as discussed in Section (3.3). The formation volume Ω_f of the vacancy has been calculated fitting the energy results of calculations on relaxed vacancy systems at different lattice parameters, as previously done for the bulk. The zero-pressure volume of the system determined by the fit has been used to calculate Ω_f from the definition (3.3), as the equilibrium volume of the supercell with 15 Al atoms and one vacancy minus the volume of 15 Al atoms in the perfect lattice. Our calculated result is $\Omega_f = 0.71\ \Omega_c$, where Ω_c is the bulk atomic volume, in good agreement with the experimental values of $0.60 \pm 0.02\ \Omega_c$ [93], $0.55\ \Omega_c$ [96] *et al.* and $0.68 \pm 0.1\ \Omega_c$ [41], as reviewed by Seeger *et al.* [97].
From the calculated values of the volumes Ω_f, Ω_c we can use the relations (3.7) and (3.6) to estimate the convergence of volumic effects in the vacancy energy of formation which we obtained for the 27-atom system. Some results (without jellium correction) are reported in table 3.2 on page 83, where fully calculated values (from definitions (3.1) and (3.2)) of E_f^v and E_f^a are reported, together with the estimated values of E_f^p and E_f^a evaluated from E_f^v using the second order expansions (3.6) and (3.7). The relaxation energies from the full calculations, which are obviously independent from the jellium

---

spherical approximation breaks as shown by figure 3.4 and 3.5 on page 86.

correction, are also included. The results show that while the second order expansions allow to recover a fraction of about 90% of the difference between the formation energies calculated using different definitions, this difference itself is of the order of 0.1 *eV* only. The relaxation energies contribute to the vacancy formation energy value within about the same range of 0.1 *eV*.

3.6 Vacancy migration and self-interstitial.

We assume that the migration path of one ion leaving a lattice site and moving into a previously vacant site takes place along a (110) direction (*i.e.* the vacancy moves onto a nearest neighbour site). We also assume that the surface energy for the migration has a saddle point when the atom is located midway between two vacant sites.[7]. Since for symmetry reasons no net force can be exerted on the migrating atom at the saddle point, the calculations for the fully relaxed energy migration can be performed without imposing constraints to the atomic relaxation. The results from the 16-atom and 27-atom systems are respectively 0.59 *eV* and 0.57 *eV*, to be compared with the experimental value of 0.62 *eV*[97].

The relaxation effects for the migrating vacancy calculations are bigger than those for the equilibrium vacancy. The displacement pattern observed consists of the migrating ion pushing its nearest neighbour atoms (the ones belonging to tetrahedrons of fcc lattice sites which include the two vacant sites) away from the saddle point, and pulling the second nearest neighbour atoms (the ones at the closest vertices of the two cubic centered faces containing both the vacant sites). The displacements are respectively the fractions 0.041 and 0.015 of the bulk nearest neighbour distance (cf. with the equilibrium vacancy in table 3.1). Valence charge density plots for the (100) and (110) planes containing the two vacancies are reported in figures 3.6 and 3.7 on page 87.

---

[7] For symmetry reasons at such point the energy is stationary in the (110) direction and in the (110) plane normal to it, so the assumption corresponds to saying that the point is not a local maximum for the migration energy surface.

The main difference between the self-interstitial system and the other defective systems treated in the present work is the size and range of the relaxation effects around the defect. Due to the close-packed structure of the pure metal, any supplementary interstitial metal ion is bound to strongly distort the shells of surrounding ions, so that the defect is expected to have a much higher energy of formation and a much lower mobility than smaller impurities like hydrogen. The experimental value for the energy of formation of the self-interstitial has to be obtained from the formation energy of the Frenkel defect 3.9 ± 0.5 eV [92], to which the formation energy of an isolated vacancy 0.66 eV has to be subtracted, to give $E_f^{self} = 3.2 \pm 0.5$ eV.

Our results about the self-interstitial are only preliminary. The investigated geometry is that of an interstitial Al atom sitting on the octahedral site in the middle of an Al face centered cube. Calculations have been performed for the unrelaxed and relaxed systems. The ionic relaxation is constrained by symmetry not to break the octahedral point symmetry around the defect, which correspond to the full cubic point group of rotations and inversion (48 operations) around the defect site. Our calculated results (at constant volume) are 9.7 eV and 2.8 eV for the unrelaxed and relaxed interstitial, with the six nearest neighbour atoms resulting displaced of 19% (≈ 0.7 *a.u.*) of their original distance from the interstitial. As a final remark we note that some evidence exists for another possible self-interstitial geometry arrangement for fcc metals[92], in which Al interstitial atoms produced by electron or neutron irradiation and analysed by X-ray diffusion scattering[104] appear to be positioned in a (100) dumbbell arrangement centered on an empty regular lattice site[105]. The investigation on the energetics of that system geometry is an issue left open for future work.

The results obtained for the defect energetics in Al are summarised in table 3.3 on page 85 . The comparison between the results of various theoretical calculations is shown in the table to be overall rather good. The APW calculations of references [62] and [61] do not suffer from the pseudopotential approximation, the only approximation left being the LDA. The calculations of reference [166] make use of a mixed-basis approach, in which the KS orbitals are expanded on a superposition of atomic pseudowavefunctions and plane waves, and give the value for the vacancy formation energy in closest agreement with the one we obtain[8].

The comparison with experiment must take into account the fact that the experiments consist of high temperature measures, which should be corrected for the additional entropic contributions enabled at non-zero temperatures. The measured value with which we compare our calculated value for E_f is the experimental enthalpy of formation, in which the entropic contribution are expected to be small[98] and can be estimated from a direct dynamic simulation[53] to be of the order of 0.1 eV.

---

[8] The authors in ref. [166] have implemented their calculation on a second very similar norm-conserving pseudopotential, and both are by construction very similar to the one we have used. For this second pseudopotential they appear to obtain a rather large calculated value of $E_f^{vac} = 1\ eV$.

No. of sites in the cell	8	16	27
Relaxed (uncorrected) E_f^v (eV)	0.768	0.882	0.590
Jellium correction $\Delta E_{jell}(eV)$	0.103	-0.260	-0.043
Relaxed (corrected) E_f^v (eV)	0.871	0.622	0.547
Relaxation energy (eV)	-	-0.060	-0.075
Relaxation displacement	-	0.011	0.014

Table 3.1: Calculated values for the relaxed vacancy formation energy in Al.

	E_f^v (eV)	E_f^a (full calc.) (eV)	E_f^a (est.) (eV)	E_f^p (est.) (eV)
Ions relaxed	0.589	0.500	0.487	0.483
Ions unrelaxed	0.664	0.552	-	-
Relax. energy	-0.075	-0.052	-	-

Table 3.2: Vacancy energies of formation and relaxation energies for the 27-atom cell from full calculations at constant volume and lattice parameter. Estimates of the formation energy at constant pressure and at constant lattice parameter from equations (3.6) and (3.7) are also provided. The jellium correction is not included.

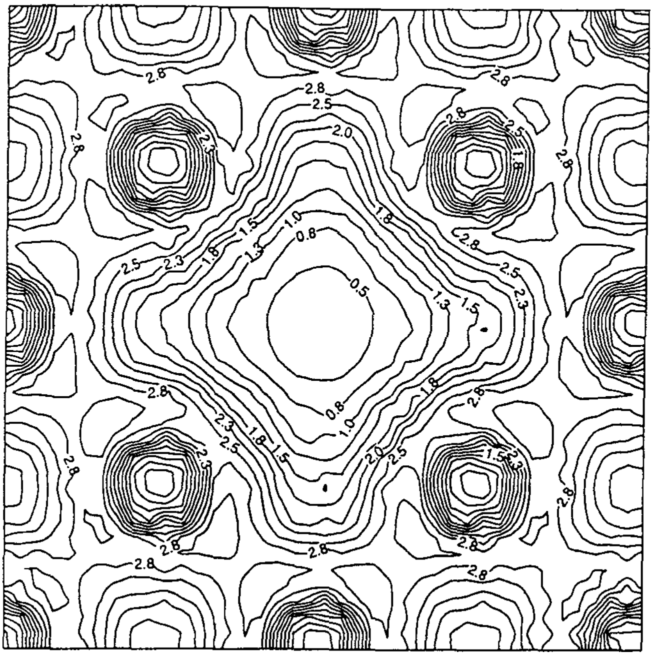

Figure 3.1: Valence charge density for the relaxed vacancy, (100) plane.

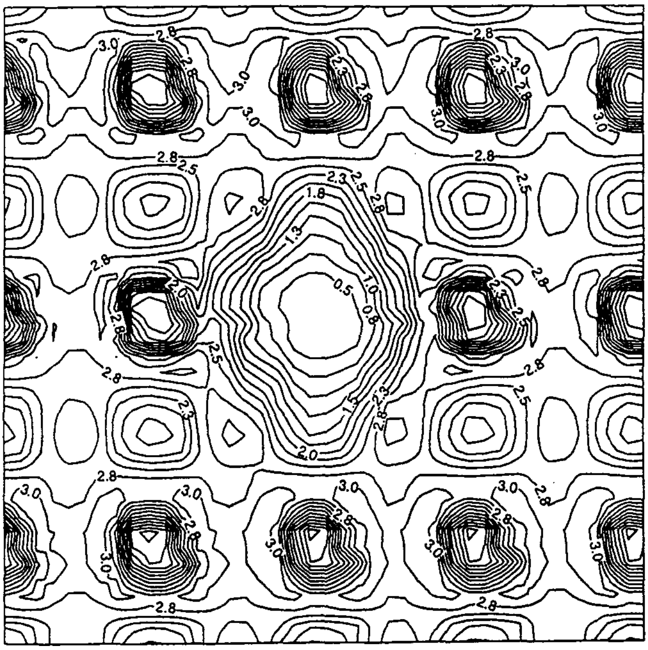

Figure 3.2: Valence charge density for the relaxed vacancy, (110) plane.

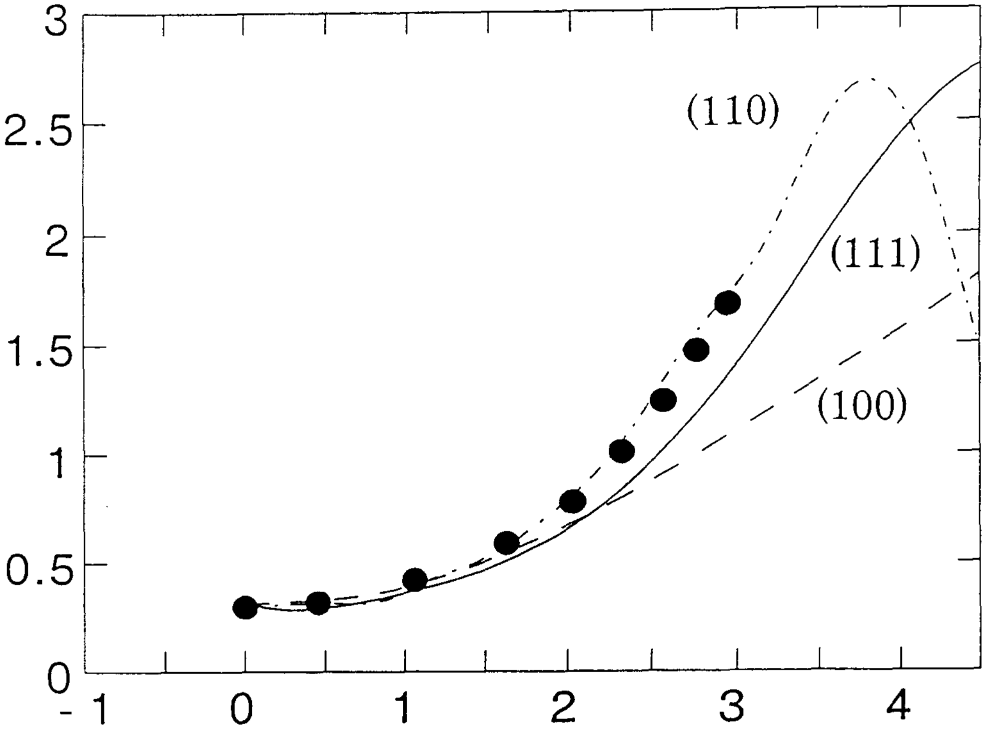

Figure 3.3: Valence electron density (units of 10^{-2} *a.u.*) as a function of the distance (*a.u.*) from the vacancy centre along the directions (110), (111), and (100). Solid circles from ref. [56] as reported in ref. [95].

	E_f (eV)	E_m (eV)	Ω_f/Ω_c	$E_f^{self.}$ (eV)
theory	0.52^a	-	-	10.2^a
	0.84^b	-	-	-
	0.73^c	0.7^c	0.66^c	3.4^c
	0.55^d	0.57^d	0.72^d	2.8^d
experiment	0.66^e	0.62^f	0.62^g	3.2^f

Table 3.3: Comparison of our calculated results for the vacancy formation and migration energies E_f and E_m, the vacancy formation volume Ω_f in terms of the atomic volume Ω_c, and the formation energy E_f^{self} of the self-interstitial, with experimental and other theoretical results. References are: (a) pseudopotential calculation of Jansen and Klein (1989)[166]; (b) LAPW calculation of Mehl and Klein (1990)[61]; (c) APW calculation of Denteneer and Soler (1990)[62]; (d) present work[59]; (e) Fluss *et al.* (1978)[52]; (f) Schilling (1978)[92]; (g) Emrick and McArdle (1969)[93]. Note that the calculation of Jansen and Klein does not include lattice relaxation.

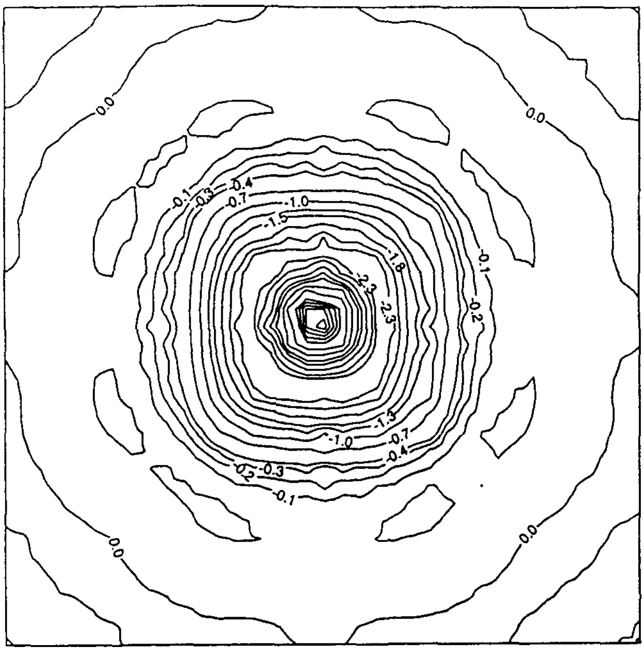

Figure 3.4: Displaced charge density for the unrelaxed 27-atoms vacancy system, plane (100). Units and length scales as in figure 3.1.

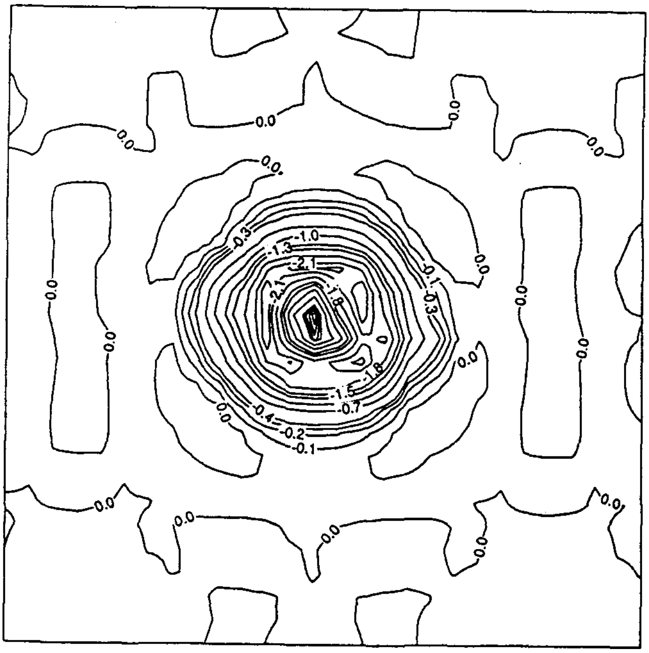

Figure 3.5: Displaced charge density for the unrelaxed 27-atoms vacancy system, plane (110). Units and length scales as in figure 3.2.

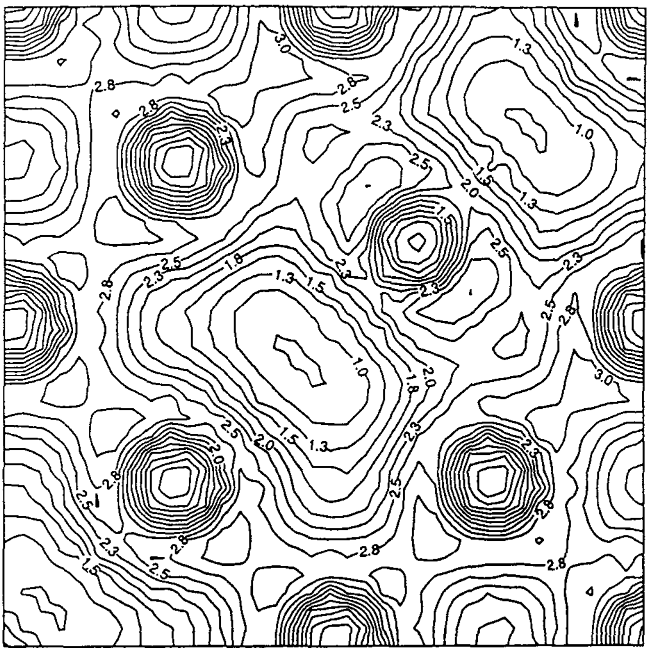

Figure 3.6: Valence charge density for the vacancy migration in the (100) plane. (27-atom system).

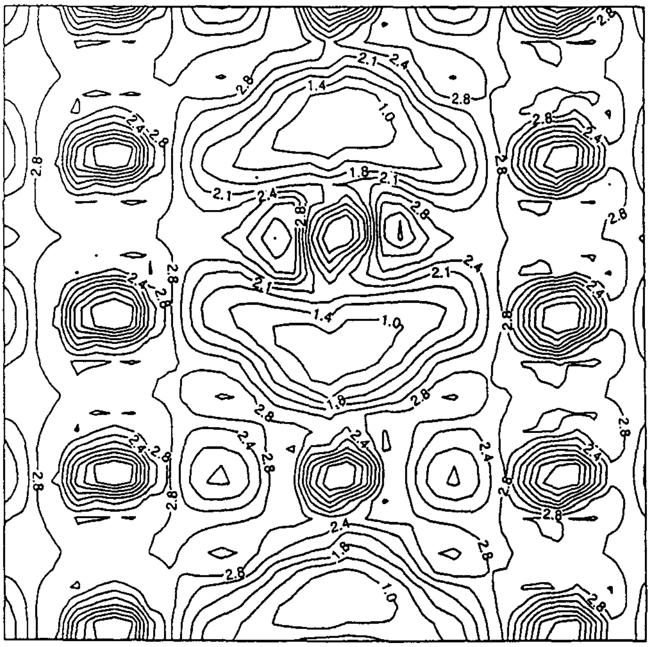

Figure 3.7: Valence charge density for the vacancy migration in the (110) plane. (27-atom system).

3.7 The hydrogen impurity and the convergence with energy cutoff.

The introduction in the calculations of an hydrogen atom represented by a bare Coulomb potential raises the problem of the total energy convergence when the potential presents singularities. The problem arises from the fact that every KS eigenstate $\psi_i(\mathbf{r})$ having non-zero value at the proton site is bound to satisfy the local exact cancellation between the kinetic and potential terms of its local energy

$$\frac{H\psi_i(\mathbf{r})}{\psi_i(\mathbf{r})} = V_{KS}(\mathbf{r}) + \frac{-\frac{\hbar^2\nabla^2}{2m}\psi_i(\mathbf{r})}{\psi_i(\mathbf{r})} = \epsilon_i \; . \tag{3.10}$$

Both these terms must be diverging for the Coulomb singularity in $V_{KS}(\mathbf{r})$ to be cancelled, and any deviation in the wavefunction from the exact fulfillment of the cancellation constraint (or "cusp condition") will lead to locally divergent terms, and to an overall variational raise of the expectation value ϵ_i [9].

The cancellation constraints imply that the eigenstates which are non-zero on the proton site (where the hermitian operator $\hat{H}$ can be extended even if the hamiltonian as a differential operator is not defined, so that the solutions ψ_i can be shown to be uniquely defined[99],[100][101]) have also discontinuous first derivatives (a "cusp") there. In the PW representation the variational convergence of the wavefunctions to the correct cusp shape is rather slow, and therefore the convergence of the ground state energy with respect to the energy cutoff used to truncate the PW basis set is also slow. The approximation introduced by the PW representation corresponds to disregarding the potential matrix elements involving plane waves with kinetic energy bigger than the energy cutoff used. The error on the energy due to the potential terms ignored gets smaller and smaller while the energy cutoff is raised, and vanishes in the limit of infinite cutoff. Traditional methods are however available for correcting the energy within perturbation theory. In a classic work by Löwdin[102] a recipe is provided for

---

[9] Note that the expectation value coincides with the eigenvalue within the basis set representation, on which we assume that the self-consistent hamiltonian has been diagonalised.

improving the hamiltonian matrix represented on a limited basis set (*e.g.* within a first "primary" cutoff) so that its eigenvalues coincide up to second perturbative order with the eigenvalues of the full hamiltonian matrix represented on a larger basis set (up to a bigger "secondary" cutoff). The corrected hamiltonian matrix elements read

$$U_{i,j} = H_{i,j} + \Delta_{i,j} \; ; \qquad \Delta_{i,j} = \sum_{\alpha} \frac{H_{i,\alpha} H^{*}_{\alpha,j}}{E - H_{\alpha,\alpha}} \, , \tag{3.11}$$

where $H_{i,j}$ are the matrix elements on the original limited basis (indexes i, j), the index α spans the states added to get to the larger basis set, and E is an energy which has to be adjusted in the portion of the eigenvalue spectrum considered. In a self-consistent PW calculation the matrix $H_{i,j}$ represents the KS hamiltonian, and α spans the set of plane waves between the primary and secondary cutoff (these plane waves are by definition eigenstates of the KS eigenproblem in which the potential is represented within the first cutoff G_1^{cut} only). Once we have determined the occupied set of eigenstates within the first cutoff, and treating the term $\Delta_{i,j}$ within first perturbative order, we get the corrected expression for the band energy:

$$E'_{band} = E_{band} + 2 \sum_{i=1}^{N_{orb}} \sum_{G_1^{cut} < |\mathbf{G}_\alpha| < G_2^{cut}} \frac{|H_{i,\alpha}|^2}{\epsilon_i - \frac{G_\alpha^2}{2}} \, , \tag{3.12}$$

where G_2^{cut} corresponds to the second and much higher energy cutoff. N_{orb} is as usual the number of occupied orbitals, and E_{band} is the band energy from the full calculation at the primary cutoff. Note that $H_{i,\alpha} = V^{KS}_{i,\alpha}$, since kinetic matrix elements are ruled out by construction. (Moreover, the self-consistent contributions in the matrix elements $V^{KS}_{i,\alpha}$ are expected to be very small.) Since the first order treatment of the perturbation $\Delta_{i,j}$ does not imply mixing of eigenstates within the primary cutoff to evaluate the energy correction, we do not consider the second order change of the DFT energy functional due to the self-consistent charge response to the perturbation, and we evaluate the correction *once* at the final stage of the calculation as:

$$\Delta E \;=\; \sum_{\mathbf{k}_j, i} \omega_{\mathbf{k}_j} f_{\mathbf{k}_j, i} \sum_{G_1^{cut} < |\mathbf{G}_\alpha| < G_2^{cut}} \frac{| < \psi_{\mathbf{k}_j, i} | V^{KS} | \mathbf{G}_\alpha + \mathbf{k}_j > |^2}{\epsilon_i - \frac{G_\alpha^2}{2}} \, , \tag{3.13}$$

where the sum on sampling points $\mathbf{k}_j$ of weights ω_j and the occupation numbers $f_{\mathbf{k}_j, i}$ of the orbitals have been introduced.

The correction (3.13) can be calculated at different values for the secondary energy cutoff E_2^{cut} by simply evaluating the summation up to the correspondent values of G_2^{cut}. What is required from the correction is to provide extrapolated values for the total energy at high cutoffs which accurately reproduce the total energy which would be obtained at those high energy cutoffs by a full calculation. Some testing is worth doing to check on the accuracy to be expected from this correction, and to determine the minimum primary cutoff beyond which the use of the extrapolation is safe.

As a test illustration we report in figure 3.8 on page 99 a plot of the results obtained for two calculations on the tetrahedral interstitial hydrogen in a system of 27 aluminium atoms, performed at the primary cutoffs of 8 and 13 Hartree respectively. The top-left circle of each curve represents a fully-calculated result, and all the others are extrapolated using expression (3.13). At the cutoff of 13 Hartree the two curves coincide within $2 \cdot 10^{-3}$ Hartree, the extrapolation from 8 Hartree being accurate between a few percent of the energy difference it predicts. The curve also shows a further total energy lowering of about $15 \cdot 10^{-3}$ Hartree beyond the primary 13 Hartree cutoff.

The primary cutoff of 13 Hartree used in the calculations is expected to be sufficient for converged values of energy differences, and is therefore not expected to influence the results for the profiles of relative energies of hydrogen in interstitial positions. The absolute energy calculated enters on the contrary in the definition of heat of solution, and the perturbative correction described above is of some relevance in that case.

3.8 Embedded hydrogen in jellium.

The elective test to check our techniques is represented by the embedded hydrogen in jellium. This system has strong similarities with the embedded hydrogen in aluminium, and at the same time its spherical symmetry allows us the comparison with precise literature results. We have performed the calculations on this system using exactly the same parameter setting (supercell geometry, k-point sampling set, Fermi surface smoothing) which we have afterwards utilised for the pseudopotential calculations, and we have applied here the jellium correction introduced in Section (3.5). The jellium correction takes here the form of the error we make in calculating the total energy of pure jellium at the Al density. The exact value of this energy within the adopted parametrisation of the correlation energy is subtracted from the result calculated with periodic boundary conditions and BZ sampling, to give the value of jellium correction for the system considered. Such error is entirely due to BZ sampling, and is systematically subtracted from the calculated energy results.

The embedding energy of hydrogen in jellium is defined as the energy of a proton immersed in jellium of given (asymptotic) density, minus the energy of an isolated hydrogen atom (the energy of the pure infinite jellium system being the reference zero energy). In our supercell calculations we fix the volume Ω of a supercell containing N electrons to the experimental Al electron density, and we introduce in the supercell the proton and one more electron. The calculation is then performed using a secondary cutoff of at least 30 Hartee for the perturbative correction (3.13). The analytically calculated jellium energy and the exact energy value (-0.5 Hartree) of the isolated hydrogen atom are then subtracted from the obtained result, to give our theoretical prediction for the embedded hydrogen in jellium.

We have performed calculations for the 16-atom system and the 27-atom system sizes, using the same smearing and sampling set previously used for the the calculations on the vacancy systems. The comparison with LDA results in literature is made in table 3.4 on page 99 . The embedded energy values obtained, once the residual BZ sampling error has been corrected through the jellium correction, are seen to be very close to each other (the jellium correction being as small as 0.07 eV by the time we get to the 27-atom system), which suggests a good convergence of the energy with respect to system size. When compared with the literature results the agreement is also good[10], so that the maximum uncertainty of the calculation is expected not to exceed 0.2 eV.

---

[10] the oscillations in the literature results values seem to be due to the technical problem of imposing the asymptotic condition of the given jellium density while performing the calculation in spherical symmetry[88].

3.9 The heat of solution and the relative stability of interstitial sites.

As discussed in Section (3.2.2), the problem of calculating reliable numbers for the hydrogen heat of solution and for settling the issue of the relative stability of the interstitial sites could not be resolved within the models based on self consistent calculations in jellium only, or on spherical approximations for the hydrogen interaction with the metal ions. While no conclusion can be driven from those works about the relative energy ordering of the types of defect trapping (interstitial or substitutional), it seems clear from all calculations that the two possible sites for interstitial trapping (tetrahedral and octahedral) are almost degenerate in energy in the case of a single hydrogen impurity.

As in the case of hydrogen embedded in jellium, we have performed calculations for the 16-atom and the 27-atom systems, including the perturbative correction of eqn. (3.13). The energy for embedding an hydrogen as an interstitial atom into the metal crystal is again as before defined assuming the isolated atom plus the undisturbed host system as reference level. We present in table 3.5 our results for the embedding energy at the tetrahedral and octahedral sites, the relaxation energy obtained for the two systems, and the calculated relaxation displacement of the nearest neighbour atoms, in absolute units, for the two cases. The results confirm the approximate degeneracy in energy between the two interstitial sites, suggesting that the most stable site is the tetrahedral one, although in our largest supercell (and most accurate calculation) the energy difference with the octahedral site is only 0.06 eV. It is remarkable that an important role in deciding the relative stability of the two interstitial sites is played by lattice relaxation effects, which are found to be much larger for the tetrahedral interstitial site (≈ 0.35 eV) than for the octahedral site (≈ 0.05 eV). The magnitude of the relaxation displacement is also found to be much different in the two cases. The four nearest neighbour Al atoms are pushed aside much more around the tetrahedral interstitial (maintaining the tetrahedral symmetry) than the six nearest neighbour atoms are in the octahedral interstitial case.

The relative stability of the two sites is the result of a balance between different opposite effects. The pure embedding energy of hydrogen in jellium as a function of the charge density at the interstitial sites would select the octahedral site as the most stable. The embedded energy of hydrogen in jellium as a function of density has the (only) minimum on a value (0.002 *a.u.*) much lower then the average density of the Al host (0.027 *a.u.*). Within the kind of considerations which are at the basis of the "effective medium" or "quasi-atom" models[88][103], this means that in an almost uniform-electron-gas metal a small hydrogen impurity would select as its stablest position the interstitial site which has the *lowest* charge density in the perfect crystal of the host metal, and that site for Al would be the octahedral one (where the density is 0.018 *a.u.*) instead of the tetrahedral one (where the density is 0.027 *a.u.*).

However, the introduction of an hydrogen impurity in the metal creates a distribution of screening charge, represented by the traditional models by the same screening charge calculated in pure jellium. The structure of such distribution is not much density-dependent as far as the main peak position is concerned, although the phase and the amplitude of the subsequent oscillations[11] far away from the nucleus may differ[87]. The introduction of the interaction between the screening charge and the ionic potentials should therefore only depend on the geometrical correlation between (i) the distance r_{NN} of the interstitial sites from the nearest neighbour Al, (ii) the position of the main features (say, the first node r_h) of the screening charge distribution, and (iii) the position of the main attractive lobe of the atomic pseudopotential outside the core radius r_c.

Following this argument, due to Gunnarsson *et al.* [106], and considering that $r_h + r_c \approx 3.3$ *a.u.* in the present case, and that r_{NN} is about 3.3 *a.u.* for the tetrahedral site and 3.8 *a.u.* for the octahedral site, the conclusion is that the *tetrahedral* site is expected to be the most stable site from the point of view of the chemical (first-order)

---

[11] If the density of the surrounding jellium is decreased to *zero* (at which value the screening is due to the 1s atomic orbital) these "Friedel oscillations"[63] disappear without the main peak of the screening cloud having ever substantially moved from its value of about 1 *a.u.* .

interaction of the embedded atom with the pseudopotential field (the fine tuning of this effect is obviously related to the energetics of ionic relaxation around the defect in the metal). Our results confirm that a compromise between the balance of the two mentioned effects determines a quasi-degeneracy of the two interstitial positions, perhaps in favour of the tetrahedral site as the most stable, even though we cannot settle the issue of relative stability with absolute certainty given the small energy differences involved.

Our value for the hydrogen heat of solution E_{sol} reported in table 3.5 was obtained from the definition given in Section (3.3) as the embedding energy in the metal of one hydrogen atom plus the dissociation energy ΔE per H atom in the molecule H_2. We used for ΔE its experimental value[107] 2.24 eV. Our final result for the heat of solution is therefore 0.94 eV, which appears to be well converged with respect to system size, and on which we estimate an overall accuracy of 0.1 eV with respect to systematic errors in the calculations. This result becomes 0.2 eV lower if we cancel the LDA errors introduced with the hydrogen potential. This is commonly done in literature[88][76] when evaluating the embedded hydrogen energies by using in the subtraction the local spin density (LSD) value (-13.4 eV [106]) instead of the exact value (-13.6 eV) for the total energy of the isolated H atom, and corresponds to assuming that the LDA error on the screened proton in the metal is similar to the LSD error in the isolated atom[12] In any case the agreement of our result with the experimental values 0.83 eV[74] and 0.66 eV[71] is satisfactorily.

A plot of the full ground state charge distribution in the (110) plane for the tetrahedral interstitial hydrogen is provided in figure 3.9 on page 101, showing that the screening charge distribution is contained within the region of the nearest neighbour atoms and interstitial empty sites.

The charge difference for the unrelaxed interstitial is shown in figure 3.10 (page 101) on a more detailed contour scale. The structure of the underlying lattice of metal atoms is

---

[12] The LDA error on the isolated H atom total energy is known to be large, the LDA energy of the atom being only -12.0 eV, but it is due to causes which do not occur in the embedded atom system[106]. The LSD energy value for H is therefore the one used for the correction.

still visible on the sites occupied by the two metal atoms neighbouring the interstitial on the (110) plane, as was found for the vacancy screening (cf. figure 3.5 on page 86). In the outer defect region the charge redistribution is remarkably spherical, and is found to drop down to a few thousandths of the bulk average density in the regions midway between the hydrogen and its images in neighbour supercells, supporting the hypothesis that even if the Friedel oscillations of the screening charge can be long-ranged, the supercell results for the energetics of the defective systems can be expected to be independent from such oscillations[62].

3.10 Interstitial energy profiles and H binding to a vacancy.

The determination of the height of the energy barrier which the the H atom has to surmount in the diffusion process poses the technical problem of defining an opportune coordinate to parametrise the different non-equilibrium positions of the migrating impurity. The diffusion path on which we have performed the calculations consists of a series of hydrogen positions along the (111) direction between the tetrahedral and the octahedral sites in the fcc lattice. Our parametric coordinate was the distance between the the hydrogen position and the center of mass of the metal atoms in the cell (which is also by symmetry on the (111) line starting from the lattice site at the origin in each of the supercells we have used). Constraints on the forces were applied during the ionic relaxation in the calculations to keep fixed in each run the value of such coordinate, since the ions would have otherwise relaxed to an equilibrium position with the hydrogen located in some interstitial site. Namely, at each step of the ionic relaxation the calculated (111) force component on the hydrogen atom was set equal to zero, and the average force along the (111) direction on the metal ions was subtracted to the individual forces on each Al ion. Note that if the height of the diffusion barrier is given by the maximum value of a set of energies calculated with a minimum procedure at fixed values of some coordinate parameter, it does not matter which parameter in particular is chosen, as far as it maps the diffusion process continuously, for the barrier height determination.

The energy profiles obtained are displayed in figure 3.11 on page 102. The energy zero has been set according to the definition of the embedded energy of the atom in the metal, and the energy values at the interstitial sites are therefore the same as those reported in table 3.5. The two sets of data refer to the calculations results obtained without (upper curve) and with (lower curve) the perturbation correction, and they are seen to differ only by a constant shift, so that the relative energies at different positions result well converged with respect to the PW energy cutoff. In each of the two sets the open circles (connected by a cubic spline interpolation curve as a guide for the eye) refer to the result obtained from the 16-atom system calculations, and the black diamonds result from the calculations on the 27-atom system. We calculate the migration energy as the difference from the top of the barrier to the lowest interstitial site, and obtain 0.20 eV for the 16-atom system and 0.15 eV for the 27-atom system.

The continuation of a similar energy profile beyond the tetrahedral site and towards an empty regular lattice site (figure 3.12 on page 103) summarises the results of some further calculations, which we have performed to study the energetics of the hydrogen atom binding to a vacancy. The aim was in this case to determine the geometry of the binding, which in the history of the theoretical modelling has been variously predicted to be substitutional, with the hydrogen sitting in the center of the vacancy, or off-centre, with the hydrogen displaced from the vacant lattice site (see Section 3.2.2).

Again in the present case considerations made on the basis of pure effective medium theory would predict the stable hydrogen position to be substitutional, due to the energetically favourable low charge density at the vacancy centre in the isolated vacancy system. On the contrary, an hydrogen impurity sitting on a tetrahedral site neighbour to the vacancy would be predicted by a model focused on the interaction between the hydrogen screening charge and the ionic pseudopotential field, in analogy with the discussion in section 3.9 on the relative stability of the interstitial sites.

Our results show the stable hydrogen position to be strongly off-centre, close to a tetrahedral site and only slightly displaced from it towards the vacant site. The entity of the displacement from the tetrahedral site is about 16% of the distance between the vacant lattice site and the tetrahedral site. This suggests that the direct interaction of the hydrogen with the three atoms at the basis of the tetrahedral unit having the vacancy at its upper vertex is the mechanism which largely determines the vacancy trapping position. The trapping energy, defined as the energy difference between this trapping position and the most stable hydrogen interstitial energy, is found to be 0.34 eV in the 27-atom system and 0.19 eV in the 16-atom system. A contour plot of the valence electron density in the (110) plane is provided in figure 3.13 on page 104.

Results concerning the interstitial hydrogen energy profiles and the hydrogen binding to the vacancy are for obvious symmetry reasons the most difficult to predict in terms of approximate models (in particular the spherical solid model[76][77]). These models nearly always neglected the lattice relaxation around the defect, or in few occasions found it energetically unimportant. The role played by the lattice relaxation is found from our results to be determinant, in particular for the energetics of system geometries with the impurity close to the tetrahedral site. The meaning of any comparison of our estimated energy barrier with the higher predictions from early models, which give values around 0.5 eV, is therefore doubtful[13].

The experimental situation for the migration energy is not very clear. The most reliable measurements are probably those reported in references [110], [114] and [111], performed at temperatures above about 600 ^oK, and giving values of 0.42 eV, 0.40 eV and 0.61 eV respectively. In particular in ref. [111] (Hashimoto and Kino, 1983) the authors observe a substantial decrease of the hydrogen activation barrier when the the temperature is lowered down to 300 ^oK, and suggest a picture of hydrogen freely migrating at room temperatures, while the diffusion at high temperature resents of the

---

[13] The two predictions for the migration energy which we were able to find in literature are both obtained from calculations performed with the hydrogen in strongly asymmetric positions between the interstitial sites. The metal ions are represented with model Al pseudopotentials and treated within the "spherical solid model" approximation. The results 0.50 eV[78] and 0.53 eV[79] appear nonetheless in excellent agreement with the most recent experimental results 0.47 eV [108] and 0.52 eV [109] available at the time.

trapping effects due to vacancies.

Some further indirect evidence of a rather low diffusion barrier for hydrogen diffusion in Al at low temperatures can be derived from measurements of the diffusion coefficient of positive muons. The muons do not self-trap (if not on impurity atoms) in aluminium, while they can be observed in localised states in pure copper[97][112][84], which has also fcc structure. The activation energy for hydrogen diffusion in copper is well established to be 0.4 eV [113][115], and therefore it unlikely that the same quantity in aluminium could be greater than this. Our somewhat low value for the migration energy is therefore not necessarily in contrast with the available experimental evidence. Our value 0.34 eV for the binding energy of hydrogen to a vacancy is in fairly good agreement with the measured trap binding enthalpy 0.52 ± 0.10 eV[116]. It is worth noticing that measured values like these have to be extracted from computational modelling used to fit the available observed data, typically by simulating the defect diffusion at the experimental temperatures between trapping sites. These models imply the use of input parameters such as the experimental diffusion coefficient in the perfect lattice[117], and therefore they suffer to some extent from the uncertainties on the value of such parameters[117][118]. Early calculations predict larger values for the hydrogen-vacancy binding energy (1.2 eV [72], 1.0 eV [87]). Effective medium theory calculations performed in conjunction with the experimental work of reference[116] gave in more recent times a predicted value of 0.52 eV, in excellent accord with the observed value.

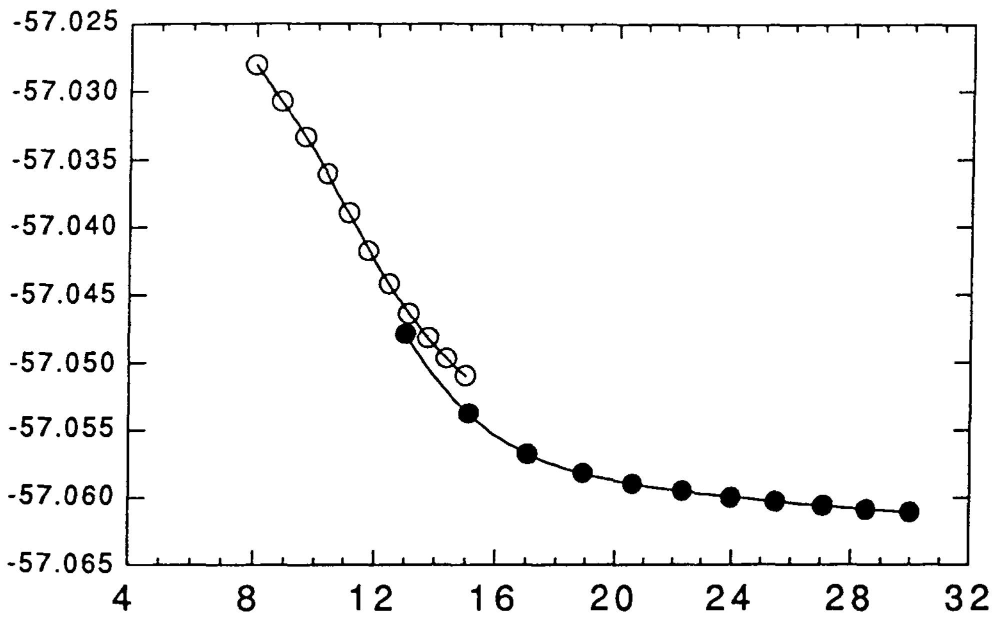

Figure 3.8: A test of the perturbative correction (3.13). The plot shows the fully converged total energy for hydrogen at the tetrahedral site in a system of 27 aluminium atoms at a sequence of values of the secondary cutoff energy. White and black symbols show the results for the primary cutoff energy is set equal to 8 and 13 Hartree respectively. (All quantities in atomic units).

	16-atom	27-atom
ΔE (eV) uncorrected	1.36	1.57
ΔE (eV) corrected	1.51	1.50
ΔE (eV) reference	$1.30^{a,b}$, 1.51^{c}	

Table 3.4: Embedding energy ΔE of hydrogen in jellium (energy of embedded hydrogen system minus energy of jellium plus isolated hydrogen). The difference between the uncorrected and corrected ΔE is the jellium correction (see text). The reference values of ΔE are those of (a): Almbladh *et al.* (1976)[76]; (b) Zaremba *et al.* (1977)[103]; (c): Nørskov (1979)[88].

	16-atom		27-atom	
	tet.	oct.	tet.	oct.
ΔE (eV) no pert.	-1.08	-0.96	-1.11	-1.07
ΔE (eV) with pert.	-1.29	-1.15	-1.30	-1.24
E_{sol} (eV)	0.95		0.94	
Relax. energy (eV)	0.36	0.04	0.32	0.05
Relax. displ. ($\AA$)	0.12	0.03	0.12	0.04

Table 3.5: Results of calculations on hydrogen at tetrahedral (tet) and octahedral (oct) sites for periodic systems having 16 and 27 aluminium atoms. The embedding energy ΔE (energy of fully relaxed system with hydrogen minus energy of perfect crystal plus isolated hydrogen atom) is given without and with the perturbative correction (see text). The energy of solution E_{sol} is obtained by adding to ΔE the experimental dissociation energy per atom of the H_2 molecule (2.24 eV). Also shown are the relaxation energy (energy of unrelaxed minus energy of relaxed systems) and the relaxational displacement of nearest neighbour aluminium atoms.

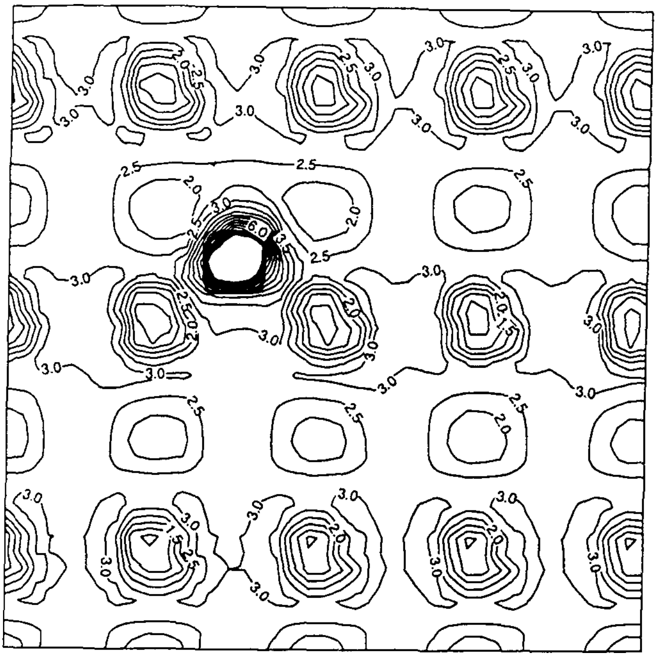

Figure 3.9: Contour plot of the electron density on the (110) plane passing through hydrogen at the tetrahedral site in a system of 27 aluminium atoms. Values marked on contours indicate the electron number density in units of 10^{-2} electrons per Bohr radius cubed (in these units the average electron density is 2.7).

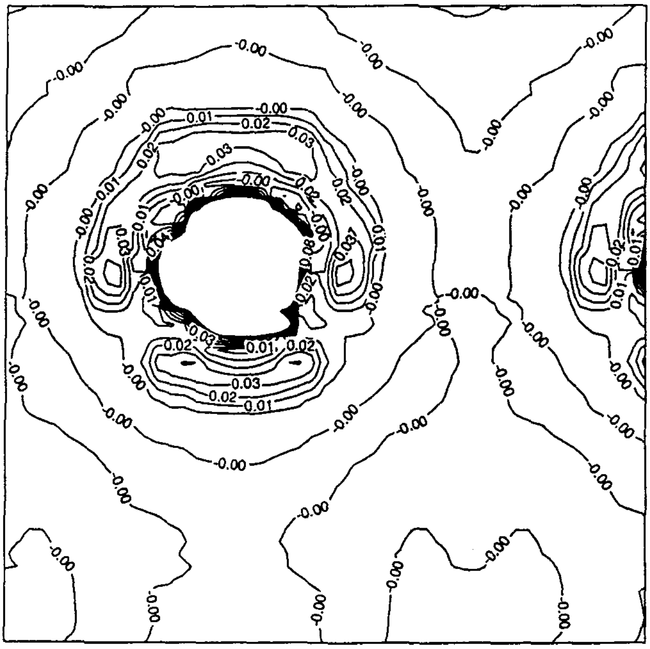

Figure 3.10: The screening electron density (see text) corresponding to the fully relaxed tetrahedral interstitial. Units and scale as in the figure above.

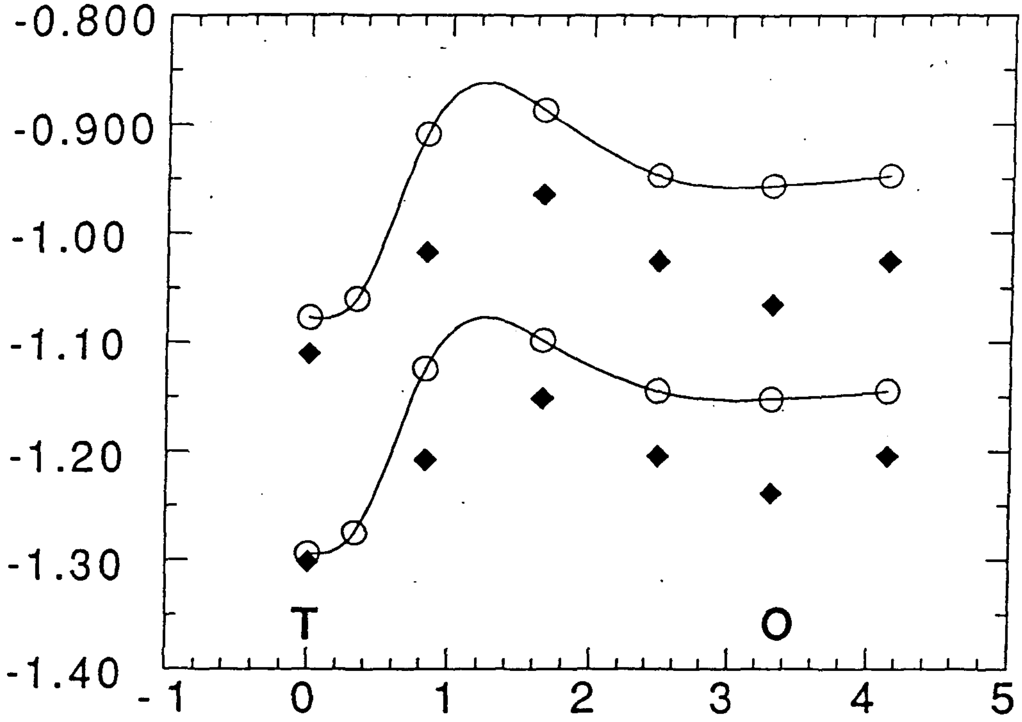

Figure 3.11: Profile of the total energy (eV)of the fully relaxed system as a function of proton position ($a.u.$) along the straight line in the (111) direction between tetrahedral (T) and octahedral (O) sites. White circles and black diamonds show results for the 16-site and 27-site systems respectively. The upper and lower sets of symbols show respectively results obtained without and with the perturbative correction.

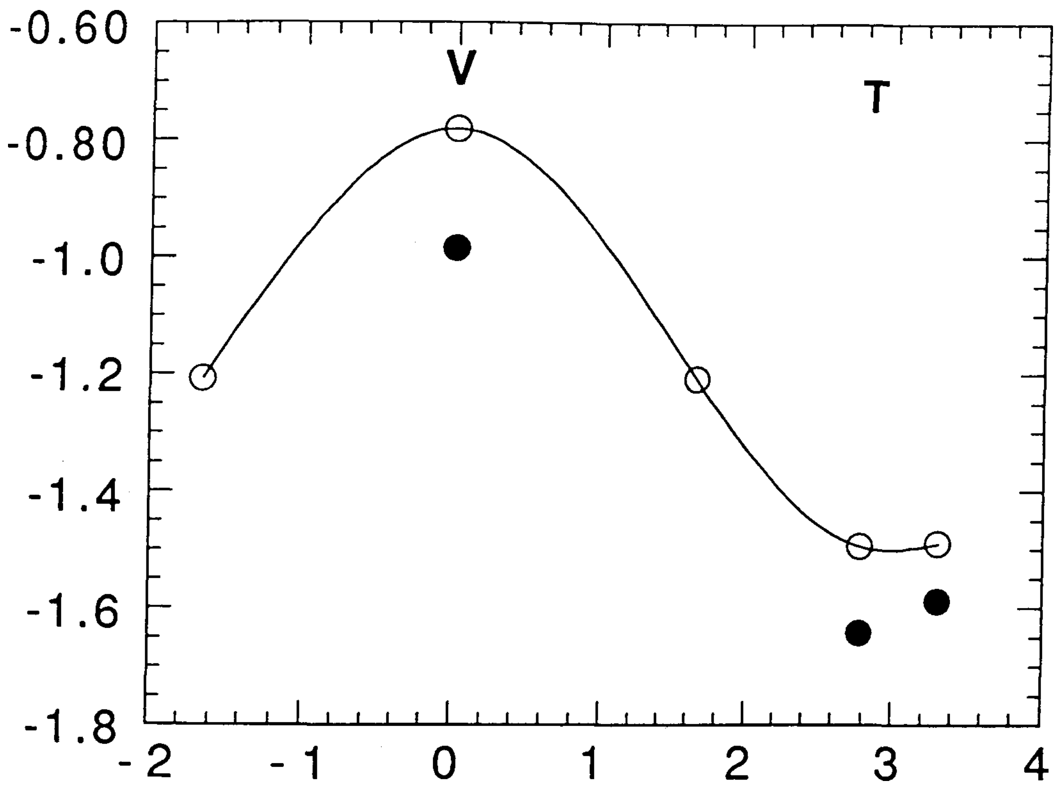

Figure 3.12: Profile of the total energy (eV) of the fully relaxed hydrogen-vacancy system as a function of proton position $(a.u.)$ on the straight line in the (111) direction between the centre of the vacancy (V) and a neighbouring tetrahedral site (T). White and black circles show respectively the results obtained for the 16-atom and 27-atom systems.

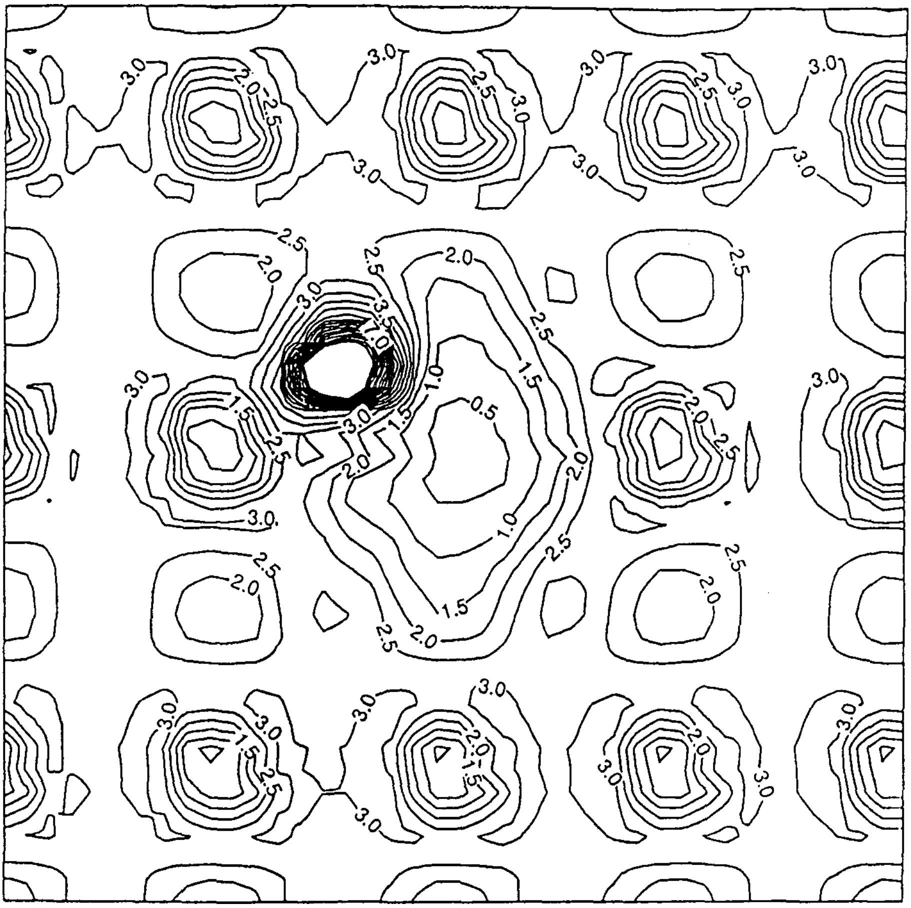

Figure 3.13: Contour plot of the electron density in the vacancy-hydrogen system. The density is shown on the (110) plane passing through the vacancy centre and the proton at its most stable position. Values marked on contours indicate the electron number density in units of 10^{-2} electrons per Bohr radius cubed (in these units the average electron density is 2.7).

4 Ab initio total energy calculations on parallel computers.

4.1 Introduction.

In the present chapter a brief discussion is provided of the problem of performing total energy calculations on parallel computing machines. These machines are already a competitive alternative to the use of vectorial supercomputers in most scientific applications, and are expected to play an increasingly important role in the practice of theoretical physics calculations. The analysis of the computational features of a DFT-LDA-PW computer code suggests a number of possible parallelising strategies, which take into account the prospective evolution of the machine architectures and the associated larger sizes of physical systems which are expected to enter the range of ab initio treatment in the very near future.

The calculations on defective systems of ceramic insulators reported in the present work involve the use of large supercells and high PW energy cutoffs, and are therefore extremely demanding in terms of computer memory, while high computational speed is required to ensure a reasonable time scale for obtaining the results. These calculations have been performed on a parallel machine (a 64-node Meiko Computing Surface in Edinburgh University) using a parallelised code CETEP specifically designed for the features of this machine, on which it was tested for the first time in conjunction with the calculations on MgO reported in Chapter 5. In the present brief chapter we summarise the general ideas at the basis of the parallelisation strategy implemented in the code. For a more complete and technically detailed discussion, reference [119] with the original analysis of the problem should be consulted.

4.2 Scaling of computations with respect to system size.

We assume here that a DFT total energy minimisation has to be performed which makes use of a large PW basis set[1]. The energy functional to be minimised includes "band" energy terms from each electron orbital of each BZ sampling point used in the calculation, and an electronic interaction contribution evaluated from the total electron density, which is itself calculated as a sum over sampling points and occupied orbitals. The minimisation corresponds to the self-consistent solution of the KS set of equations, but can be performed without explicitly solving such set, using some global approach of the kind pioneered by Car and Parrinello[16], like the conjugate gradients technique used in this work (see Sections 2.2 and 2.3).

All the minimisation techniques suitable for large scale calculations have the common feature of optimising iteratively a set of N_{orb} electronic orbitals $\{\psi_i\}$, each represented by a vector of N_{plw} complex numbers. The hamiltonian terms are diagonal in either real or reciprocal space, so that Fast Fourier Transforms (FFT) are invariably used to transform the orbitals in the appropriate space where the integration of the energy contributions is a single sum on the space mesh index. The FFT operations scale like $N \log N$, where N is the dimension of the transformed vector, and dominate the calculations with a time load (or "time complexity") $O(16 N_{orb} N_{plw} \log_2 N_{plw})$ for each transform[2] in the case of small systems. For big systems the orthonormalisation of orbitals scaling like $O(N_{orb}^2 N_{plw})$ is the dominant part of the computation. Since the number of PW for a given energy cutoff is proportional to the volume of the system, and so is in usual conditions the number of orbitals, the time complexity of the calculations for large systems will eventually scale like the cube of the system volume.

---

[1] Algorithms using different basis sets can be efficiently parallelised, but the typical scalings in the calculations are different than in our case, and are not treated here.

[2] The FFT need twice the the number of points in each dimension than PW in each orbital. The G-space sphere transformed is therefore eight times bigger than the energy cutoff sphere, and has to be inscribed into a FFT cubic grid of G-vectors having roughly twice its volume. This accounts for the prefactor 16 in the expression.

The minimum memory storage required for the calculations is also obviously increasing when the size of the system increases. The most efficient calculation strategy should limit to the minimum (or better avoid) the use of slow-access disk memory. The minimal use of memory in a calculation involves the allocation of memory space for at least one full set of wavefunctions $\{\psi_i\}$, so that the memory needed scales like the square of the number of atoms, for a given system density.

Even assuming that a fast non-parallel machine can fit the memory requirements of a single large calculation[3], the speed of one processor in such machine depends on the available technology and is not an adjustable parameter, so that if an unreasonable time is needed to perform the calculation, the calculation is in practice out of the range of the available technology. This can be the case of large ab initio dynamic simulations, which require a modest amount of memory if compared with the requirements of the largest energy minimisations feasible on the same given machine, but which are extremely slow (typically months of processing are needed for a single run) in computing the desired results.

For an application which would be exceedingly demanding for a single processing unit in terms of computer memory and computation time, the *only* alternative left is the use of parallelisation, *i.e.* the distribution of the computational load on a (virtually unlimited) number of concurrent computing subunits. The typical parallel machines of the kind used in this work, to which the present analysis will be limited, can be thought as a group of computing subunits (nodes) sharing information along the computation through special data-transfer routines arranged in some efficient communication topology, and each having a specific local amount of dynamic memory.

The nodes used in our calculations (carrying an Intel i860 microprocessor and 16 Mbytes of dynamic memory each) were arranged in the hypercube communication topology, in which each node shares a communication link with n "nearest neighbour" other nodes, each of which is thought as located on the opposite side of a $n-$dimensional

---

[3] At the time of the calculations performed in the present work the best alternative serial computer available was the CRAY X- MP/416, limited in memory to only about 100 Mbytes for normal utence.

hypercube's edge. Dimensions up to $n = 6$ were available, corresponding to a nominal peak performance of 5 Gflops[4] and a total of 1 Gbyte of distributed memory, to be compared with the 0.25 Gflops and 0.13 Gbyte of a Cray X-MP/416 used in serial mode. It is noteworthy that the next-generation processor of Cray technology performs 1.4 times faster *only*, given the 0.33 Gflops delivered by a Cray Y-MP/8128 in serial mode, while the substantial increase of peak performance of this latter machine resides mainly in the improved memory (1 Gbyte) and in the enlarged number of processors (from four to eight, with a theoretical peak performance of 2.7 Gflops, using full parallelism). Given the computational load scaling of the existing total energy algorithms[5] two or three orders of magnitude in the overall machine speed are needed for approaching successfully systems ten times the current sizes, and it is highly unlikely that the single-processor technology could respond to such need.

On the other hand "Teraflop" parallel machines using typically thousands of processing nodes are already under study, while machines ten times the size and using about ten times faster communications than the one we use are already operative[6]. The use of these machines for scientific production is still in the pioneering stage, with much to be improved in the handling of fast-communication networks and faulty hardware situations (the occurrence of software-unrecoverable hardware faults being roughly proportional to the number of node boards).

In the following sections we provide a brief analysis of some alternative strategies for mapping a total energy calculation on the typical node-network of the present generation of parallel machines, in the light of the prospective performance of the next-generation machines, predictably in the speed range of 10 to 1000 Gflops.

---

[4] The "flop" unit corresponds to one real single precision floating point operation per second.

[5] Some first-principles computational techniques scaling ***linearly*** with the system, size have been proposed[120][121], but have not yet entered the standard practice of calculations.

[6] For example, the "Delta machine", at Caltech, with 512 i860 processors operating concurrently.

4.3 Possible parallelisation strategies.

The minimum amount of data in a PW calculation corresponds to the memory required to store the complex arrays of the wavefunctions coefficients. If N_{ions} is the total number of pseudo-atoms in the supercell, the number of plane-waves N_{plw} in the basis set scales like $(100-1000)\ N_{ions}$, the number of orbitals N_{orb} like $(1-10)\ N_{ions}$, and the number N_k of BZ sampling points like $1/N_{ions}$. As mentioned in the former section, the computer-time load of the techniques minimising the DFT energy functional by iterative orbital optimisation scales like $O(N_{orb}^2 N_{plw})$, to be compared with the time complexity $O(N_{plw}^3)$ of the solution of the KS eigenproblem through direct matrix inversion on the PW basis set.

We therefore concentrate on the problem of parallelising the computations by dividing into subunits the data on which an iterative algorithm operates[7], with a discussion of the degree of efficiency of the computations when assigning each data subunit to a separate processing unit of the parallel machine. The analysis on possible parallelisation strategies has the goal of minimising the computer time spent in communications. The "perfectly" efficient parallel calculation is the one during which almost no time is spent in communicating information between processing units[8], and in which all the (identical) nodes are loaded evenly up to maximum work capacity without ever exceeding their maximum resident memory. In real calculations the amount of communications required in performing the FFT of the orthogonalisations of orbitals is determinant. Some possible parallelisation strategies are enumerated in the following.

(1) The single BZ sampling point k_i could be assumed as a first candidate subunit. Each node would be assigned all the computations corresponding to one sampling point. Orthogonalisations and FFT would be performed serially on each node. Communications would be required only to sum the charge density

---

[7] This approach is called "data driven" parallelisation.

[8] It should be noted that when *no* communication is needed between concurrent processors, the calculation is strictly speaking no more parallel, since no synchronisation of different processing units, and therefore no parallel machine, is needed.

scalar field and to sum the energy and forces contributions. This approach can be of some use for calculations using extremely high energy cutoffs on systems requiring high precision BZ sampling (for example, for computing defect energetics or elastic properties of medium sized systems of transition metal atoms modelled by highly transferable pseudopotentials). Although it is always possible to define groups of k-points as the calculation subunit, it is on the other hand necessary to use in the calculations at least as many sampling points as concurrent nodes. For large systems requiring very few (or only *one*) sampling points, it is often impossible, for pure memory requirements, to use as few node units, and this approach becomes totally inadequate.

(2) Another candidate subunit could be a group of orbitals at a given k-point. The obvious advantage of this approach would be the possibility of performing the FFT serially on each node. This can often be done with the use of dedicated hardware on each node. The orthogonalisation between orbitals would on the other hand involve large data communications between nodes, which would represent by far the most cpu intensive operation for large system sizes[9].
The basic operation performed concurrently in the calculations would be the band updating: the band-by-band technique described in Section 2.3.2 would therefore be incompatible with this choice of parallelisation strategy, so that some other minimisation algorithm would be needed to synchronise the updating of the wavefunctions and reduce to the minimum the operations which ensure the orthogonality of orbitals.
Although feasible ways to perform the orthogonalisation have been suggested[119], it is moreover clear that within this parallelisation approach the full FFT mesh would have to be stored on each node, with a correspondent memory load *per node* of $O(16N_{plw})$, scaling linearly with the volume of the system. As in

---

[9] It could appear that the time needed to communicate data should be bound to be anyway negligible when compared to the time spent in processing data. This is not the case due to (i) the complicated patterns of the communication network (ii) the intrinsic slowness of the available communication software, compared with the speed of the serial operations performed on the nodes.

the preceding strategy, the dynamic memory per node (which is assumed to be fixed, like the peak speed performance of each processor) would be at some stage saturated going to large system sizes.

(3) A third possible parallelisation data subunit consists of portions of the real space and reciprocal space represented in the calculations. Since the PW basis set is a subset of a G-space mesh, and the repeating supercell in the calculation is also mapped onto a real-space mesh, it is straightforward to distribute equally the two spaces onto nodes. Each orbital is spread in this case onto each node, and each node deals serially with each orbital's components on a limited region of either real or reciprocal space. The operations involved in the computation of total energy and forces are all local in one of the two spaces, so the corresponding computations can be performed concurrently, without communicating anything else than the *scalar* sub-integrals of the various quantities evaluated on each node. The same argument applies to the orthonormalisation procedure. The FFT is on the other hand an intrinsically non-local operation, since every plane-wave coefficient in each wavefunction's expansion has a transformed contribution on each of the wavefunction's values on the real space mesh, and vice versa. Every FFT therefore involves in this approach a global redistribution of all data fields.

If a fixed *physical volume* is assigned to each node, the amount of memory required on each single node scales like $O(N_{orb}N_{plw}/N_{nodes})$, like in the parallelisation strategy (2), but a very limited additional space is needed to perform the FFT, since the FFT mesh is spread on all the nodes.

(4) The last two strategies could be combined into a parallelisation scheme in which the asymptotic memory requirement per node is fixed. Since the total storage needed scales like the square of the system volume, this means that for extremely large calculations (on systems of several thousands of atoms) a number of nodes is needed which itself scales like the squared system's volume, each node corresponding to the values of a fixed number of bands on a fixed

region of space (the topology of which is, as above, otherwise completely arbitrary). FFT operations again involve full communications, while now further communications of data fields are needed to evaluate at each node the partial scalar products between the "resident" orbitals and the orbitals permanently stored on other nodes. The updating of orbitals is performed concurrently in each group of bands, so that if the number of such groups is very limited some feature can be retained of the smooth "band-by-band" updating technique described in Section (2.3.2), by updating concurrently one band of each group at time.

4.4 Sources of efficiency loss and the strategy adopted.

The goal of parallelisation is to distribute a computational load onto a finite number n of processing units in such a way that the overall speed of the computation is n times faster than it would be if the whole computation were loaded onto one single unit (even if this is not really possible because of memory limitations). In each of the parallelisation strategies described in the former section only negligible parts of the calculation have to be performed by one processor only, or *repeated* exactly by all processors. One example is represented by the input operation of the global calculation parameters, like the geometry of the supercell and the total number of ions in it, which cannot be performed any faster than it would using a single processor. This and other sources of efficiency loss from the ideal parallel performance are regrouped below into categories.

I *Residual sequential operations* are in practice a number of operations, like the updating of the ionic positions during the run according to Hellmann-Feynman forces, parallelising which would be an unnecessary complication. They are performed identically at each node.

II The *uneven distribution of computations* is normally a more serious source of efficiency loss. It is typical of the case in which the load of work cannot be distributed exactly between nodes because (i) there is some incompatibility between the data structures and the node number (for example, using the strategy (2) of last section with an odd number of orbitals and an even number of nodes) or (ii) when the amount of work per node cannot be predicted in advance, since depends on the calculation features (for example, still with strategy (2), if different orbitals require a different number of conjugate gradient steps to be optimised within the same (fixed) energy convergence tolerance.

III The *overheads of processor synchronisation* are another source of efficiency loss. They occur whenever a piece of information has to be communicated to a node (or to all nodes) before the whole run can proceed. A typical example is the scalar product of two orbitals in strategies (3) and (4): even if the workload of this operation is equally divided between nodes, and the associated computation is performed concurrently, the stages of the computation which require the knowledge of the scalar product's value have to wait until each node's partial contribution to the product is summed before the calculation can proceed. This latter summation can be thought as being performed at one single node: during the time it takes, after which the result can be communicated to all the remaining nodes[10], the whole computation is not parallel.

IV Finally, with *overheads of data communications* it is usually meant the time spent in communicating data between nodes. During this time, which depends on the communication software and hardware and on the complexity of the parallelisation topology, the nodes are inactive. In total energy calculations using PW this time is almost all spent in transferring large real or reciprocal

---

[10] Many of the operations mentioned in point (I) are in fact performed in this way, communicating a result instead of evaluating it at each node, to avoid instabilities due to the rounding noise at different nodes.

space data fields between nodes, as it happens for example during each FFT procedure within parallelisation strategies (3) and (4) of last section.

For the calculations on defects in ionic compounds presented in the next chapter, we adopt the parallelisation strategy (3), and therefore we choose to distribute in equal parts the real and reciprocal space grids associated to our supercell calculations. This choice is dictated by physical considerations, given that all the contributions to the total energy functional can be reduced to single-index sums (*i.e.* local operations) in the discrete real space or momentum space representations. This is also true for the scalar products needed to accomplish the orthogonalisation of the orbitals. Once the domain of each sum is equally distributed on the nodes, the sums are performed concurrently, and the subtotals *only* need to be communicated between nodes.

The FFT, on the contrary, are not local operations, and in the parallelisation strategy chosen they involve large amounts of data communication. This problem is avoided by strategy (1) or (2) of last section, which assign to each concurrent node all the operations associated with a group of sampling points or with a group of orbitals. However, the kind of physical systems which we consider (large supercells of insulating materials) rules out the possibility of loading onto a single node all the data corresponding to a single BZ sampling point, while the number of available nodes is always much larger than the number of k-points needed, so that strategy (1) is ruled out in our case. Moreover, the maximum size of the systems we study is already in the region in which the time complexity of the orthonormalisations takes over the time complexity associated to the FFT (in spite of the latter's large prefactor), so that strategy (2) is also ruled out, since it implies communications when evaluating the scalar products between orbitals. These communications are needed also in strategy (4), differing from the one we adopt in the fact that only some of the orbitals are represented on each node, so that the same portion of real and reciprocal space must be assigned to more than one node at time. The systems we can investigate with the available machine (limited to 64 nodes) are however still small enough to make this further subdivision unnecessary in our calculations.

The implementation of the FFT operation represents, from what said so far, the (only) source of efficiency loss which cannot be avoided when parallelising the algorithm. A careful distribution of the data structures onto the nodes has however been implemented in the parallel code CETEP, which proves very useful in reducing the time spent in performing the communications.

In the calculations, the reciprocal space FFT grid is distributed equally on the nodes, paying attention to the fact that not all the G-vectors are inside the energy cutoff sphere while distributing the computational work between nodes. In particular each node is assigned an equal number of *columns* of G-vectors in the k_x direction[11]. Some of them are totally outside the cutoff sphere within which the coefficients of the orbitals can be different from zero. The number of these columns is kept as balanced as possible between different nodes. The real space FFT grid is organised in *planes* orthogonal to the x direction. The integer mesh dimension N_x in such direction is normally chosen to be a multiple of the number of nodes used in the calculation, so that an equal number of real space grid planes corresponds to each node.

The three-dimensional FFT can be factorised into lower-dimensional integrals. With the asymmetric assignment of the two spaces outlined above, each node can perform the FFT either on one-dimensional G-space columns or on two-dimensional real space planes, before any communication occurs. The transformations from reciprocal to real space are performed through the sequence of a one-dimensional FFT, a set of data communications, and a two-dimensional FFT. The transformations backwards to reciprocal space consist of the same operations performed in the reversed order. In either case the communication routines have to be called only once during each global FFT.

This choice of space subdivision has eventually to be abandoned whenever the size of the system is so large that sitting one grid-plane of data on a single node is no longer possible for memory reasons. Before the system becomes so large that a parallelisa-

---

[11] It is sufficient for this that the number of mesh gridpoints in a plane $k_y k_z$ plane is a multiple of the number of nodes.

tion approach like the strategy (4) of Section 4.3 becomes unavoidable, it is obviously possible to assign to each node only portions of grid planes, performing each FFT as a series of three one-dimensional transformations, and communicating *twice* the data meanwhile. However, this is not the case for the systems treated in this work, for which the 16 Mbytes of memory on each of the 64 nodes on the Meiko i860 Computing Surface were in all applications sufficient for adopting the single communication scheme outlined above[12].

---

[12] See reference ([119]) for technical details concerning the communication routines, which were especially written for the use of this machine.

5 Calculations on defect energetics in oxide materials.

5.1 Introduction.

In this chapter we present the results of a series of calculations on defect energetics in MgO[122][123] and Li_2O[124], performed with the techniques discussed in Chapter 2 and Chapter 4. Magnesium oxide and lithium oxide are two representative examples of ionic oxides, having the rock-salt and anti-fluorite structures respectively (see figures 5.7 and 5.9 on pages 150 and 152), which display several typical features of a large class of insulating ceramics. MgO is an important mineral (constituting about 10% of the earth's lower mantle), and is used in a number of technological applications as a catalyst and as a high-temperature ceramic. Li_2O has important applications in nuclear reactors technology[125], in solid-state batteries[126], and as a fast ionic conductor at high temperatures.

These compounds are strongly ionic. The valence charge density is almost completely located in the immediate proximity of the oxygen atoms, and a reasonable description of it is readily provided by a short-ranged spherical distribution of electrons, structurally similar to an atomic oxygen full valence shell[1]. It is therefore possible to describe successfully several properties of these materials using model representations based on pair interactions between couples of ions. The parameters in the models have to be fitted to experimental results, after which they can be used to predict other properties of the materials, and provide estimates for relevant quantities which are extremely difficult to measure experimentally, like *e.g.* the defect formation energies[2]. On the other hand, features like the distortion of the "soft" electronic cloud around the oxygen atoms in pure and defective material samples are out of the reach of classic models.

---

[1] Note, though, that the LDA O^{2-} ion is *not* stable (nor is the physical O^{2-} ion).

[2] However, for some other quantities like the optic phonon frequencies and the elastic constants, a model including *only* the pair interactions between rigid ions is not sufficient.

Moreover, when studying less "easy" oxides (for example: more covalent minerals like Al_2O_3 or SiO_2) these models become less reliable, and given the mentioned difficulty in performing the experiments, some support from fundamental theory is required, to assess the cases in which some pair potential description is still reliable, and to provide some means of investigation in all the other cases.

In the following sections of this chapter we discuss some of the existing classical models which have been proposed at different times for the investigation of several ionic solids, we refer to the Hartree-Fock technique as an alternative to DFT schemes for studying these materials from first principles (Section 5.2), and we summarise the work done so far within the DFT-PW technique. In Section 5.3 we provide some details of the calculations we have performed, with the results obtained from test calculations on perfect crystals. We then address the problem of studying the energetics of charged defects with the supercell method, and we report the results of some ancillary model calculations which we have performed to monitor the convergence of results with respect to cell-size (Section 5.4). In Section 5.5 we present results for the energetics and the ground state charge densities for Schottky defects in MgO, and Frenkel defects in Li_2O, and for the associated systems of migrating point defects (the two migrating vacancies in MgO, and the migrating Li vacancy and interstitial in Li_2O).

5.2 Modelling of ionic solids and alternatives to DFT calculations.

5.2.1 Classical models.

To state an operative definition, a crystal can be considered ionic if the crystal potential can be accurately approximated as a sum of pair potentials between the constituent atoms, and if the long range interaction is dominated by the Coulomb term in which formal charges are adjusted to represent the degree of ionicity of the atoms in the solid[127]. The short range part of the approximate pair potential represents a compromise between Pauli exclusion, band dispersion, and residual covalent effects. A very common simple analytic form used for the short range interaction is the Buckingham potential

$$V_{\alpha,\beta} = A_{\alpha,\beta} e^{-r/\rho_{\alpha,\beta}} - \frac{C_{\alpha,\beta}}{r^6} , \tag{5.1}$$

where the coefficients A, ρ, C of the pair interaction potential between the atomic species labeled by the indexes α, β are usually fitted on perfect lattice properties. An improvement on this ("rigid ion") model can be made by taking into account the electronic polarisability of the ions. The most common way to do this consists of formally subdividing the ionic charge into a "core" and a "shell" component

$$Z_{ion} = Z_{core} + Z_{shell} , \tag{5.2}$$

and then allowing for a controlled splitting of the two charges from the original ionic site, the (massive) core being connected to the (massless) shell by a harmonic spring. Each subdivision of charges and each spring constant introduces further degrees of freedom for the fit of experimental data, improving the flexibility of the model. [3] This "shell" model[128] has the virtue of being physically sensible, in spite of the fact that the mentioned harmonic coupling between cores and shells is not derived from fundamental considerations, and has been proven in many circumstances to be transferable within reasonably similar systems with unchanged parametrisation[129].

The empirical parametrisation of the shell model potentials is normally adjusted by means of a least squares fitting procedure using as input the experimental data for the lattice parameter and the elastic and dielectric constants[4], and the resulting potential is checked by calculating the phonon dispersion curves[132]. However, even if the parametrisation proves accurate for the harmonic properties of the perfect crystal (and for the internal structure of the unit cell, when the ions positions are not fixed by

---

[3] Negatively charged shells are usually associated to the cations in the ionic materials (and not to the anions only), even if no valence electrons are left on the cations in the solid, and even if the core electrons polarisability is expected to be small, as in the case of Li_2O.

[4] Some attempts have also been made to fit the parameter from full quantum mechanical calculations[130][131]

symmetry, as it happens *e.g.* for non cubic minerals like $\alpha-Al_2O_3$[133]), this only gives confidence on the accuracy of the potential and its first and second derivatives at the normal interatomic separations.

The study of defects, on the contrary, requires accuracy of the representation not only on the region probed by elastic and dielectric data, but also on a more internal region of the pair potential, in the case of interstitial defects, and external region, in the case of vacancies. Experimental data from relevant physical samples to fit the empirical potentials in the regions outside the perfect ionic spacing are in many cases not available, and there are serious doubts whether the normally fitted potentials can be relevant in these cases. The problem is expected to be particularly acute in the case of high symmetry (*e.g.* cubic) ionic solids, where the properties of the perfect crystal sample the potential on a very limited region.

In spite of these difficulties, the results from pair potential models for the leading defect energies in a large number of ionic materials, including alkaline-earth monoxides like MgO[134][137][135][136] and SrO[135], transition metal monoxides like MnO[137] and ZnO[138], and oxides with fluorite and anti-fluorite structures like UO_2[141] and Li_2O[142], are in good agreement with the experimental results.

5.2.2 Hartree-Fock techniques.

Apart from work based on models, there has been a considerable effort on the ab initio energetics of ionic compounds including oxygen. The strong localisation of charge around the anions, the quasi-spherical shape of its distribution, and the consequent leading role which is expected for exchange effects, rather than correlation, in the electron-electron interaction, makes of these systems very convenient and sensible subjects for the theoretical analysis based on the Hartree-Fock (HF) technique. The pure HF approach treats the (non-local) exchange exactly, and corresponds to the variational ansatz of a single Slater determinant at each BZ sampling point treated. The self-consistent solution of a set of single particle differential equations at each sampling point is derived from a stationarity condition for the total energy expression much in the same way as for the derivation of the KS system (1.9).

HF techniques have been widely used by physicists and chemists for the study of structural properties of molecules, and standard software for these systems has been available for a long time. The basis sets used are almost invariably gaussian-like, parametrised on the basis of prior knowledge of the electronic structure of the isolated atoms. The study of solids introduces the problem of the incorrect behaviour of the HF density of electronic states at the Fermi energy[143][144]. The implementation of an HF Linear Combination of Atomic Orbitals is also a non-trivial task, for the presence of non-local exchange terms involving a large number of four center integrals, and due to the non-orthogonal nature of the basis sets. Some difficulties are also related to the correction which should be added to the single particle screened potential to take into account the correlation effects (which are not included in the HF results by definition). This last issue can however be handled by the inclusion in the scheme of correlation-only density functional expressions[145][146] for the correlation energy, depending on the electronic charge density and its derivatives.

At least one very general software package for HF calculations in solids has been implemented (CRYSTAL[148][149]) and applied to several classes of compounds. In particular the properties of a large number of ionic crystals have been investigated in different high-symmetry geometries[150][151][152][153].

However, the treatment of *defects* in oxides introduces a severe increase of the size of the systems which have to be treated. A practical strategy for computing the energetics of defects while keeping small the subsystem on which full quantum mechanical calculations are performed, is the "embedded cluster" method. The underlying idea is that an explicit treatment of the electronic problem is needed only at the defect site and on a number of neighbouring ionic sites, while all that is required in the larger surrounding zone is that the correct variation of the lattice electrostatic potential is well represented. This outer zone can therefore be modelled by a shell of ions represented by point charges[154][155], or by ion-shell harmonic couples (*i.e* using the shell model[156]). To complete the system representation a suitable second outer shell can be included in the calculations, normally as a uniform medium or as a shell model lattice with the correct dielectric properties.

The resulting model, similar in spirit to the Mott-Littleton model[157] for the far-field displacement in a polarisable material, provides an economical framework within which the energetics and the electronic structure of isolated defects can be investigated without the approximations associated with the use of periodic boundary conditions. Although the results of calculations on isolated defects (vacancies, or substitutional atoms) in materials like MgO and U_2O are found to be in good agreement[155] with those of the fully modellistic calculations which they are meant to support, the truly "ab initio" content of this approach can be biased by limitations in the HF basis-set convergence, and by the limited size of the tractable clusters. The method has nevertheless recently produced good results on a number of defect systems in Oxides like F-type centres[158] substitutional anion impurities in MgO[159], and substitutional Li trapped-hole centres in MgO[160], and has been proven useful to derive defect interionic potentials for model calculations[161].

The problems connected with a proper termination of the cluster, and with embedding the cluster in the appropriate Madelung field, have been recently revisited by Pisani and co-workers[162]. These authors propose to couple the cluster with the correct crystalline environment by a self-consistent procedure which takes into account, through appropriate correction terms, the electronic structure of the perfect crystal, which can be separately calculated with the ab initio HF technique. The method, which has already provided encouraging results on various systems including oxides[163], is probably the most sophisticated HF-based technique developed so far which can treat defects in solids without the approximations imposed by the use of periodic boundary conditions.

5.2.3 Previous DFT-PW calculations.

The volume of work available in the literature about defective ionic systems treated in the DFT-PW formalism is not comparable to the large quantity of papers based on model or ab initio HF techniques, at least as long as second-row anions like oxygen are present in the material. In particular, we could not find in literature any report on previous attempts to calculate the energetics of isolated defects in ceramic oxides, on which this work concentrates. The reason is simply connected to the extremely large basis sets needed to treat the strongly peaked oxygen *p*-orbitals in a large supercell, so that it is only very recently that calculations of this kind have entered the reach of computational technologies, due to the concurrent effect of improvements in the efficiency of minimisation algorithms, improvements in the convergence properties of the pseudopotentials, and escalation of the available computing power.

Although the pseudopotential density functional techniques have been applied successfully to study some perfect oxide crystals in normal conditions[164], or their electronic structure in high pressure regimes[165], the study of larger systems with these techniques has been limited to few cases[166]. Most of the work has however been devoted to the investigation of silicates[167], and their phase-dependence on pressure[168]. (Note that silicates are not strictly ionic materials due the semi-covalent nature of the Si-O bond.) In particular some calculations have been recently performed on the energetics of oxygen vacancies (neutral and charged) in SiO_2 ($\alpha-$cristobalite[169] and $\alpha-$quartz[170]), even though the vacancy defects cannot be considered to be isolated in the system geometries investigated[5]. The calculations presented in the following sections[122] correspond as far as we know to the first documented application of the well established DFT-LDA-PW technique to the investigation of isolated defects in ionic oxides.

---

[5] The vacancies are located on neighbouring lattice sites of different SiO_4 tetrahedral units[169].

5.3 Test calculations and periodic boundary conditions.

5.3.1 Setting up of calculations.

Before attempting calculations on defects in MgO and Li_2O, we have made extensive calculations on the properties of the perfect crystals, which can be checked both with with experiment and with previous theoretical investigations. Before reporting on our work on perfect crystals, we summarise briefly the calculation ingredients and parameters used throughout the work.

The main problem in the representation of ions comes from the oxygen pseudopotential, which requires an high cutoff treatment. The pseudopotential we used was derived[26] within the RRKJ procedure discussed in Section 2.4.1, and represented in the KB form (eqn. (2.33)). The optimisation wavevector q_c for the p-wave was set equal to 5.7 *a.u.* . The reference atomic configurations used to construct it were $2s^2 2p^4$ for the s and p components, and $2s^2 2p^{2.5} 3d^{0.5}$ for the d component, with real-space cut-offs for the three components equal to 1.25, 1.25 and 1.45 *a.u.* respectively.

A severe test of the general quality of an oxygen pseudopotential is provided by the study of the convergence with respect to the PW energy cutoff of the physical properties of the isolated oxygen dimer, which can be investigated to check at the same time the transferability properties of the pseudopotential. The short equilibrium length of the dimer and the highly asymmetric electronic distribution around each atom which is associated to the molecule's ground state, concur to provide an ideal small test system to prove the quality of a pseudopotential (which is always a compromise between transferability and convergence properties), and make sure that the pseudopotential can be used with absolute confidence in the calculations on larger systems.

To avoid the problems connected with the molecule polarisation, a useful comparison can be made with results from other LDA calculations performed with "hard" pseudopotentials forced to convergence at extremely high energy cutoffs, and with "soft" potential constructed with different optimisation schemes recently introduced. In table 5.1 on page 133 we report a comparison of our results for the dimer with those obtained from reference [171] using a recently introduced scheme for "ultrasoft" pseudopotentials[172], and with those of the standard unoptimised pseudopotential of reference [11]. Our calculated results are obtained for the molecule in a cubic box of edge 10 *a.u.*, using the Γ-point to sample the Brillouin zone, exactly as it was done in reference [171]. The bond length, ground state vibrational frequency and binding energy of the dimer are seen to be well converged with respect to the literature results by the time we get to a cutoff of 600 *eV* (44.1 *Ry*).

Optimisation is not needed for magnesium or lithium pseudopotentials. We have used in these cases two pseudopotentials generated with the standard Kerker method[173]. The reference all-electron atomic configurations for Mg were $3s^2$ for the *s*-component, and $3s^{0.5}3p^{0.25}3d^{0.25}$ for *p*- and *d*-components, with real space cutoffs ("core radii") of 1.38, 1.98 and 2.03 *a.u.* . The real-space cut-off for Li was 1.5 *a.u.* for components *s* and *p*, for which the atomic configurations used were $2s^2$ and $2s^{0.75}2p^{0.25}$ respectively (the *d*-wave was not treated explicitly in the generation process). For both Mg and Li pseudopotentials the *s*-wave component has been treated as local, to minimise the bias due to the KB representation, given that in most systems treated the spherical components of the electronic orbitals are by symmetry expected to be the most important, while the electronic charge in the ionic solids investigated is known in advance to be radically different (lower) than in the neutral atoms case. All pseudopotentials have been shown to be highly transferable over the required energy ranges, and to be free of the "ghost" states which can sometimes afflict the Kleinman-Bylander representation form[24].

For all the calculations on the perfect crystals we used a PW energy cutoff of 1000 *eV* (73.5 *Ry*), while for the calculations on the larger defective systems we used a *minimum* cutoff of 600 *eV* (41.1 *Ry*), corresponding to the range of 600-700 plane waves per atom. The first higher cutoff was used to guarantee the excellent convergence needed for the evaluation of elastic properties, while the second more limited cutoff was found enough to guarantee the convergence of energy differences within 10^{-3} *eV* per atom in all systems.

Other points of technique are as follows. In the Mg atom there is an appreciable overlap between the 3*s* and 2*p* orbitals, which means that the non-linear core correction[27] described in Section (2.4.2) may be significant in our case. The correction was therefore implemented and used in test calculations, as reported in the next section. The sampling of Brillouin zone is much less important for highly insulating oxides than it is in metals. The BZ sampling points were generated by the standard Monkhorst-Pack scheme[32]. The exchange-correlation energy was represented by the Perdew Zunger form[146][6].

All the ab initio total energy minimisations were performed using the preconditioned conjugate gradients technique developed by Teter *et al.*[19] already described in Section (2.3.2), using the code CETEP (Cambridge-Edinburgh Total Energy Package)[119] on a 64-node Meiko Computing Surface in Edinburgh University and a 32-node Intel iPSC/860 in Daresbury Laboratory. For details on the parallelisation strategy adopted by the code, Section 4.4 should be consulted.

5.3.2 Results for the perfect crystals.

We briefly illustrate here the results obtained from our calculations on the perfect crystals, as a check of our techniques, to be compared with experimental data. Apart from giving us the opportunity to test the adequacy of some calculation setting features like the pseudopotentials used and the chosen cutoffs, the calculations on the unit cells allow to investigate the convergency of the BZ sampling at very low computer time costs.

Once the target supercells have been chosen, (in our case a 16-ion and a 32-ion cell for MgO, and a 48-ion supercell for Li_2O), the perfect-crystal calculations using those supercells and any chosen sampling set can be reproduced using the unit supercell and

---

[6] Some evidence of a "better" behaviour in ionic materials of different exchange and correlation energy forms has been reported[165].

an appropriate "folded out" set of sampling points, leading to the same total energy within numerical accuracy. Our tests show that Γ-point sampling only is not really adequate even for the 32-ion and 48-ion systems, but that the Monkhorst-Pack four-point set[32] (eight points in the full BZ, reduced to four because of the inversion symmetry) should be extremely accurate, giving an error of less than 0.01 eV in the total energy per cell. However, for calculations on the distorted unit cells which we need to fit the elastic constants and the transverse optic frequencies, the four-point set is not adequate, and we have used 16 or 32 k-points in this cases.

The core correction due to the non-linear dependence of the exchange-correlation energy on electron density can produce important effects if there is a significant overlap between core and valence wavefunctions[27]. This effect is negligible for oxygen, but there is slight overlap for the magnesium atom, as shown in figure 5.1 on page 128, which makes the correction worth investigating[7]. Its effects turn out to be small, and will be noted below where appropriate. Our calculated values of the equilibrium lattice parameter a_0, the bulk modulus, the three elastic constants C_{11}, C_{12}, C_{44}, the zone-centre transverse optic frequency and the four phonon frequencies at the X-point for MgO are listed in table 5.2 on page 134. The reported value of lattice parameter does not include the core correction, which reduces it by 0.5 %. This variation is well within the uncertainty from other sources. For comparison, the use of the Wigner form for exchange-correlation[174], instead of the form we have used, increases the lattice parameter by 0.9 %. However, the core correction is included in the TO frequency, which is the only case where it was found to be significant: without the correction, the frequency results lower by 0.8 THz. Our calculated results for some perfect lattice properties of Li_2O are reported in table 5.3 on page 135. As for MgO, the evaluation of phonon frequencies has been made through the "frozen phonon" technique, *i.e.* directly from the fitted curvature at the minimum of the total energy function calculated for each phonon at various amplitude displacements in the harmonic regime. The very

---

[7] Although this correction has been used in the past for calculations on bulk properties of ionic materials[164][165], no report of the size of its effects has been made.

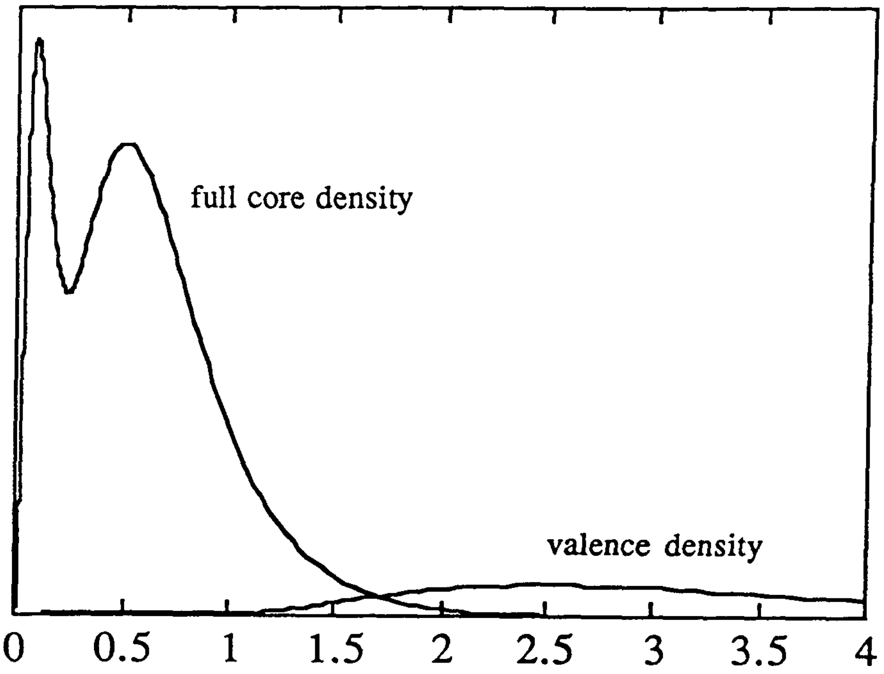

Figure 5.1: Contributions to the electron density $\rho(r)$ as a function of radial distance r (*a.u.*) due to core electrons and valence electrons in the neutral Mg atom, showing the slight overlap in the region 1.5 - 2.0 *a.u.* .

good agreement with experiment of all the perfect lattice properties investigated is what should generally be expected from calculations of this kind, and gives us confidence that the technical aspects of the calculations are under adequate control. To provide some reference point for the results of calculations on defective systems, we show in figures 5.2 and 5.3 on page 136 the calculated ground state density distributions for the valence charge in the perfect crystals. In both cases the strongly ionic nature of the compounds is very clear, the charge being almost completely localised on the oxygen atoms.

5.4 Defect energetics in periodic boundary conditions.

The goal of our calculations is to provide a theoretical estimate for the energy of formation of Schottky defects in MgO and Frenkel defects in Li_2O. Both kind of defects involve the presence in the solid of a couple of *isolated* point-defects of opposite charge: an anion vacancy and a cation vacancy for the Schottky defect in MgO, and a cation vacancy and a cation interstitial for the Frenkel defect in Li_2O. The calculations could in principle be performed using supercells big enough to contain the defect couples at a distance from each other such that the two point defects could be considered isolated in the same sense as they are in the real systems (the screened Coulomb interaction being obviously long-ranged both in the theoretical model and in the experimental samples). However, because of the limited size of the supercell which can be investigated in material like these, the calculations have to be performed sitting a single vacancy or interstitial in each repeated cell. The overall defect charge state which is to be investigated has to be therefore defined when setting in each defect calculation the total electronic charge (*i.e.* the number of electrons) present in the supercell.

Vacancies in MgO carry a net charge: a Mg vacancy is formed by removal of a Mg core without changing the number of valence electrons, while an O vacancy is formed by removing an O core together with 8 valence electrons; the net charges of the Mg and O vacancies are thus $-2e$ and $2e$ respectively. The Li vacancy in Li_2O is constructed in an analogous way, while the Li interstitial is formed by adding a Li core without introducing an additional valence electron, the vacancy and the interstitial having thus net charges of $-e$ and e respectively.

We note that other charge states are also possible. For example, under suitable conditions, F-centres consisting of one or more electrons bound to an oxygen vacancy can be formed[158]. These different states have not been studied here. We also did not investigate in the present work the unoccupied acceptor and donor energy levels associated with the vacancy defects, although these are clearly of great interest.

Because of the net charges carried by the defects, the sum of the core and electron charges in each supercell is not zero when a vacancy or an interstitial are present. This introduces a formal divergence in the total energy per supercell, due to the long-ranged nature of the Coulomb interaction. Moreover, a correction has to be devised for the spurious interaction of the vacancies and of the interstitials with each other's polarisation fields. Note that neither of these problems was present in the case of the calculations on vacancies and interstitials in Al reported in Chapter 3, because of the short-ranged metal screening and of the uncharged nature of the defects in the systems considered there.

These issues arise in exactly the same form in the treatment of charged defects with empirical interaction models. An established way to treat charged defects in periodic boundary conditions is to suppose the net charge of cores and electrons to be compensated by a uniform background. This eliminates the mathematical divergence at $G = 0$ in the total energy expression in the PW formulation[181]. The procedure has been applied both in model calculations[182] and ab initio calculations[183] involving charged defects in periodic boundary conditions. In particular in the model calculations on defects in KCl and CaF_2 of reference [182] (Leslie and Gillan, 1984), a systematic comparison was made with the results obtained with the same model potential but without the use of periodic boundary conditions (*i.e.* on truly isolated defects represented in the Mott-Littleton scheme[157]), showing perfect agreement between the two approaches. These authors also introduced a simple physical argument from which a correction term for the residual Coulombic interaction between defects can be derived[182]. Following their procedure, we calculate the leading contribution to the defect-defect interaction energy ΔE by regarding the defects as a superlattice of repeated point charges. The correction term ΔE represents the Coulomb energy per cell of a periodic array of point charges with a neutralising background immersed in a structureless dielectric of the same dielectric constant as the perfect crystal, and is given by

$$\Delta E = -\frac{1}{2}\alpha q^2/\epsilon_0 L \ , \tag{5.3}$$

where q is the net defect charge, ϵ_0 is the static dielectric constant of the bulk crystal,

L is the lattice parameter of the supercell and α is an appropriately defined Madelung constant. Each defect formation energy is obtained by subtracting the energy of the perfect system from that of the defective system. Since we are interested in the energetics of isolated defects, the correction ΔE is subtracted from the result to obtain an improved value.

In order to support the correctness of this procedure, we have performed a series of calculations on vacancy energetics in MgO in periodic boundary conditions using the shell model with a well established parametrisation for the pair interaction potentials. The goal of these calculations was (i) to analyse the converge of the Schottky formation energy and of the vacancy migration energies with respect to the size of the supercell, and (ii) to check the agreement of these results with the literature results on isolated defects obtained from the conventional Mott-Littleton method using the same potential parameters[8].

The parametrisation of Sangster and Stoneham[136] was used for the pair interaction potentials, with the potentials represented in the standard Buckingham form[9] of eqn. (5.1), in which the Mg and O ions in the shell-model have the ionic charges of 2e and -2e. The calculations were performed using the code SYMLAT[184] on the CRAY X-MP/416 in Rutherford Appleton Laboratory, Oxford. We report in table 5.4 on page 137 our results for the empirically calculated Schottky energy, including the Madelung correction (5.3), and for the cation and anion vacancy migration energies, for supercell sizes going up to over 400 ions. Results from the same interaction model obtained by the Mott-Littleton method[185] are also reported for comparison.

It is clear from the results in table 5.4 that the supercell values for all the defect energies converge rapidly with increasing cell size to the Mott-Littleton values for isolated defects. With a supercell size of 32 ions, the residual error in the Schottky energy E_S is about 0.7 eV, *i.e.* about 10 % of its value. This accuracy can already

---

[8] In appealing to empirical modelling in this way, we are making the (reasonable) assumption that the asymptotic dependence of the energies on supercell size will be qualitatively the same in ab initio and empirical treatments.

[9] This potential form is also sometimes referred to as "Born-Mayer-Huggins" form.

be considered satisfactory, although the full ab initio treatment of the 54-atom or 64-atom supercells would perhaps be desirable to remove residual convergence errors. As would be expected in the hypothesis of large cancellation of the convergence errors, the migration energies converge faster than the Schottky energy, and are already rather well converged for systems of 32 lattice sites, the absolute errors being about 0.3 eV. Although we performed some model calculations also on Li_2O, to establish a "first guess" set of ionic position for the ab initio calculations requiring lattice relaxation (as reported in the next section), we did not repeat the full analysis done in the case of MgO. The convergence of the corrected results with respect to supercell size was assumed in this case to be achieved for our biggest (48-atoms) supercell. This supercell has a bigger volume (approximately 20%) than the MgO 32-atom supercell[10], while the charge of the defects investigated is half than it is in MgO. The expected size of the error due to spurious interaction between defects in repeated cells is therefore at least four times smaller in Li_2O than it is in MgO.

---

[10] Note that both supercells are body-centered cubic, and the two materials have almost identical dielectric constant ϵ_0 (9.86 for MgO and 9.78 for Li_2O).

Approach	E_{cut} (Ry)	d $(a.u.)$	ω (cm^{-1})	E_{bind} (eV)
ref. a				
V($r_c = 1.8$ $a.u.$)	20	2.41	1840	9.7
	25	2.40	1780	9.8
V($r_c = 1.5$ $a.u.$)	20	2.29	1760	10.0
	25	2.30	1760	10.1
	30	2.30	1800	10.1
V($r_c = 1.2$ $a.u.$)	20	2.49	1130	9.1
	30	2.32	1650	9.8
	50	2.30	1610	9.8
BHS (ref. b)	40	2.40	1170	9.0
	85	2.30	1490	9.6
	125	2.29	1660	9.8
This work	29.4	2.39	1914	-
	44.1	2.27	1539	9.8

Table 5.1: Energy cutoff convergence of the equilibrium distance d, the ground state frequency ω and the binding energy E_{bind} of the oxygen diatomic molecule compared with the theoretical results of (a): Laasonen and Car [171], using the optimisation method due to Vanderbilt[172] (for three different values of the core radius r_c), and with (b): the reference pseudopotential of Bachelet *et al.*[11]. See text (page 124) for the details on the pseudopotential used in the present work.

	calculated	experimental
a_0 (Å)	4.17	4.21^a
B (Mbar)	1.54	1.55^b - 1.62^c
C_{11} (Mbar)	3.03	2.90^d
C_{12} (Mbar)	0.76	0.88^d
C_{44} (Mbar)	1.69	1.60^d
TO(Γ) (THz)	12.39	12.23^c
TA(X) (THz)	8.65	8.96^b
LA(X) (THz)	12.57	12.65^b
TO(X) (THz)	13.24	13.15^b
LO(X) (THz)	16.36	16.61^b

Table 5.2: Calculated and experimental values of lattice parameter a_0, bulk modulus B, elastic constants C_{ij} and five phonon frequencies of MgO. Phonon modes are the transverse optic mode at the Γ-point and the transverse and longitudinal acoustic and optic modes at the X-point of the Brillouin zone. References to experimental work are (a): Wyckoff[175]; (b): Sangster *et al.*[176]; (c): Anderson and Andreatch[177]; (d): Jasperse *et al.*[179].

	calculated	experimental
a_0 (Å)	4.50	4.60
c_{11} (Mbar)	2.14	2.02
c_{12} (Mbar)	0.15	0.22
c_{44} (Mbar)	0.69	0.59
TO(Γ) (THz)	14.1	12.6
R(Γ) (THz)	16.5	15.7
TA(X) (THz)	8.5	7.7
LA(X) (THz)	15.0	14.3
TO(X) (THz)	11.8	11.1
LO(X) (THz)	22.2	22.0
TR(X) (THz)	17.8	16.2
LR(X) (THz)	7.1	8.0

Table 5.3: Comparison of calculated and experimental values for lattice parameter a_0, elastic constants C_{ij}, and selected phonon frequencies of Li_2O. Acoustic, optic and Raman modes are denoted by A, O and R, longitudinal and transverse branches being distinguished by the initial letters L and T; Γ and X in parentheses indicate modes at the zone centre and at the X point of the Brillouin Zone. Experimental values are taken from ref. [180].

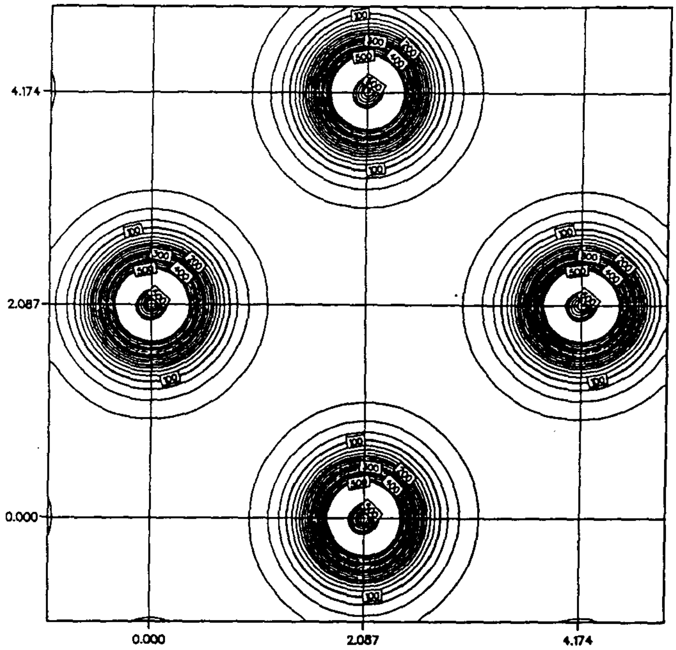

Figure 5.2: Contour plot of the calculated valence electron density (units of 10^{-2} Å^{-3}) on the (100) plane in perfect-crystal MgO. The contours are uniformly spaced at intervals of 25×10^{-2} Å^{-3}. Intersections of the grid lines mark regular-lattice sites. Distance along the edge of the plot is indicated in angstrom units.

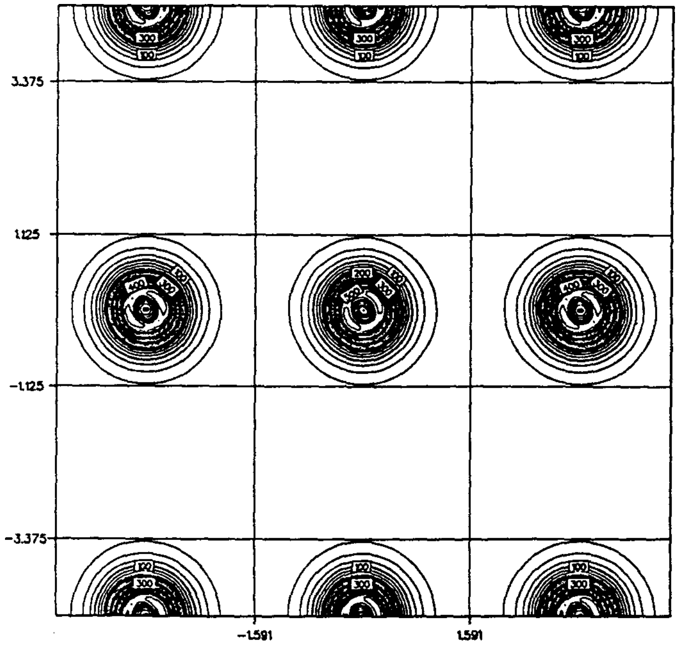

Figure 5.3: Contour plot of the calculated electron density on the (110) plane in perfect crystal Li_2O (antifluorite structure). Units as above.

no. of ions	E_S (eV)	ΔE_m (eV)	
		cation	anion
16	7.03	1.58	1.53
32	7.03	2.36	2.48
54	7.41	2.15	2.23
64	7.34	2.22	2.32
128	7.55	2.11	2.21
250	7.60	2.08	2.19
432	7.63	-	-
Mott-Littleton	7.72	2.07	2.11

Table 5.4: Values for the Schottky energy E_S and the cation and anion migration energies ΔE_m in MgO calculated in periodic boundary conditions using the empirical shell-model potential of Sangster and Stoneham[176]. Results are shown for a range of different sizes of supercell, and include the Madelung correction (see equation (5.3) on page 130). Also shown are the defect energies calculated from the same interaction model for the infinite crystal using the Mott-Littleton method (Sangster and Rowell [185]).

5.5 Defect energetics.

5.5.1 Schottky and Frenkel formation energies.

The Schottky energy E_S in MgO is the sum of the energies needed to extract a Mg^{++} ion and an O^{2-} ion to form two relaxed isolated vacancies, minus the cohesive energy per ion pair in the solid. For a given supercell size, we therefore calculate the energies of (i) the perfect crystal[11]; (ii) the system formed from (i) by extracting a Mg core; (iii) the system formed from (i) by extracting an O core and eight electrons. The Frenkel pair formation energy E_F in Li_2O is the the energy required to extract a Li^+ ion forming a relaxed Li^- vacancy, plus the energy needed to form a relaxed Li^+ interstitial, so that we need supercell calculations for the perfect lattice, the vacancy system and the interstitial system all performed at the fixed number of electrons of the perfect lattice case.

The calculated values for E_S and E_F are small energy differences of large total energy results, and therefore some attention has to be paid to ensure the maximum possible cancellation of errors when performing the subtractions. As previously mentioned, we made use for all supercell systems of the Monkhorst-pack 4-point sampling set for all the defect energetics calculations on the 16-atom and 32-atom cell in MgO and on the 48-atom cell in Li_2O, the sampling error expected for the largest system sizes on the total supercell energy being smaller than 0.1 eV.

For the 16-atom MgO calculations we used the PW energy cutoff of 1000 eV. The 32-atom and 48-atom calculations on MgO and Li_2O used a cutoff of 600 eV, corresponding to a number of plane-waves to represent each orbital in the range of 15000-20000. The justification for this lower cutoff comes from tests performed with different cutoffs on the (unrelaxed) vacancy formation energies in the 8-atom system. These calculations

---

[11] We really only need one calculation on the unitary cell system with the sampling set which is equivalent to the one we use for the supercell (cf. Section 5.4).

show that the cutoff decrease from 1000 eV to 600 eV changes the value of the Schottky energy for this system by less than 0.05 eV, in spite of a total energy difference per unit cell of about 2 eV between the two calculations, due to imperfect convergence with respect to cutoff.

Ionic relaxation could have been performed using the Hellmann-Feynman forces on the ions and some iterative minimisation scheme (for example, using the conjugate gradients technique on the ionic degrees of freedom). We have, though, found it more practical to adopt a less "automatic" procedure. For the MgO 16-atom cell the cubic symmetry of the vacancy leaves only one relaxational degree of freedom when a vacancy is created. The minima have therefore been determined by one-dimensional fit of the total energy curves along the only displacement coordinate. In the MgO 32-site cell and in the Li_20 48-site cells the degrees of freedom are many more, and we have simply used the output coordinates from our model calculations described in Section 5.4. This procedure is justified by the known accuracy of the shell-model results on the properties of the materials we investigate, although it could be only of partial help, or irrelevant, or even misleading, for materials with more complicated electronic structures than those of our case.

In any case the magnitude of the residual forces acting on the ions at the end of the electronic minimisation gives clear indications on the differences between the model and the first-principles ionic minima, and allows an estimation of the residual total-energy decrease which would be recovered by the complete ab initio relaxation of atoms. In our calculations the residual Hellmann-Feynman forces using the model-relaxed positions were always less then 0.4 $eV/Å$, (and practically always much less than this much), and harmonic models of the further relaxation indicate that the energy lowering could not exceed 0.1 eV, which is not very relevant given the size of errors from other sources in the calculations (see discussion on page 131) and the *much* larger magnitude of the experimental error bars. Our results for the energetics of vacancy defects in the two materials investigated are reported in table 5.5 on page 142. Ions extraction or immersion energies are corrected with the Madelung correction (5.3) for the residual Coulomb interaction between periodic defect images in different supercells.

The formation energy of Schottky defects in MgO is so large that its precise experimental determination, due to the extremely low concentration of defects even close to the melting point, is very difficult. The measured values range in the interval 5-7 eV[142], and therefore the agreement within about 0.5 eV between our results and the results of the pair potential models (see discussion on page 131 and results in table 5.4 for the uncomplete convergence with respect to supercell size) is an important support for the validity of these models.

The experimental uncertainty on the Frenkel formation energy in Li_2O is also rather large. The formation energy 2.53 eV from reference [187] is probably the most reliable experimental value, being the result of a careful computer-fitting analysis of a very large amount of data (from a wide temperature range for the conductivity measurements). Given these uncertainties, our calculated value 2.20 eV in table 5.5 can again be considered in satisfactory agreement with both the experimental results and the empirical-model predictions.

The effect of the vacancy defects on the surrounding charge distribution can be studied by subtracting the ground state density of the perfect lattice from that of the unrelaxed defective system. Contour plots of these density differences for the Mg and O vacancies in MgO in the (100) and (110) planes are shown in figures 5.4 and 5.5 on pages 143 and 144. The units used for the density are $10^{-2}/\text{Å}^3$, the lengths are expressed in Å, and the ions (in the rock-salt structure) are at the intersections of the superimposed grid.

The structure of the density response to the magnesium vacancy can be analysed on the (100) direction on both planes in figure 5.4. The small amount of charge present on the cation and in the region immediately around it in the perfect lattice is repelled by the negatively charged vacancy, to create a region of negative (shaded) difference. The main structure of the charge response is on the (six) neighbouring oxygen ions, and takes the form of a distortion of the p-like orbitals pointing towards the vacancy, whose lobes are displaced to create the double peak-trough structures visible on the oxygen sites.

In the case of the (positive) oxygen vacancy in figure 5.4, the leading effect is a charge transfer to the spherical region surrounding the vacant site and corresponding to the six nearest neighbours Mg atoms, which are less efficiently ionised in the absence of the oxygen in the center of the octahedron they constitute. The transfer is mainly from the *p*-orbitals pointing to the vacancy of the nearest neighbour oxygen atoms, on which the depletion leaves the prominent quadrupole moment visible in the center of the (100) plane plot.

Similar difference plots for the Li unrelaxed vacancy and interstitial in Li_2O are shown in figure 5.6 on page 145 for the (110) plane. The interstitial site is at the center of a face-centered cube of oxygen atoms. Again here the effective negative charge of the vacancy and positive charge of the interstitial create large depletion regions (of opposite sign) around the defects, while the main effect, as for the Mg vacancy in MgO, is in the distortion of the *p*-orbitals on the oxygen ions neighbouring the defects, whose lobes relax in response to the repulsive (attractive) field of the vacancy (interstitial). It is worth noticing that these effects obtained with a first-principles description of the electronic distribution give a much more complex image of the polarisation response than what can be derived from simple dipolar models like the shell model, and could provide the insight needed for more refined modelling taking into account the shape of the electronic polarisation response[12] .

---

[12] For example, fitting the parameters of "breathing" spherical, elliptical or of more complicately shaped model shells [139][140] .

MgO	16 ions	32 ions
(1) perfect lattice (total)	-3711.197	-7384.963
(2) perfect lattice (per unit cell)	-463.900	-461.560
(3) Mg vacancy (unrelaxed)	-3667.749	-7339.924
(4) Mg vacancy (relaxed)	-3668.136	-7341.224
Mg extraction energy:		
(5) uncorrected (4) - (1)	43.061	43.739
(6) corrected	44.633	44.987
(7) O vacancy (unrelaxed)	-3284.272	-6961.171
(8) O vacancy (relaxed)	-3285.718	-6962.754
O extraction energy:		
(9) uncorrected (8) - (1)	425.479	422.209
(10) corrected	427.051	423.457
Schottky energy:		
(11) ab initio (6) + (10) - (2)	7.784	6.884
(12) experimental	5 - 7[a]	
(13) empirical model	7.72[b]	
Li_2O	48 ions	
(14) perfect lattice (total)	-7226.666	
(15) perfect lattice (per unit cell)	-451.667	
(16) Li vacancy (unrelaxed)	-7212.570	
(17) Li vacancy (relaxed)	-7213.497	
Li extraction energy:		
(19) uncorrected (17) - (14)	13.169	
(20) corrected	13.467	
(21) Li interstitial (unrelaxed)	-7236.950	
(22) Li interstitial (relaxed)	-7238.233	
Li immersion energy:		
(23) uncorrected (22) - (14)	-11.567	
(24) corrected	-11.269	
Frenkel energy:		
(25) ab initio (20) + (24)	2.198	
(26) experimental	1.58[c]-2.53[d]	
(27) empirical model	2.28[a]	

Table 5.5: Ab initio total energies of the periodic systems used to study the energetics of defective MgO, and Li_2O, with the resulting Schottky energy E_S and Frenkel Energy E_F, compared with values from experiment and from empirical modelling. *Ab initio* results are shown for the MgO 16-ion and 32-ion supercells and for Li_2O 48-ion supercell. (The individual energies are numbered to allow the relations between them to be indicated.) The correction referred to in items (6),(10),(20),and (24), is the Madelung term given in equation (5.3). References to experimental and empirical values are (a):

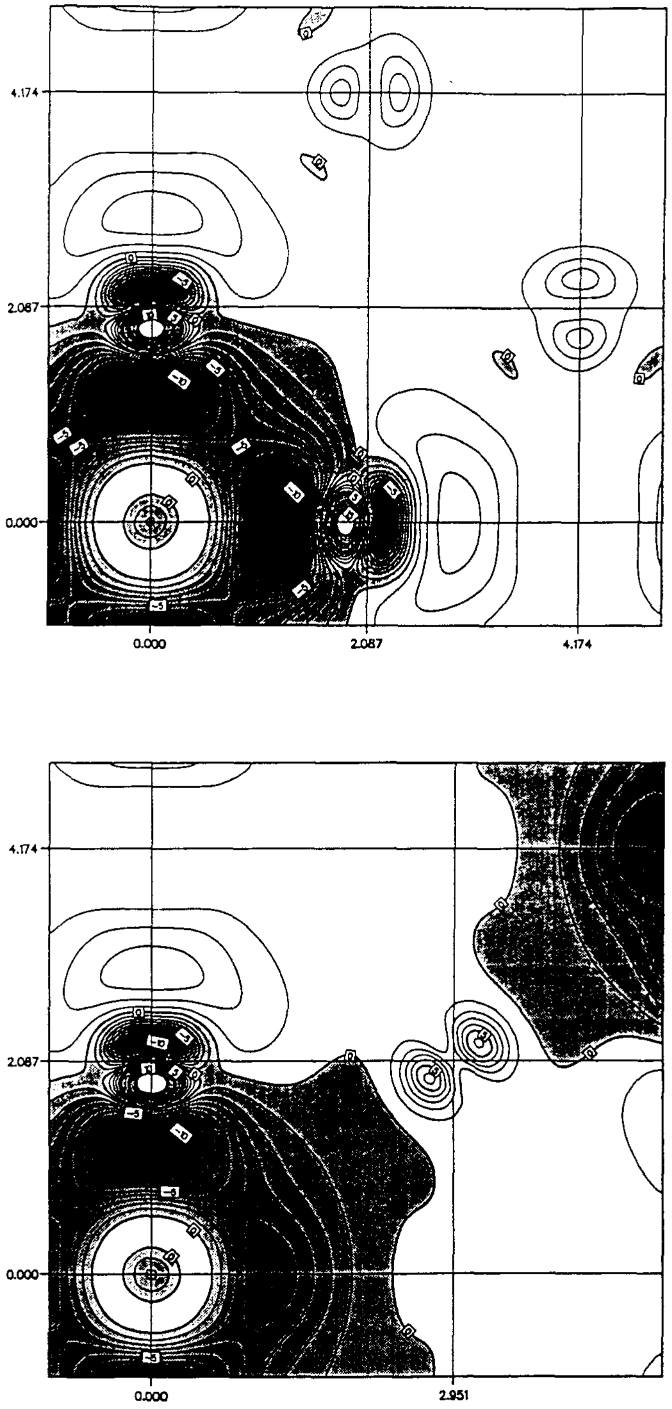

Figure 5.4: Difference valence density (defective system minus perfect crystal) for the Mg^{++} vacancy in MgO on the (100) (above) plane and the (110) plane (below). Density is in units of 10^{-2} Å^{-3}, with contours at intervals of 10^{-2} Å^{-3}, and negative regions shown shaded. Intersections of the grid lines mark regular-lattice sites, with the vacancy site at the origin of coordinates. Distance along the edge of the plot is indicated in angstrom units.

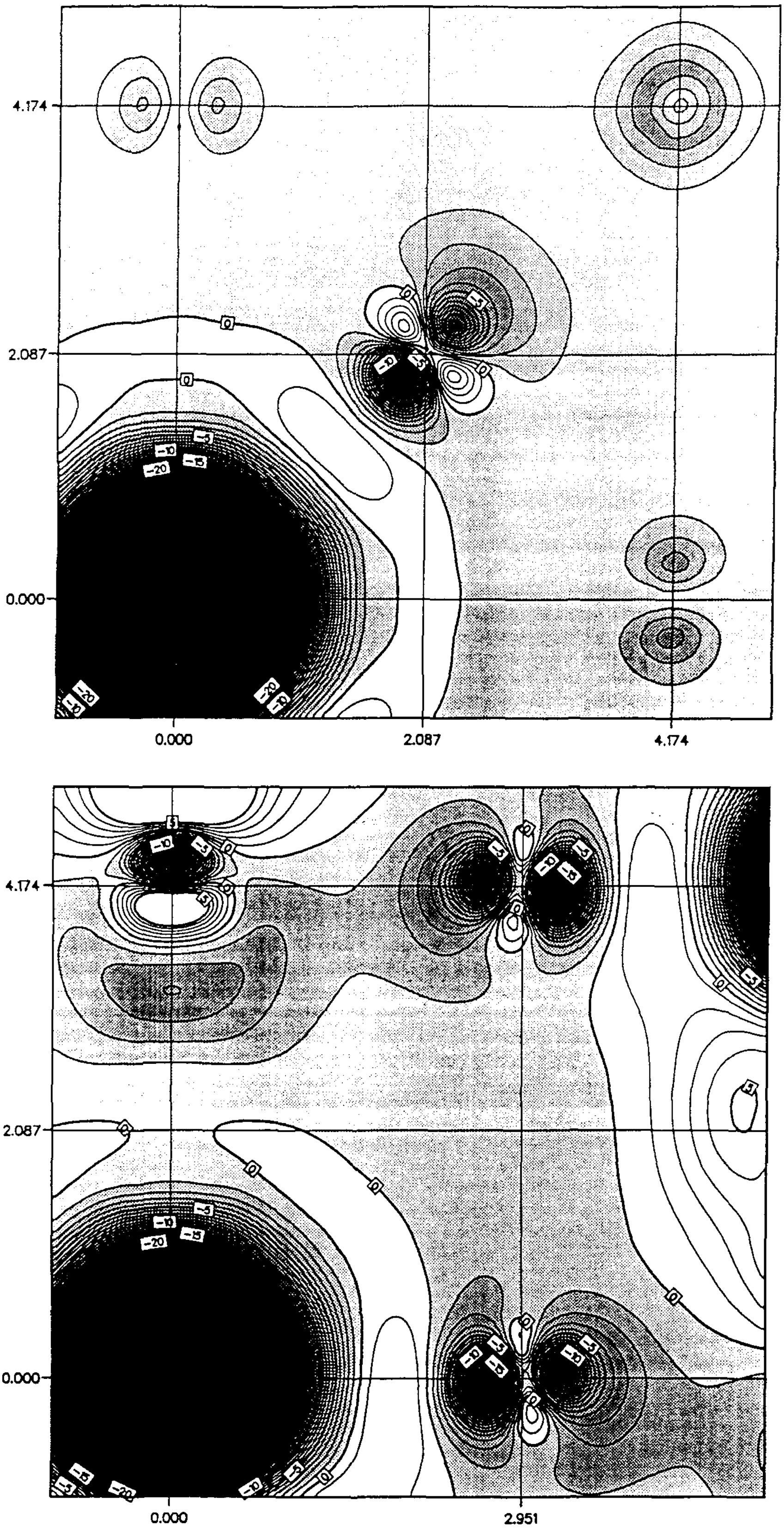

Figure 5.5: Difference valence density (defective system minus perfect crystal) for the $O^=$ vacancy in MgO on the (100) plane (above) and on the (110) plane (below). Other details are the same as for figure 5.4 (page 143).

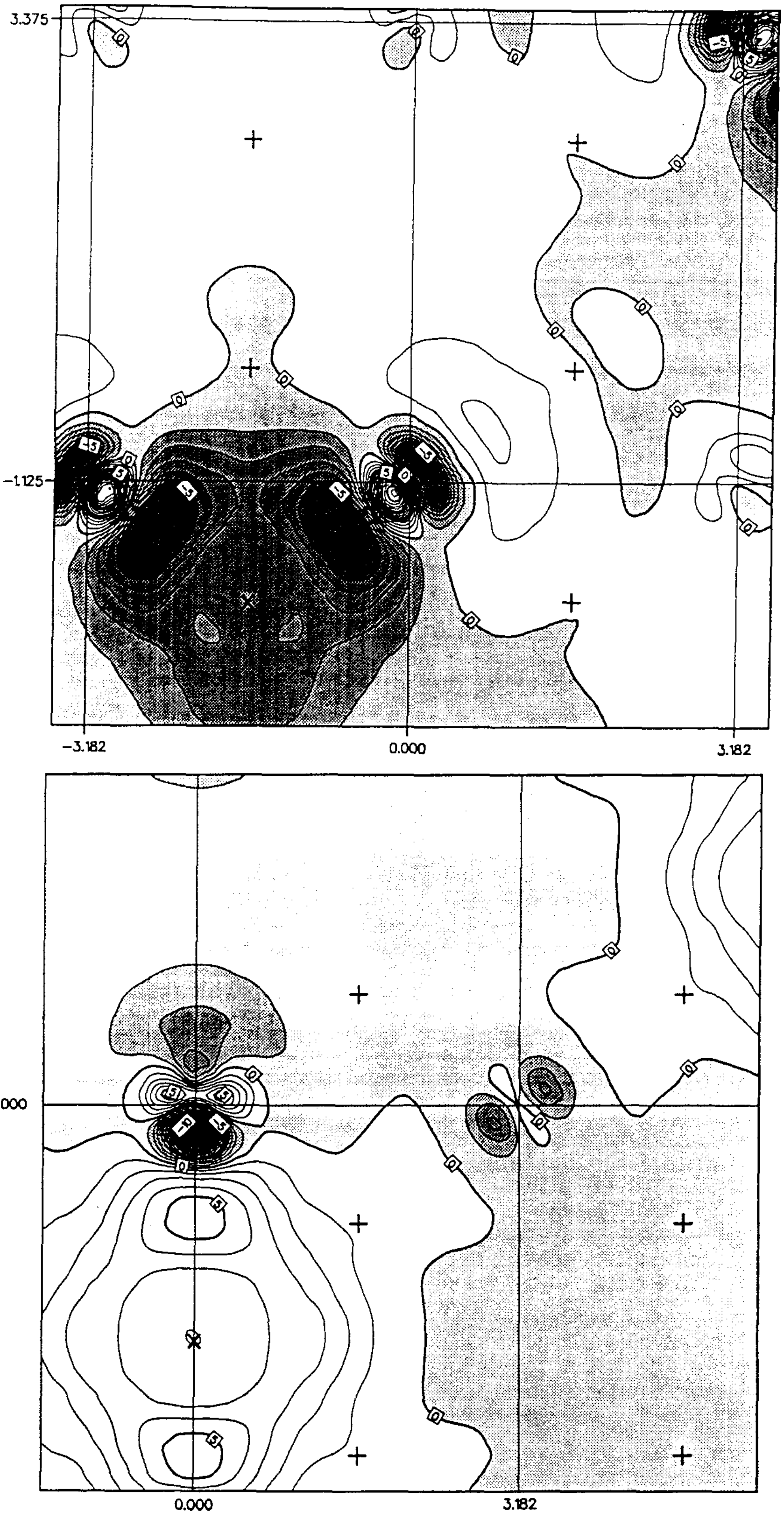

Figure 5.6: Difference valence density (defective system minus perfect crystal) for the Li^+ vacancy in Li_2O on the (110) plane (above) and for the Li^+ interstitial in the (110) plane (below). Density is in units of 10^{-2} Å^{-3}, with contours at intervals of 10^{-2} Å^{-3}, and negative regions shown shaded. Oxygen ions are at the intersections of the superimposed grid. "X" and "+" symbols denote the positions of the defects and of the lithium atoms on their regular lattice sites respectively.

5.5.2 Defect migration energies.

We turn now to consider the results of our ab initio calculations on migrating defects in the two materials. In the MgO crystal each of the sublattices of the two constituent elements has the fcc symmetry. The migration of both kind of vacancies takes place on a cubic centered face when an ion moves into the vacant site from a neighbouring sublattice site (see figure 5.7 on page150). The migration geometry is therefore similar to the migration of Al vacancies discussed in Chapter 3, and the migration energy is defined analogously for both ionic species as the difference between the energy of the fully relaxed system with one ion sitting midway between two empty sublattice sites, and the energy of the fully relaxed vacancy. Charge density plots on the (100) plane for the full valence charge of the relaxed systems of migrating Mg and O vacancies are reported in figure 5.8 on page 151.

In the anti-fluorite structure of Li_2O, the lithium ions form a simple cubic sublattice. Each Li lattice site has therefore six equivalent nearest neighbour sites to which a Li vacancy can migrate during the diffusion process (see figure 5.9 on page 152). The stationary point where the migrating ion is positioned for calculating the migration energy is again midway between two perfect Li lattice sites. The ions are then relaxed using the empirical model calculation, as was done for the relaxed vacancy case, and the residual Hellmann-Feynman forces are checked to be small enough not to affect the results for the migration energy (experimentally about 04-0.5 eV) for less than 0.1 eV.

The migration mechanism of the Li interstitial in Li_2O is less clear (the migration energy is not known experimentally). Empirical modelling on a number of materials having the fluorite and anti-fluorite structures indicates the interstitialcy mechanism to be energetically favoured[141], in which the migrating interstitial moves onto an occupied regular site simultaneously displacing its previous occupant onto a new interstitial site (see figure 5.10 on page 153). The relaxed system saddle-point configuration has the two moving atoms disposed symmetrically with respect to the (110) mirror plane placed midway between the initial and final interstitial sites. Charge density plots on the (110) plane for the full valence charge of the relaxed systems of migrating Li vacancy and interstitial are reported in figure 5.11 on page 154.

The results obtained for the calculated migration energies are reported in table 5.6 on page 155. The results from table 5.5 for Schottky and Frenkel pairs formation energies have also been included for the biggest cell sizes. The very good agreement with experiment of all the migration energies, within an error of about 0.1 eV comparable with the spread of experimental numbers, is very encouraging.

The similarity of the cation and anion migration energies in MgO, also predicted by the empirical models, is confirmed by our result. The charge density plots in figure 5.8 show two completely different ground state charge distributions for the two migrating ions at the saddle point. This, however does not necessarily imply differences of the energetic barriers for the two migrations, since from the point of view of a Madelung model with formal charges ± $2e$ the two system configurations in the figure are one the mirror image of the other. The completely ionic nature of the ground state distributions even during the migration, (the Mg ions being invisible in the contour plots) could account for this apparent discrepancy between the enormous difference in size between the two migrating ions and the close similarity of the two migration barriers.

Good agreement, finally, is also found for the Li migration energy in Li_2O, which appears to underestimate the experimental results by less than $0.1eV$[13], while no experimental result is available for the interstitial migration energy.

5.5.3 Concluding remarks.

The calculations reported in the present chapter represent a first step towards the ultimate objective of accumulating a systematic data base for the energetics of defects in ionic materials. The results are encouraging, suggesting that the "first-principles" techniques we used are adequate to the class of systems investigated. It is noteworthy

---

[13] Note that the Madelung correction (5.3) cancels away when we evaluate the emigration energy as a difference of two energies. This reflects the fact that the macroscopic dielectric screening in the material does not depend on the position of the charged defect in the lattice.

that the generality of the methods we use prevents these results from being biased by particular choices of model parameters, localised basis sets, or special embedding techniques.

A first possible extension of the present results is the investigation of the other charge states and of the electronic structures associated to the defects studied. This would consist of the study of the vacancy defect systems not restricted to a single pre-defined total number of electrons in each supercell, and to the sole occupied energy levels. The relevance of this kind of study is connected with the important role which the energetic ordering of the possible charge states in defective systems has in determining the mechanical, optical, and chemical properties of oxide materials (in particular, in the case of rare earth ceramics like CeO_2, pure[194] or in solid solution[195]).

Another natural continuation of the present work is the investigation of ionic or semi-ionic materials for which the empirical models are not (or are only partially) reliable. This is particularly important in the case of materials for which the experimental evidence is incomplete and in need of theoretical support. An extension of the work to the study of grain boundaries and surface reconstructions and defects in oxide materials would also be of great relevance, to provide insight into sintering and catalysis processes at the fundamental level, for which there is a severe lack of experimental evidence. Some improvements in the present calculations and some refinement of the techniques, before extending their use to different materials, are, however, needed.

The possibility of investigating bigger systems is the first of the improvements needed. The ions in the materials investigated exert long-ranged Coulomb forces on each other, and each charged defect creates an extended polarisation region, distorting the surrounding lattice of ions and the associated electronic distribution. As discussed in the previous sections, the supercell method provides an elegant solution to the "termination problem" typical of the cluster-based approaches, but it also introduces the new problem of the spurious interactions between the defects polarisation fields.

In the case of bulk defects treated here, the volume of the supercells scales like the cube of the distance between the repeated defects. In the limit of extremely large systems the calculations are dominated by the orthonormalisation of orbitals, which scales like the cube of the system's volume (no. of atoms). An obvious advantage would be gained adopting some improved calculation strategy in which the computational workload were reduced to scale linearly with the volume of the system. The encouraging results of some recent investigations in this direction[120][121] suggest that suitable and robust algorithms for this purpose will be available in the very near future.

Another independent source of improvement will be represented by the introduction of very large parallel computing machines ("Teraflop machines"), which are expected to extend the reach of the techniques we have used to supercells containing several hundreds of atoms. The availability of machines of this kind, about two orders of magnitude more powerful than what is available at the moment (and definitely outside the reach of any foreseeable progress of non-parallel computing devices) will also automatically solve another, more minor, problem which we encountered in the present calculations.

In our calculations the direct relaxation of the ionic lattice around the defects using the Hellmann-Feynman forces results slow and ultimately unpractical. This problem was partially cured in the calculations by using as "first guess" positions the relaxed ionic coordinates obtained from an empirical model, and in our case no further atomic relaxation was ever needed for reaching good energy minima. However, some preliminary results on another system chosen as an example of more structurally complicated metal oxide (*e.g.* α-Al_2O_3 [133] [14]) show that this is not always the case, so that a fully ab initio technique for accomplishing the ionic relaxation is in general needed. Since efficient and robust algorithms for this purpose are already available (like the CG technique, applied to the atomic position and constructing the search directions from the Hellmann-Feynman forces), no other difficulty than the temporary limitation of computing resources prevents this particular problem to be solved in the course of a first-principles investigation like the one we have reported in the present chapter.

---

[14] The results of this particular study belong to a later stage of our investigation on oxide materials, and are not reported in the present work.

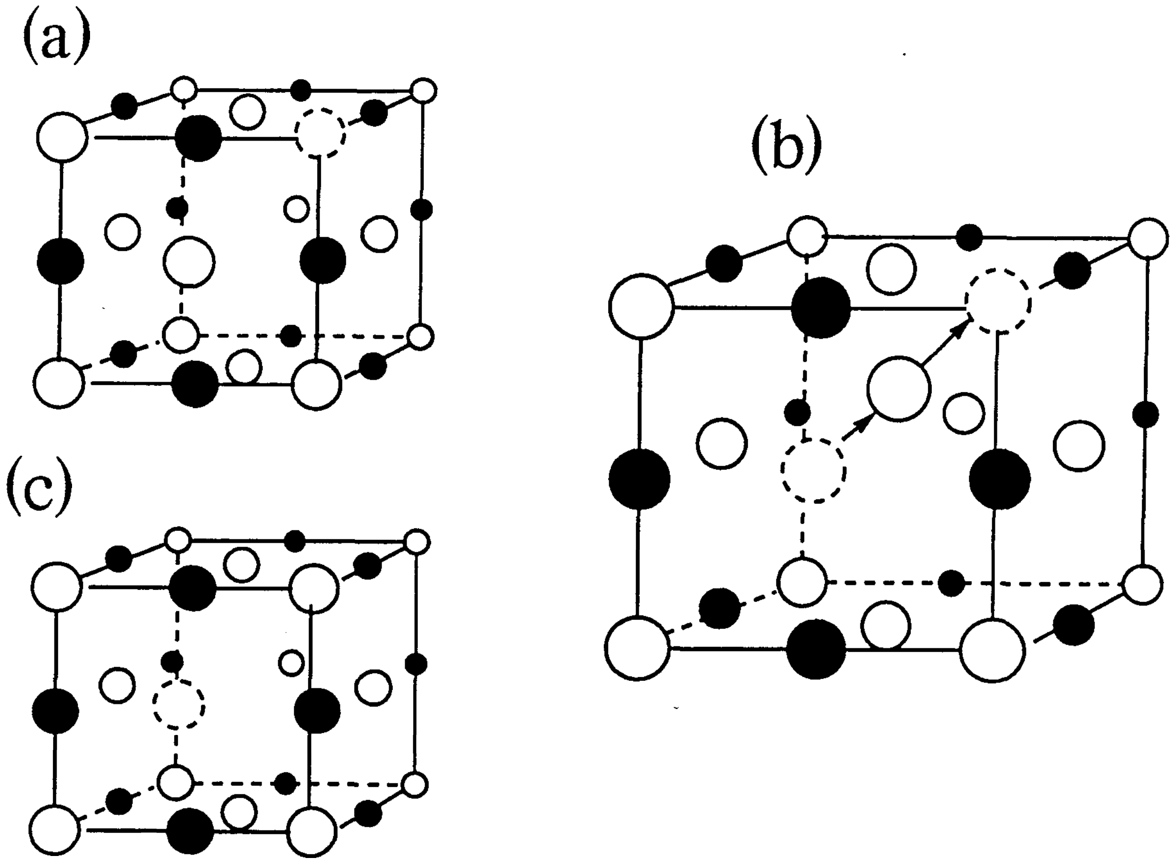

Figure 5.7: The rock-salt structure and the migration of a vacancy in MgO. Each atomic species occupies a fcc sublattice, the two sublattices being shifted of $a_0/2$ along the (100) direction one with respect to the other. The vacancies of both kind diffuse along the (110) directions. (a): vacancy in the stable position; (b): migrating ion at the saddle point midway between two regular lattice sites; (c): stable vacancy in the new position. The migration energy is the difference between the energies calculated at (b) and either at (a) or at (c).

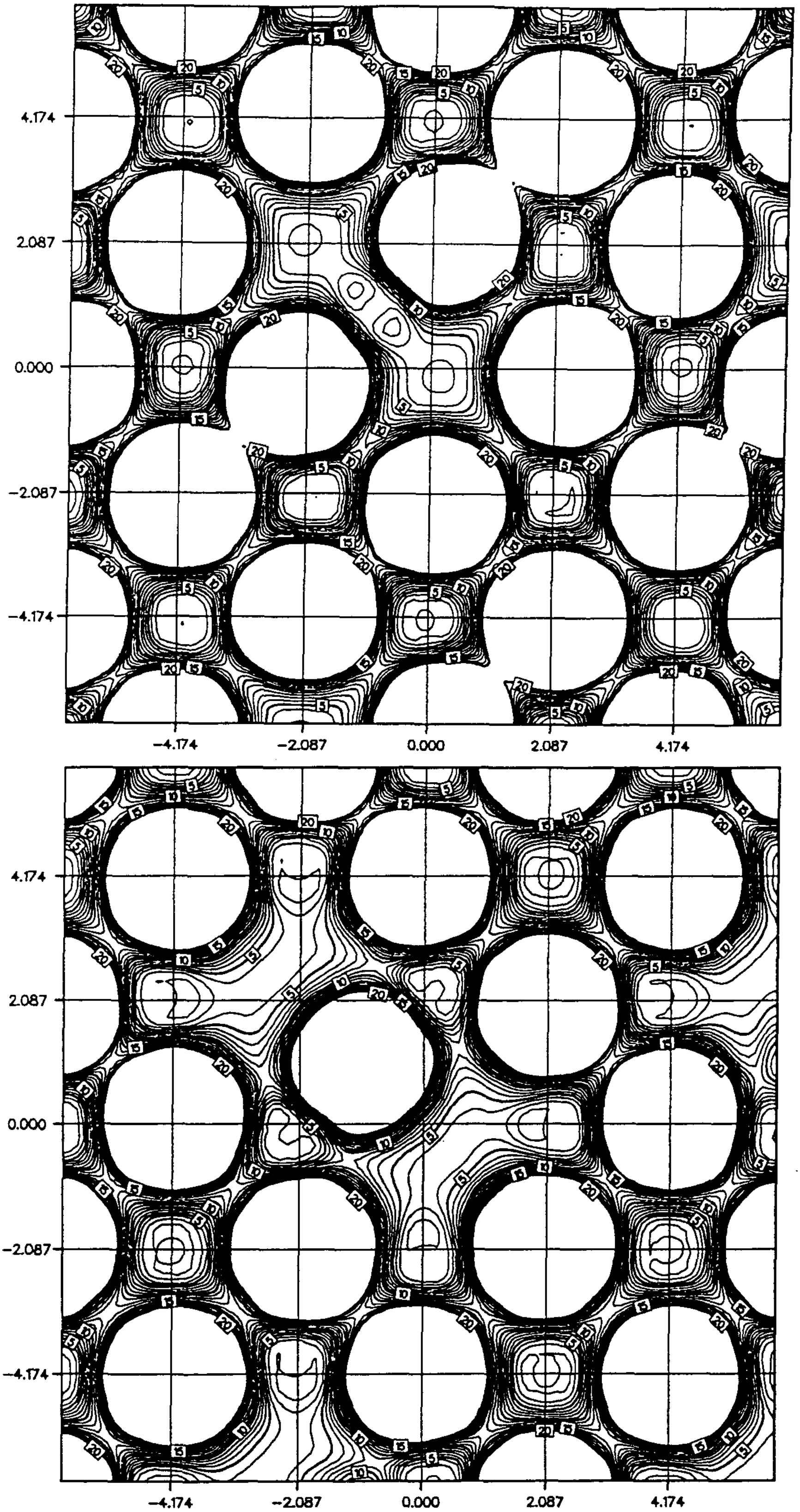

Figure 5.8: Total valence electron density on the (100) plane for the migrating Mg^{++} vacancy (above), and the migrating $O^{=}$ vacancy (below). In both cases the system is fully relaxed, with the migrating ion held at the saddle-point, midway between initial and final sites. Units of density are 10^{-2} Å^{-3}, with contours at intervals of 10^{-2} Å^{-3}. The plots are cut off for densities above 20×10^{-2} Å^{-3}. Distance along the edge of the plot is indicated in angstroms.

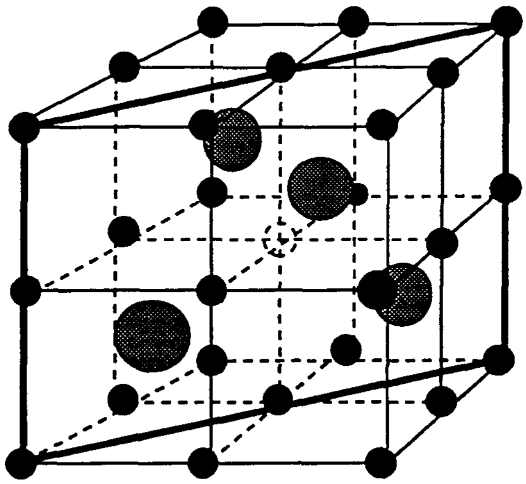

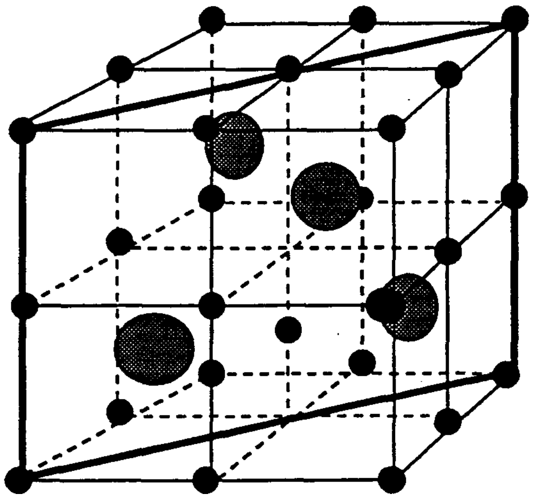

Figure 5.9: The anti-fluorite structure and the migration of a Li vacancy in Li_2O. Li and O atoms are represented by small black circles and large grey circles respectively. The vacant Li lattice site is at the center of the cube (above). The migration takes place along a (100) direction, with one of the six Li nearest neighbour atoms moving into the vacant site. The saddle-point position (below) corresponds to the migrating Li atom placed midway between the initial and final vacancy positions.

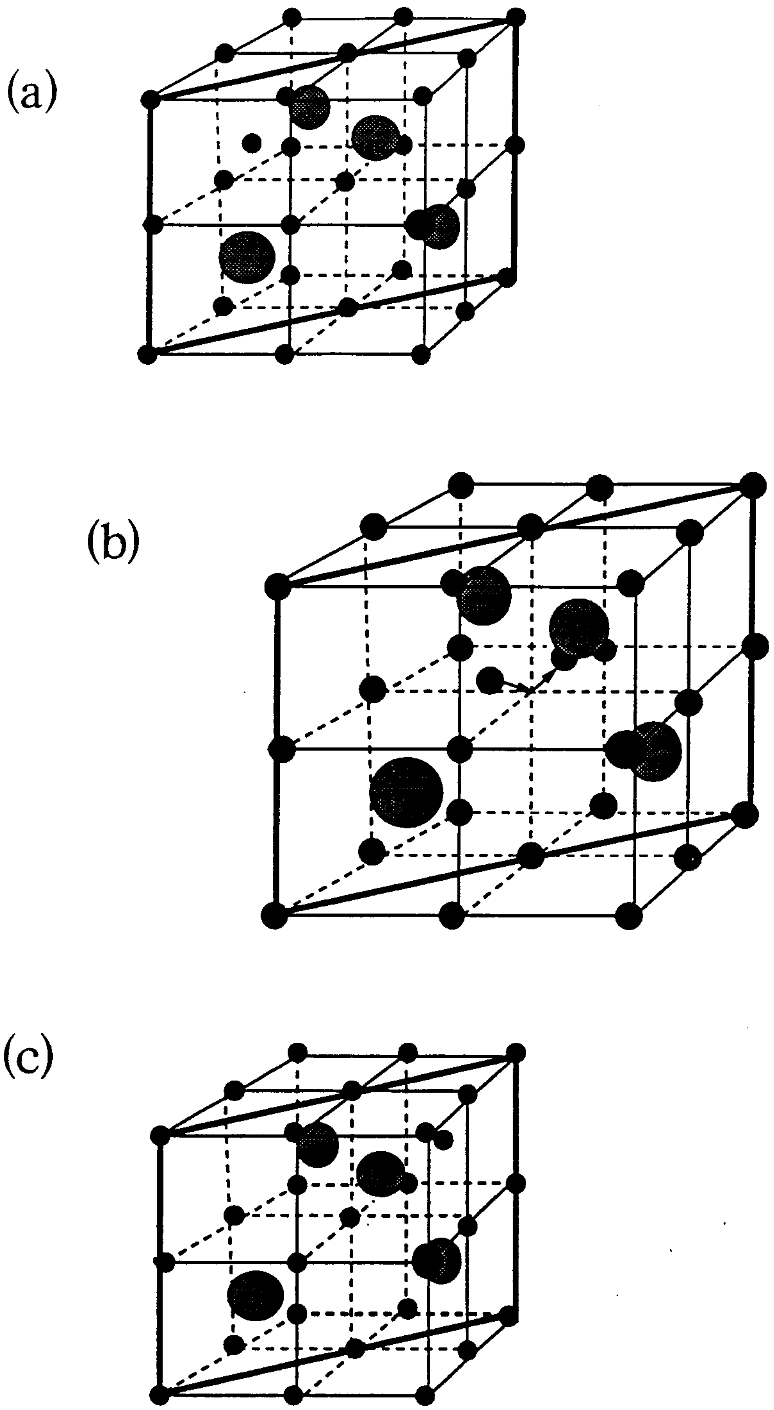

Figure 5.10: The migration of a Li interstitial. (a): the original interstitial position is at the center of a cube of Li atoms not containing an O atom (the front-top-left cube). (b): the interstitial atom moves on the (110) plane (identified by the thick-lined contour) and displaces another Li atom from its regular lattice position. The saddle-point configuration consists of the two atoms symmetrically displaced on the (110) plane from the regular site. (c): the final position of the interstitial is at the center of the rear-top-right cube of Li atoms.

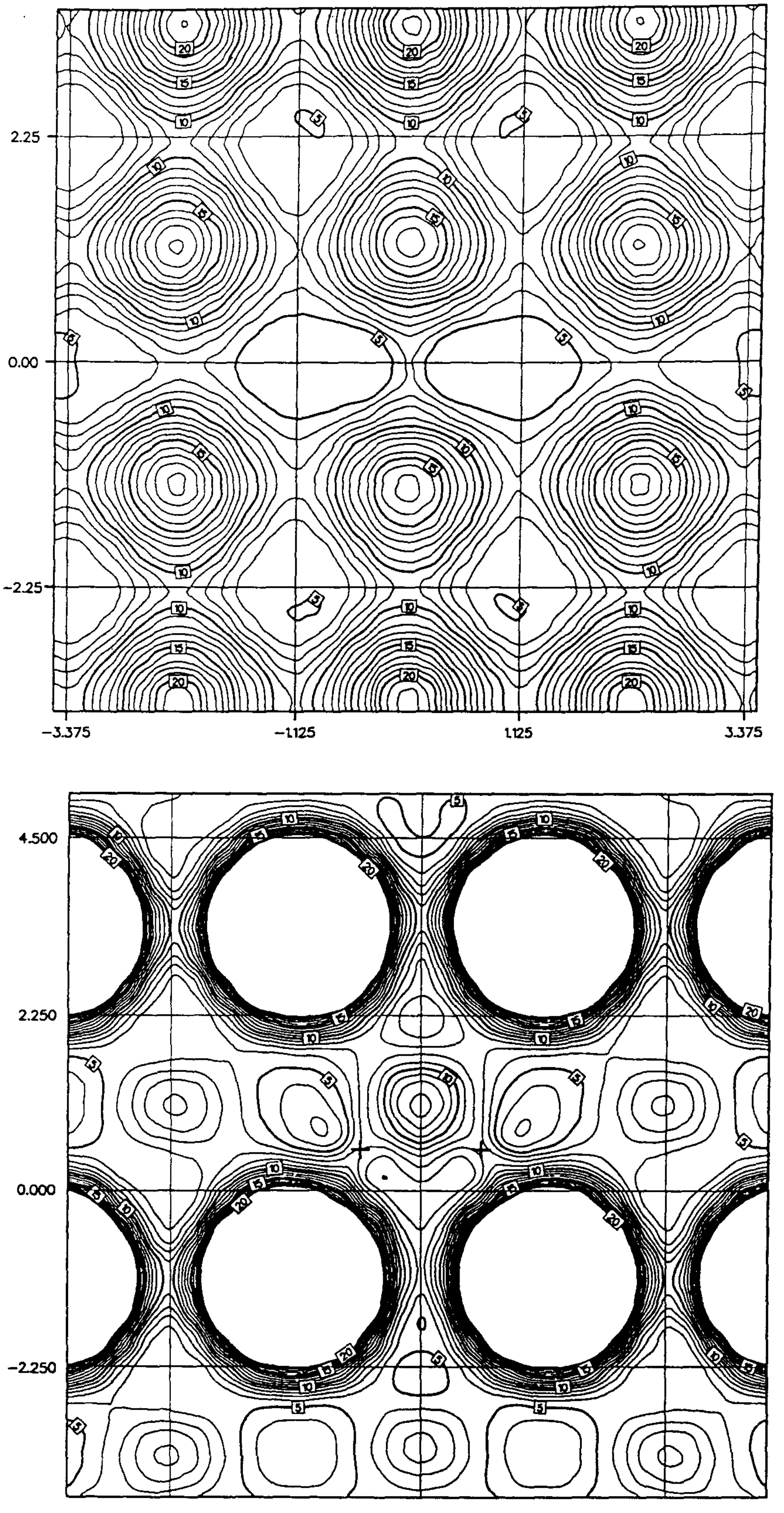

Figure 5.11: Total valence electron density on the (100) plane for the migrating Li$^+$ vacancy (above) and on the (110) plane for the Li$^+$ interstitial (below). In both cases the system is fully relaxed, with the regular lattice positions of lithium atoms at the intersections of the superimposed grid. The migrating ion in the figure above is at the coordinate origin, the initial and final vacant sites being to the left and right. The two atoms involved in the interstitial migration are marked by crosses. The regular site on which Li atoms interchange is at the coordinate origin. Units and scales as in figure 5.8

	calculated	empirical	experimental
MgO			
E_S (eV)	6.88	7.72^h	$5\text{-}7^a$
ΔE_m (eV) cation	2.39	2.07^h	2.2^b, 2.28^c
ΔE_m (eV) anion	2.48	2.11^h	2.42^d, 2.61^e
Li_2O			
E_F (eV)	2.20	2.28^i	1.58^f, 2.53^g
ΔE_m (eV) (vacancy)	0.34	0.27^l	0.40^g, 0.49^g
ΔE_m (eV) (interstitial)	0.58	0.51^l	–

Table 5.6: Ab initio results for the Schottky energy E_S and the cation and anion vacancy migration energies ΔE_m in MgO, and for the cation Frenkel energy E_F and the vacancy and interstitial migration energies ΔE_m in Li_2O. The ab initio values for MgO and Li_2O are from 32-ion and 48-ion systems. Experimental results are from references: (a): Wuensch *et al.*[193]; (b): Duclot and Departes[188]; (c): Sempolinski and Kingery[189]; (d): Shirasaki and Harma[190]; (e): Shirasaki and Yamamura[191]; (f): Ohno *et al.*[186]; (g): Chadwick *et al.*[187] . Results for empirical models are from references: (h): Sangster and Rowell[185]; (i): Mackrodt[142]; (l): This work.

Conclusions.

In this work we have presented the results of a series of defect-energetics calculations in Al host and in the ionic oxides MgO and Li_2O. The two kinds of materials and their electronic structures are very different, and the physics of isolated defects in them (*i.e.* the modalities of the electronic screening, the energies involved in the formation of the defects, and the energy barriers for defect diffusion) is accordingly different.

The results for the vacancy in Al demonstrate that a careful first principles treatment can lead to a very accurate description of this point defect, without introducing previous experimental knowledge other than the ionic core charge, or assuming arbitrary approximations in the self-consistent treatment, as was customary in the past. The agreement with experimental findings and with the few other very recent fully ab-initio results (obtained from other DFT-based approaches) shows that this system is under good technical control.

The addition of a hydrogen impurity in the Al host metal introduces further technical difficulties, connected with the necessity of high energy cutoff treatment in large supercells of the metallic system. By carefully tailoring the minimisation algorithm, and by paying special attention to the issues connected with BZ sampling, we have obtained for the first time successful results from fully ab initio calculations on H impurities in Al. These results have a special value in the light of the technological importance of metal hydrides. Moreover, there is still no clear experimental picture for (1) the localisation of the hydrogen impurity, (2) the role played by lattice relaxation in the different self-trapped geometries, (3) the features of the hydrogen binding to a vacancy defect, and (4) the modalities of its diffusion in the metal host.

Apart from satisfactorily reproducing the observed values of experimentally measured quantities like the hydrogen heat of solution, the aim of our investigation was to provide some theoretical insight into these issues.

The investigation of defects in ionic ceramics like MgO and Li_2O within the DFT-PW formalism constitutes the second part of this work. A main result of these calculations is that they clearly show the adequacy of the DFT-LDA pseudopotentials-supercell method for the study of large systems of ionic materials, in spite of the non-unifom ground state distributions and of the large (but a priori unknown) charge redistribution from the isolated atoms case.
As results of our supercell calculations, very accurate predictions could be obtained for a wide range of bulk and defect properties in MgO and Li_2O, *e.g.* the formation energies of Schottky and Frenkel pairs and the migration energies of point defects of different charge and size. This suggests that for materials of this kind the techniques we have used are a valid alternative to the use of localised basis sets or of cluster-embedding techniques for obtaining results which are correct within the experimental accuracy.
Overall, our results are in strong support of the empirical models for ionic materials, but they can also represent a valid source of information for improved modelling. The defects we investigated in MgO and Li_2O carry net charges, and they are expected to induce a strong polarisation of the surrounding lattice and to distort the electronic distribution on the nearest neighbour ions. While our results agree with the empirical predictions on lattice relaxation around the defects, they also show that the defect-induced charge density displacements are considerably more complex than the dipolar polarisation implied by most empirical models.

Given the very high energy cutoff treatment required by the presence of oxygen, supercell calculations generally involve almost prohibitive demands of computer time and memory allocation. An important factor in rendering these calculations nowadays possible has been the recent improvements in the total energy minimisation algorithms, which have enabled a more effective treatment of the technical aspects of large-systems calculations. Another advance is the availability of "smooth" pseudopotentials, constructed by means of increasingly sophisticated and effective optimisation techniques. Some features of our calculations on oxides consist of the use of a minimisation algorithm with minimal memory requirements, and of a carefully optimised smooth pseudopotential for oxygen. In spite of this, these calculations would not have been feasible without the help of a large parallel supercomputer. The calculations required the use a fortran code (CETEP) explicitly adapted to these kind of machines, using machine-dedicated FFT and communication routines. The data-driven parallelisation strategy in the code was designed and implemented (by M.C.Payne and L.J.Clarke, in Cambridge and Edinburgh Universities) taking into careful account the time-complexity scaling of the various operations at large system sizes.

As the first application of this code to reach conclusion, our calculations on MgO represent also the first example of a series of large-scale ab initio total energy calculations in the DFT-LDA-PW framework using supercells and pseudopotentials *ever* to be successfully completed (in September 1991[122]) on a parallel supercomputer. Much of the human-time investment in this part of the present work was spent in extensive machine and code testing, and in overcoming technical difficulties of various kind which were encountered in the course of the computations. As well as marking a step forward in the ability of computational practice to treat technologically important materials like ionic oxides, we believe that the results of this part of the work also provide a timely illustration of the progress in the first-principles investigation of solids which has been stimulated in very recent times by parallel computational techniques.

Appendix A.
Entropy Correction: results for Al.

We report here the results of some further calculations on Al perfect-lattice properties which we performed to demonstrate the validity of the BZ sampling procedure discussed in Sections (2.5.2) and (2.5.3).

A.1.1 Convergence of the corrected total energy.

Assuming the widely used "gaussian broadening" technique as a starting point, we have implemented the entropy correction for the normalised gaussian smearing function $g(x)$ in the form:

$$g(x) = \frac{2}{\sigma\sqrt{\pi}} e^{-(\frac{\epsilon-\mu}{\sigma})^2} \qquad \Delta E_{corr}(\sigma) = -\frac{\sigma}{2\sqrt{\pi}} \sum_{\mathbf{k}_j,i} w_{\mathbf{k}_j} e^{-(\frac{\mu-\epsilon_i(\mathbf{k}_j)}{\sigma})^2} , \qquad (A.1)$$

(cf. equation (2.76)), where as usual σ is the smearing width, $w_{\mathbf{k}_j}$ is the weight of the BZ sampling point $\mathbf{k}_j$, and μ is the Fermi energy self-consistently extracted from the ground state occupations f_i of the orbitals and from the charge conservation condition $\sum_i f_i = N_{el}$. The occupations are evaluated by integration of the smearing function up to the Fermi level for each orbital of eigenvalue ϵ_i :

$$f_i = f(x_i) = \int_{-\infty}^{x_i} g(t)dt \qquad x_i = \frac{(\mu - \epsilon_i)}{\sigma} . \qquad (A.2)$$

We report in figure A.12 on page 164 the effects of the correction defined by equation (A.1) when applied to bulk aluminium at a series of different broadening widths σ . The calculations were performed using a set of 256 sampling points, constructed "folding out" in the primitive BZ the set given by (±1/4, ±1/4, ±1/4)[15] in units of the reciprocal space basis vectors corresponding to the fcc superlattice with 64 Al atoms

---

[15] For a cubic supercell this set corresponds to the mean value point introduced in reference [30].

per cell[16]. This rather large sampling set allows us to derive meaningful conclusions on the stability of the corrected results even at small values of σ, for which many sampling points are needed to extract correct ground state energy values. From the results in the figure, it is clear that the correction recovers most of the deviation of $E(\sigma)$ from the unsmeared ground state energy E_0 (cf. eqn. 2.67), so that the ground state can be reproduced within a tolerance of 10^{-2} eV even starting from an uncorrected energy 1 eV or more higher.

As a test on the BZ convergence of the corrected total energy, we have calculated this quantity for bulk Al for a series of different sampling sets and broadening widths. All the sampling sets were obtained as above as the equivalent of a set of eight BZ points in a supercell calculation, since we are interested in determining which sampling set and smearing width should be used for obtaining a chosen absolute accuracy in a supercell calculation of given size. Note that in an actual supercell calculation on a disordered metal system, the greater dispersion of the self-consistent eigenvalues (which in the bulk case at different k-points are largely degenerate) is expected to *improve* the accuracy of our statistic correction.

The results of the calculations are illustrated by figure A.13 on page 164, showing the corrected total energy per Al atom as a function of the number of points in the sampling set for the values ($\sigma = 3.2, 1.6, 0.8, 0.4, 0.2, 0.1$ eV). While no good convergence can be assumed for the energy calculated at $\sigma = 0.1$ eV before 256 sampling points are used (empty circles), the convergence progressively improves at higher values of σ, being already reached for $\sigma \doteq 3.2$ eV (full circles) within an accuracy of 10^{-2} eV using 32 sampling points only. The number of orbitals used in the calculations should be always sufficient to span the energy spectrum widened by the broadening procedure. The triangles in figure A.13 show that the subtracted energy correction is overestimated if a broadening width $\sigma = 6.4$ eV is used, for which not enough states were included in the calculations.

---

[16] The sampling set is reduced by inversion, but not by other symmetry operations, from the full set of 512 points.

A.1.2 The elastic constant C_{44} .

The physical quantities of interest in total energy calculations are usually differences of total energies, so that cancellation of energies is hoped for when the results are needed with better precision than what can be expected within the accuracy of the calculated energy itself. The BZ convergence of most physical quantities is known from experience to be much faster than the convergence of the total energy.

There are, however, circumstances in which cancellation of errors cannot be expected to help. A typical case occurs when there are relevant differences in the electronic structures of the two systems to which the energy values in the subtraction correspond. In this case using the same BZ sampling set to integrate very dissimilar band energies does not lead to cancellation of errors. Another case occurs when there is no obvious way to asses a sampling set which in the two systems has the same physical significance. The accuracy of "mean value" or "special" points of the BZ depends on the symmetry properties of the integration domain[30][32], and is not preserved if in one of the systems such symmetry is broken. These problems are obviously most serious in the case of metals, due to the slow convergence of results with BZ sampling.

As a further test of our BZ integration scheme we have calculated the C_{44} elastic constant in Al. Elastic properties are determined by the harmonic fit of an energy curve around the minimum, the energies in the fit being very small (of the order of 10^{-2} eV per atom) and the bulk point-symmetry being broken when imposing a strain to the crystal cell. C_{44} is obtained by shear strain, so that the electron density in the metal is not changed to first order in the deformation. For this reason, there can be no large *positive* contribution to C_{44} from the band energy in the metal in the free electron gas approximation, so that the response of the crystal to shear stress is totally due to structure-dependent factors, *i.e.* depends on the ionic positions.

The structure-dependent contributions to the total energy can be expressed in a second order perturbation expansion in the strength of the (weak) pseudopotential:

$$U_{struct} = U_E + \sum_{g} W(g) v(g)^2 F(g) \qquad W(g) = \sum_{\mathbf{g}} |S(\mathbf{g})|^2 , \qquad \text{(A.3)}$$

where $S(\mathbf{g})$ is the structure factor, W(g) is summed on all equivalent reciprocal lattice vectors, $F(g)$ is essentially a negative monotonic function not depending on the pseudopotential $v(g)$ and slowly converging to zero, and U_E is the usual Madelung term.

Local model pseudopotentials $v(g)$ for aluminium have a zero in G-space representation at about 1.5 k_f, in close correspondence to the position of the (111) set of reciprocal perfect lattice vectors (which is about 1.6 k_f). This gives a simple qualitative argument to conclude that a shear deformation splitting the (111) set away from the minimum of $v(g)^2$ would lower the band energy contribution to the energy[42][43], or, in other words, to conclude that the band energy component to the elastic constant C_{44} is negative.

The Madelung energy of any ionic configuration can be readily calculated with no BZ sampling errors through Ewald summation, and its contribution to the elastic constant is known since long ago to be large and positive[196], while the experimental value of C_{44} for pure Al is much smaller[197][198]. From this evidence it is clear that a large cancellation takes place in determining the value of C_{44}, with the Madelung contribution slightly prevailing, so that the fcc structure of the metal is stable with respect to shear deformation.

Since BZ sampling errors occur *only* in the large and negative band energy contribution to C_{44}, and since no cancellation can be expected for these errors as discussed above, the theoretical calculation of C_{44} within standard total energy procedures is technically extremely difficult, and we are not aware of a successful calculation of this kind in literature[199], although some attempts have been made with standard smearing procedures[200], finding no convergence (or negative values) for C_{44}, in spite of the use of *thousands* of inequivalent BZ sampling points.

We report in table A.7 on page 163 our results for C_{44} for two smearing widths ($\sigma = 3.2\ eV$ and $\sigma = 1.6\ eV$) and various sampling point sets. The sampling sets were determined with the same procedure used for the total energy calculations described before, the geometry of the corresponding supercell being indicated in parentheses for each set (the number of atoms on each supercell is twice the number of points used in the calculation on the unit cell). Each result has been obtained from polynomial fit of nine energy values, the distorted unit cell being determined by the strain tensor $\epsilon_{ij} = \frac{1}{2}\epsilon(1 - \delta_{ij})$ for equi-spaced values of ϵ in the range [-4%, 4%] , corresponding to energy differences in the range [0, 25] meV. While the convergence is probably still uncomplete for $\sigma = 1.6\ eV$, the series of values for $\sigma = 3.2\ eV$ is converged within 10^{-2} Mbar using 108 sampling points or more.

No. of k-points	32(fcc)	64(bcc)	108(fcc)	256(fcc)
C_{44} $\sigma = 3.2\ eV$ (Mbar)	0.465	0.404	0.363	0.365
C_{44} $\sigma = 1.6\ eV$ (Mbar)	0.767	0.070	0.380	0.413

Table A.7: Results for C_{44} obtained for two smearing widths ($\sigma = 3.2\ eV$ and $\sigma = 3.2\ eV$) for various BZ sampling point sets. The number of atoms in each supercell corresponding to the sampling set used (see text) is twice the number of sampling points indicated. (The supercell symmetry is as indicated in parentheses.)

We report in table A.8 on page 165 our results for C_{44} obtained using a sampling set of 256 BZ points and a broadening width $\sigma = 3.2\ eV$. Values from some experimental measurements are also reported for comparison. The "band" contribution C_{44}^{band} is calculated as the difference between the total value and the Madelung contribution C_{44}^{E}.

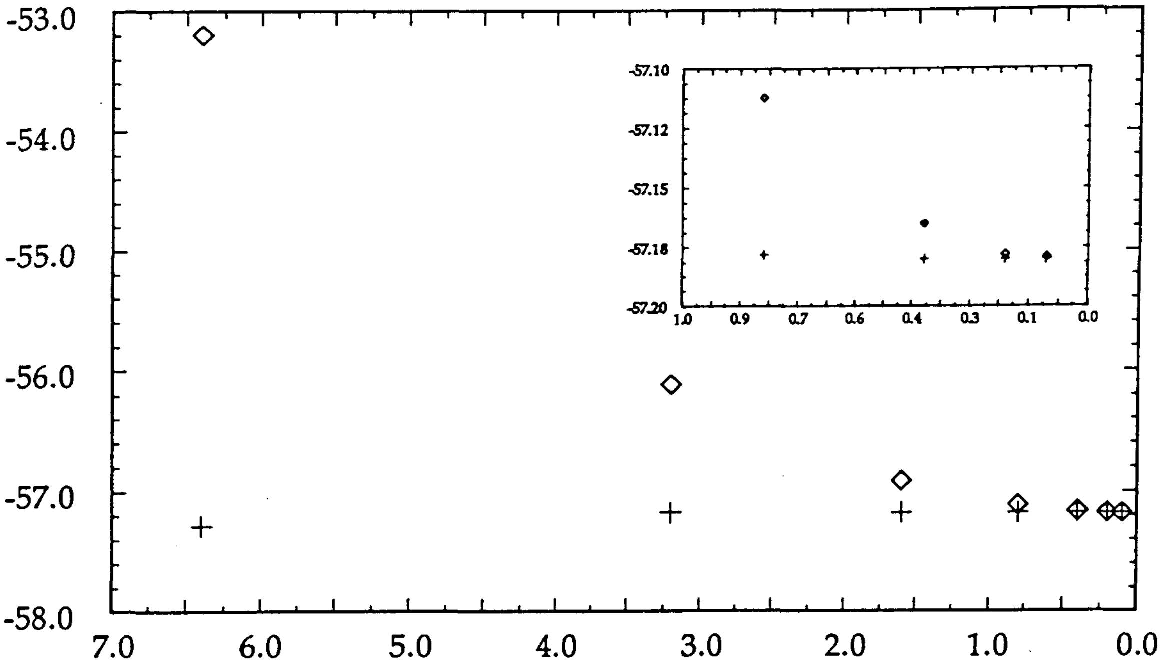

Figure A.12: Uncorrected (empty diamonds) and corrected (crosses) total energy values (eV) per unit cell in Al, obtained at self-consistency using gaussian smearing at different fixed values of the broadening width σ (eV). The corrected energy at fixed sampling set is very stable even at large values of σ within an accuracy of a few meV, as shown in the magnified scale plot.

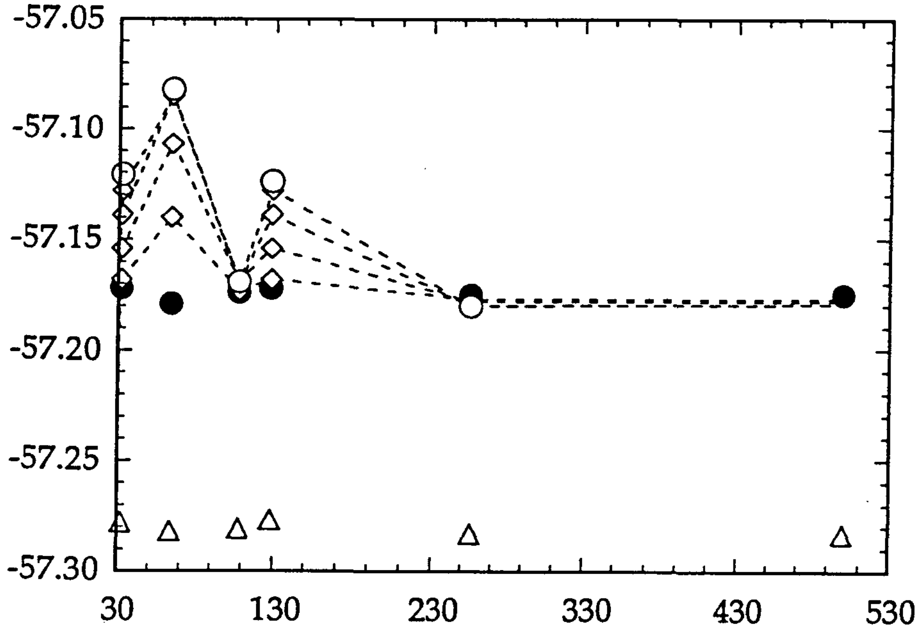

Figure A.13: Corrected total energy (eV) for $\sigma = 3.2, 1.6, 0.8, 0.4, 0.2, 0.1$ eV as a function of the number of BZ sampling points. Full and empty circles correspond to $\sigma = 3.2$ eV and to $\sigma = 0.1$ eV respectively. Triangles correspond to the correction calculated at $\sigma = 6.4$ eV, for which not enough orbitals to span the energy spectrum

C_{44}^{E} (Mbar)	C_{44}^{band}(Mbar)	C_{44}(Mbar)	C_{44}^{exp}(Mbar)
1.567	-1.202	0.365	0.309^a,0.316^b

Table A.8: Results for C_{44} obtained using 256 BZ sampling points and a smearing width $\sigma = 3.2\ eV$. The "band" contribution C_{44}^{band} is the difference between the calculated value C_{44} and the Madelung contribution C_{44}^{E}. Values from some experimental measurements (extrapolated at zero temperature) are taken from references: (a): Vallin *et al.* [197]; (b): Kamm and Alers [198] .

Acknowledgments.

The results of the research reported in this thesis owe immensely in every respect to the patient and dedicated work of my Supervisor, Professor Michael John Gillan.

I also acknowledge the great help in clarifying ideas which comes from my years-old habit of friendly discussing physics with Stefano de Gironcoli. I am deeply indebted to Nicola Marzari for his affection and for his continuous support during the work. I also thank for their everlasting support, affection, and friendship, my brother Salvatore and my friends Antonio Fiorentini and Lodovico di Caporiacco.

Bibliography

[1] P.Hohenberg and W.Kohn, Phys. Rev. **136**, B864 (1964).

[2] W.Kohn and L.J.Sham, Phys. Rev. **140**, A1133 (1965).

[3] D.M.Ceperley and B.J.Alder, Phys. Rev. Lett. **45**, 566 (1980).

[4] J. Perdew and A.Zunger, Phys. Rev. B **23**, 5048 (1981).

[5] See for example S.Vashista and W.Kohn, in *Theory of the Inhomogeneous Electron Gas*, S.Lundqvist and N.H.March ed., (Plenum, New York, 1983).

[6] See for example M.L.Cohen and V.Heine, Solid State Phys. **24**, 37 (1970).

[7] N.W.Ashcroft and D.C.Langreth, Phys. Rev. **155**, 682 (1967).

[8] C.Herring, Phys.Rev. **57**, 1169 (1940).

[9] J.C.Phillips and L.Kleinman, Phys. Rev. **116**, 287 (1959).

[10] D.R.Hamann, M.Schlüter and C.Chiang, Phys. Rev. Lett. **43**, 1494 (1979).

[11] G.B.Bachelet, D.R.Hamann and M.Schlüter, Phys. Rev. B **26**, 4199 (1982).

[12] W.H.Press, B.P.Flannery, S.A.Teukolsky and W.T.Vetterling, *Numerical Recipes: the Art Of Scientific Computing*, (Cambridge University Press, Cambridge, 1990) ch 10, p 301.

[13] R.Fletcher and C.M.Reeves, Comput.J. **7**, 149 (1964).

[14] R.Fletcher, *Practical Methods for Optimisation* vol 1 (Wiley, New York, 1980) p 63.

[15] P.E.Gill, W.Murray and M.H.Wright, *Practical Optimisation*, (Academic Press, London, 1981).

[16] R.Car and M. Parrinello, Phys. Rev. Lett.**55**, 2471 (1985).

[17] M.J.Gillan, J.Phys: Condensed Matter **1**, 689 (1989).

[18] I.Štich, R.Car, M.Parrinello and S.Baroni, Phys. Rev.B **39**, 4997 (1989).

[19] M.P.Teter, M.C.Payne and D.C. Allan, Phys. Rev. B **40**, 12255 (1989).

[20] R.P.Feynman, Phys. Rev. **56**, 340 (1939).

[21] M.C.Payne, M.P.Teter, D.C.Allan and J.D.Joannopoulos, in press.

[22] A.De Vita, I Štich, M.J.Gillan and M.C.Payne, to be published.

[23] L.Kleinman and D.M.Bylander, Phys. Rev. Lett. **48**, 1425 (1982).

[24] X.Gonze, P.Käckell and M. Scheffler, Phys. Rev. B **41**, 12264 (1990).

[25] A.M.Rappe, K.M.Rabe, E.Kaxiras and J.D.Joannopoulos, Phys. Rev. B **41**, 1227 (1990).

[26] J.S.Lin, A. Qteish, M.C.Payne and V.Heine, to be published.

[27] S.G.Louie, S.Froyen and M.L.Cohen, Phys. Rev. B **26**, 1738 (1982).

[28] G.Engel and R.J.Needs, Phys. Rev. B **41**, 7876 (1990).

[29] B.Farid, and R.J.Needs, Phys. Rev. B **45**, 1067 (1992).

[30] A.Baldereschi, Phys. Rev. B **7**, 5212 (1973).

[31] D.J.Chadi and M.L.Cohen, Phys. Rev. B **8**, 5747 (1973).

[32] J.Monkhorst and J.D.Pack, Phys. Rev B **13**, 5188 (1976).

[33] N.D.Mermin, Phys. Rev. **137**, A1441 (1965).

[34] A.De Vita and M.J.Gillan, to be published.

[35] C.L.Fu and K.M.Ho, Phys. Rev. B **28**, 5480 (1983).

[36] R.J.Needs, R.M.Martin and O.H.Nielsen, Phys. Rev. B **33**, 3778 (1986).

[37] I.J.Robertson and M.C.Payne, J.Phys.:Cond. Matt. **2**, 9837 (1990).

[38] M.Methfessel and A.T.Paxton, Phys. Rev. B **40**, 3616, (1989).

[39] J.Callaway and N.H.March, Solid State Phys. **38**, 136 (1984).

[40] S.de Gironcoli, (private communication).

[41] W.A.Harrison, *Pseudopotential Theory of Metals*, (New York, Benjamin, 1966).

[42] V.Heine and D.Weaire, Phys. Rev. **152**, 603 (1966).

[43] V.Heine and D.Weaire, Solid State Phys. **24**, 250 (1970).

[44] R.M.Nieminen, M.Manninen, P. Hautojärvi and J.Arponen, Solid State Comm. **16**, 831 (1975).

[45] M.Manninen R.M.Nieminen P. Hautojärvi and J.Arponen, Phys. Rev B **12**, 4012 (1975).

[46] R.Chang and L.M.Falicov, J.Phys. Chem. Solids **32**, 465 (1971).

[47] Z.D.Popovic, J.P.Carbotte and G.R.Piercy, J.Phys.F.: Met.Phys. **4**, 351 (1974).

[48] P Minchin, A.Meyer and W.H.Young,J.Phys.F.:Met.Phys. **4**, 2117 (1974).

[49] R.Evans and M.W.Finnis, J.Phys.F.:Met.Phys. **6**, 483 (1976).

[50] W. Triftshäuser, Phys. Rev. B **12**, 4634 (1975).

[51] A.S.Berger, S.T.Ockers and R.W.Siegel, J.Nuclear Mat. **69-70**, 734 (1978).

[52] M.J.Fluss, L.C.Smedskjaer, M.K.Chason, D.G.Legnini and R.W.Siegel, Phys. Rev. B **17**, 3444 (1978).

[53] G.Jacucci, R.Taylor, A.Tenenbaum and N.V.Doan, J.Phys.F.:Met.Phys. **11**, 793 (1981).

[54] C.B.So and C.H.Woo, J.Phys.F.:Met.Phys. **11**, 325 (1981).

[55] B.Chakraborty, R.W.Siegel and W.E.Pickett, Phys. Rev. B **24**, 5445 (1981).

[56] B.Chakraborty and R.W.Siegel, Phys. Rev. B **27**, 4535 (1983).

[57] L.S.Goodwin, PhD Thesis, Cavendish Laboratory, University of Cambridge (1987).

[58] A.De Vita and M.J.Gillan, J.Phys.:Cond. Matt. **3**, 6225 (1991).

[59] A.De Vita and M.J.Gillan, J.Phys.:Cond. Matt. **4**, 599 (1992).

[60] R.W.Jansen and B.M.Klein, J.Phys.:Cond. Matt. **1**, 8359 (1989).

[61] M.J.Mehl and B.M.Klein, 1990 Preprint.

[62] P.J.H.Denteneer and J.M.Soler, Solid State Comm. **78**, 857 (1991).

[63] J.Friedel, Phil.Mag. **43**, 153 (1952).

[64] N.J.Puska and R.M.Nieminen, Phys. Rev. B **29**, 5382 (1984).

[65] M.S.Daw and M.I.Baskes, Phys. Rev. B **29**, 6443 (1984).

[66] H.Sugimoto and Y.Fukai, Phys. Rev. B **22**, 670 (1980).

[67] Y.Fukai and H.Sugimoto, Adv. Phys. **34**, 263 (1985).

[68] J.K.Nørskov and F.Besenbacher, J.Less-common Met. **130**, 475 (1987).

[69] J.P.Bugeat and E.Ligeon, Phys. Lett. **71A**, 93 (1979).

[70] T.Springer, in *Hydrogen in Metals I*, ed. G.Alefeld and J.Völkl (Springer, Berlin, 1978).

[71] W. von Eichenauer, Z.Metallkd. **59**, 613 (1968).

[72] Z.D.Popovic and M.J.Stott, Phys. Rev. Lett.**33**, 1164 (1974).

[73] Z.D.Popovic, M.J.Stott, J.P.Carbotte, and G.R.Piercy, Phys. Rev. B **13**, 590 (1976).

[74] C.E.Ransley and H.Neufeld, J.Inst.Met. **74**, 599 (1948).

[75] S.Estreicher and P.F.Meier, Phys. Rev. B **27**, 642 (1983).

[76] C.O.Almbladh and U. von Barth, Phys. Rev. B **13**, 3307 (1976).

[77] M.Manninen and R.M.Nieminen, J.Phys.F.:Met.Phys. **9**, 1333 (1979).

[78] L.M.Kahn, F.Perrot and M.Rasolt, Phys. Rev. B **21**, 5594 (1980).

[79] F.Perrot and M.Rasolt, Solid State Comm. **36**, 579 (1980).

[80] F.Perrot Phys. Rev. B **16**, 4335 (1977).

[81] M.L.Cohen and V.Heine, Solid State Phys. **24**, 37 (1970).

[82] J.P.Bugeat,A.C.Chami and E.Ligeon, Phys. Lett. **58A**, 127 (1976).

[83] K.Doremburg, M.Gladish, D.Herlach, W.Mansel, H.Metz, H.Orth, G.Pulitz, A.Seeger, W.Wahl and M.Wigand, Z. Phys. **B31**, 165 (1978).

[84] O.Hartmann, E.Karlson, L.O.Norlin, D.Richter and T.O.Niinikowski, Phys. Rev. Lett.**41**, 1055 (1978).

[85] M.D.Whitmore and J.P.Carbotte, J.Phys.F.:Met.Phys. **9**, 629 (1979).

[86] J.K.Nørskov , Solid St.Comm. **24**, 691 (1979).

[87] D.S.Larsen and J.K.Nørskov J.Phys.F.:Met.Phys. **9**, 1975 (1979).

[88] J.K.Nørskov, Phys. Rev. B **21**, 2131 (1980).

[89] M.J.Stott and E.Zaremba, Phys. Rev. B **22**, 1564 (1980).

[90] N.J.Puska, R.M.Nieminen and M.Manninen, Phys. Rev. B **24**, 3037 (1981).

[91] G.Solt, M.Manninen, and H.Beck, J.Phys.F.:Met.Phys. **13**, 1379 (1983).

[92] W. Schilling, J.Nucl.Mater. **69**, 465 (1978).

[93] R.M.Emrick and P.B.McArdle, Phys. Rev. **188**, 1156 (1969).

[94] R.Stumpf, X.Gonze and M.Scheffler, Research Report of the Fritz Haber Institute, (1990).

[95] W.E.Pickett and B.M.Klein, Phys. Rev. B **29**, 1588 (1984).

[96] E.Babić, R.Girt, R. Krsnik, B.Leontić and I. Zorić, Phys. Letters (Netherlands) **33A**, 368 (1970).

[97] A.Seeger, D.Wolf and H.Mehrer, Phys. Stat. Solidi (b) **48**, 481 (1971).

[98] M.J.Gillan, Phil. Mag. A **43**, 301 (1981).

[99] T.Kato, Trans. Am. Math. Soc., **70**, 195 (1951).

[100] T. Kato, Trans. Am. Math. Soc., **70**, 212 (1951).

[101] T. Kato, Commun. Pure Appl. Math., **10**, 151 (1957).

[102] P.O.Löwdin, J.Chem.Phys. **19**, 1396 (1951).

[103] E.Zaremba, J.H.Rose, L.M.Sander and H.B.Shore, J.Phys.F: Metal Phys. **7**, 763 (1977).

[104] P.H.Dederichs, J.Phys.F.:Met.Phys. **3**, 471 (1973).

[105] P.Ehrhart, H-G.Haubold and W.Schilling, in: Advances in Solid State Physics, vol. XIV, O.Madelung and H.J.Queisser eds. (Pergamon Press, Oxford, 1974) p 87.

[106] O.Gunnarsson and B.I.Lundqvist, Phys. Rev. B **13**, 4274 (1976).

[107] H.Beutler, Z. Phys.Chem. B **27**, 287 (1934).

[108] W. von Eichenauer and A. Pebler, Z.Metallkd. **48**, 373 (1957).

[109] S.Matsuo and T.Hirata, Trans. Natl. Res. Inst. Met **11**, 22 (1969).

[110] W. von Eichenauer, K.Attenbach, A. Pebler, Z.Metallkd. **52**, 682 (1961).

[111] E.Hashimoto and T.Kino, J. Phys. F: Metal Phys.**13**, 1157 (1983).

[112] K.W.Kehr, D.Richter, J.M.Welter, O.Hartmann, E.Karlsson, L.O.Norlin, T.O. Niinikowski, and A. Youanc, Phys. Rev. B **26**, 567 (1982).

[113] L.Katz,M.Guinan and R.J.Borg, Phys. Rev. B **4**, 330 (1971).

[114] K.Papp and E.Kovacs-Csetenyi, Sci. Metall. **15**, 161 (1981).

[115] G.Perkins, and D.R.Begeal, Ber. Bunsenges. Phys. Chem. **76**, 863 (1972).

[116] S.M.Myers, P.M.Richards, W.R.Wampler and F.Besenbacher, J.Nucl.Mater. **165**, 9 (1989).

[117] S.M.Myers, P.Nordlander, F.Besembacher, J.K.Nørskov, Phys. Rev. B **33**, 854 (1986).

[118] S.M.Myers, F.Besembacher and J.K.Nørskov, J.Appl.Phys. **58**, 1841 (1985).

[119] L.J.Clarke, I.Štich and M.C.Payne, Comp.Phys.Commun., in press.

[120] G.Galli and M.Parrinello, Bull.Am.Phys.Soc. **36**, 835 (1991).

[121] S.Baroni and P.Giannozzi, Europhys. Lett. **17**, 547 (1992).

[122] A.De Vita, M.J.Gillan,J.S.Lin, M.C.Payne, I.Štich and L.J.Clarke, Phys. Rev. Lett.**68**, 3319 (1992).

[123] A.De Vita, M.J.Gillan, J.S.Lin, M.C.Payne, I.Štich and L.J.Clarke, in press.

[124] A.De Vita,I.Manassidis and M.J.Gillan, Europhys. Lett. **19**, 605 (1992).

[125] T. Tone, N. Fujisawa and Y. Seki, *Nucl. Tech./Fus.* **4**, 573, (1983).

[126] K. Noda, Y. Ishii, H. Ohno, H. Watanabe and H. Matsui, *Adv. Ceram.* **25**, 155 (1989).

[127] C.R.A.Catlow and A.M.Stoneham, J.Phys. C **16**, 4321 (1983).

[128] B.G.Dick and A.W.Overhauser, Phys. Rev. **112**, 90 (1958).

[129] A.M.Stoneham and J.H.Harding, Ann.Rev.Phys.Chem. **37**, 53 (1987).

[130] R.G.Gordon and Y.S.Kim, J.Chem. Phys **56**, 3122 (1972).

[131] N.H.March, in *Computer Simulation of Solids*, ed. C.R.A. Catlow and W.C.Mackrodt, (Springer-Verlag, Berlin, 1982) p 97.

[132] C.R.A.Catlow and M.Dixon, in *Computer Simulation of Solids*, ed. C.R.A. Catlow and W.C.Mackrodt, (Springer-Verlag, Berlin, 1982) p 130.

[133] I.Manassidis, A.De Vita and M.J.Gillan, *Proc. 4th Int. Conf. on Computational Phys., Prague, 24-28 August 1992*, (World Scientific, Singapore) in press.

[134] A.Seeger and H.Mehrer, in *Vacancies and Interstitials in Metals*, (North Holland, Amsterdam, 1969).

[135] W.C.Mackrodt and R.F.Stewart, J.Phys.C **12**, 5015 (1979).

[136] M.J.L.Sangster and A.M.Stoneham, Phil. Mag. B **43**, 597 (1981).

[137] C.R.A.Catlow, W.C.Mackrodt, M.J.Norgett and A.M.Stoneham, Phil.Mag.**35**, 177 (1977). Phil.Mag.**40**, 161 (1979).

[138] W.C.Mackrodt, R.F.Stewart,J.C.Campbell and I.H. Hillier, J. de Physique C **6**, 64 (1980).

[139] U.Schröder, Solid State Commun. **4**, 347 (1966).

[140] M.J.Sangster, J.Phys.Chem Solids **35**, 195 (1974).

[141] C.R.A.Catlow, Proc. Roy. Soc. A **353**, 533 (1977).

[142] W.C.Mackrodt, in *Computer Simulation of Solids*, ed. C.R.A. Catlow and W.C.Mackrodt, (Springer-Verlag,Berlin,1982) p 175.

[143] N.W.Ashcroft and N.D.Mermin, *Solid State Physics*, Holt-Saunder International Editions (1976), p 335.

[144] H.J.Monkhorst, Phys. Rev. B **20**, 1504 (1979).

[145] R.Colle, A.Fortunelli and O.Salvetti, J.Chem.Phys **80**, 2654 (1984).

[146] J.P.Perdew, Phys. Rev. B **33**, 8822 (1986).

[147] J.H.Harding, Rep.Prog.Phys. **53**, 1403 (1990).

[148] R.Dovesi, C.Pisani, C.Roetti and V.R.Saunders, Phys. Rev. B **28**, 5781 (1983).

[149] C.Pisani,R.Dovesi and C.Roetti, in *Lecture Notes in Chemistry*, (Springer-Verlag, Heidelberg, 1988).

[150] R.Dovesi, C.Ermondi, E.Ferrero, C.Pisani and C.Roetti, Phys. Rev. B **29**, 3591 (1984).

[151] M.Causà, R.Dovesi, C.Pisani and C.Roetti, Phys. Rev. B **33**, 1308 (1986).

[152] R.Nada, C.R.A. Catlow, R.Dovesi and C.Pisani, Phys. Chem. Min. **17**, 353 (1990).

[153] M.Causà, R.Dovesi, C.Pisani and C.Roetti, Surface Sci. **215**, 489 (1989).

[154] R.W.Grimes, C.R.A. Catlow and A.M.Stoneham, J. Phys.: Condens. Matter **1**, 7367 (1989).

[155] R.W.Grimes, C.R.A. Catlow and A.M.Stoneham, J. Chem.Soc., Faraday Trans. **2**, 485 (1989).

[156] J.H.Harding, A.H.Harker, P.B.Keegstra, R.Pandey, J.M.Vail and C Woodward, Physica B **131**, 151 (1985).

[157] N.F.Mott and M.J.Littleton, Trans. Faraday Soc. **34**, 485 (1938).

[158] R.Pandey and J.M.Vail, J.Phys.:Cond. Matt. **1**, 2801 (1989).

[159] R.Pandey, J.Zuo and A.Barry Kunz, Phys. Rev. B **39**, 12565 (1989).

[160] J.Zuo, R.Pandey and A.Barry Kunz, Phys. Rev. B **44**, 7187 (1991).

[161] R.Pandey, J.Zuo and A.Barry Kunz J.Mater.Res. **5**, 623 (1990).

[162] C.Pisani,R.Dovesi, R.Nada and L.N.Kantorovich, J.Chem.Phys. **92**, 7448 (1990).

[163] C.Pisani,R.Dovesi, R.Nada and S.Tamiro, Surface Sci. **216**, 489 (1989).

[164] S.Froyen and M.L.Cohen, Phys. Rev. B **29**, 3370 (1984).

[165] K.J.Chang and M.L.Cohen, Phys. Rev. B **30**, 4774 (1984).

[166] H.J.F.Jansen, Phys. Rev. B **43**, 7267 (1991).

[167] D.C.Allan and M.P.Teter, Phys. Rev. Lett. **59**, 1136 (1987).

[168] J.R.Chelikowsky, H.E.King, N.Troullier, J.L.Martins and J.Glinnemann, Phys. Rev. Lett. **65**, 3309 (1990).

[169] D.C.Allan, M.P.Teter, J.D.Joannopoulos, Y. Bar-Yam and S. T. Pantelides, in *Atomic Scale Calculations in Materials Science*, ed. J.Tersoff, D.Vanderbilt and V.Vitek, MRS Conf. Proc. Vol. **141**, 255 (1989).

[170] Y.Bar-Yam, S.T.Pantelides, J.D.Joannopoulos, D.C.Allan and M.P.Teter, in SiO_2 *and its Interfaces*, ed. S. T. Pantelides and G. Lucovsky, MRS Conf. Proc. Vol. **105**, 223 (1987).

[171] K.Laasonen and R.Car, Phys. Rev. B Rap.Comm. **43**, 6769 (1991).

[172] D.Vanderbilt, Phys. Rev. B Rap.Comm.**41**, 7892 (1990).

[173] G.P.Kerker, J.Phys. C **13**, L189 (1980).

[174] E.P.Wigner, Phys. Rev. **46**, 1002 (1934).

[175] R.W.G. Wyckoff, *Crystal Structures*, (Wiley, New York, 1963).

[176] M.J.L. Sangster, G.Peckham and D.H.Saunderson, J. Phys. C, **3**, 1026 (1970).

[177] O.L. Anderson and P. Andreatch, J.Am.Ceram.Soc. **49**, 404 (1966).

[178] A.J.Cohen and R.G.Gordon, Phys. Rev. B **14**, 4593 (1976).

[179] J. R. Jasperse, A.Kahan, J.N.Plendl and S.S.Mitra, Phys. Rev. **146**, 526 (1966).

[180] T.W.D.Farley, W.Hayes, S.Hull, M.T.Hutchings, M.Alba and M.Vrtis, *Physica B* **156** & **157**, 99 (1989).

[181] J.Ihm, A.Zunger and M.L.Cohen, J.Phys.C **12**, 4409 (1979).

[182] M.Leslie and M.J.Gillan, J.Phys. C **18**, 973 (1985).

[183] C.G.Van de Walle, P.J.H.Denteneer, Y Bar-Yam, and S.T.Pantelides, Phys. Rev. B **39**, 10791 (1989).

[184] M.Leslie, Solid State Ionics **8**, 243 (1983).

[185] M.J.L.Sangster and D.K.Rowell, Phil. Mag. A **44**, 613 (1981).

[186] H.Ohno, S.Konishi, K.Noda, H.Takeshita, H.Yoshida, H.Watanabe and T.Matsuo, J.Nucl.Mater. **118**, 242 (1983).

[187] A.V.Chadwick, K.W.Flack, J.H.Strange and J.H.Harding, *Solid State Ionics*, **28** - **30**, 185 (1988).

[188] M.Duclot and C.Departes, J. Solid State Chem. **31**, 377 (1980).

[189] D.R.Sempolinski and W.D.Kingery, J.Am.Ceramic Soc. **63**, 664 (1980).

[190] S.Shirasaki and M.Harma, Chem. Phys. Lett. **20**, 361 (1973).

[191] S.Shirasaki and H.Yamamura, Jap. J. Appl. Phys. **12**, 1654 (1970).

[192] R.A.Catlow, M.J.Norgett, and T.A.Ross, J.Phys.C **10**, 1627 (1977).

[193] B.J.Wuensch,W.C.Steele and T.Vasilios, J.Chem.Phys. **58**, 5258 (1973).

[194] T.X.T.Sayle, S.C.Parker and C.R.A.Catlow, in press.

[195] S.Meriani, Material Science and Engineering **A109**, 121 (1989); S.Meriani, V.Sergo and C.Schmid, *Proceedings of Symposium on Advanced Ceramics, 54th session of the Indian Ceramic Society*, 1990.

[196] K.Fuchs, Proc. Roy. Soc. (London) **A151**, 585 (1935).

[197] J.Vallin, M.Mongy, K.Salama and O.Beckman, J.Appl.Phys. **35**, 1825 (1964).

[198] G.N.Kamm and G.A.Alers, J.Appl.Phys. **35**, 327 (1964).

[199] neither is M.L.Cohen (private communication), nor are the authors in ref. [200].

[200] V.Heine and R.J.Needs, (private communication).